AD-A166 375 ON THE EVOLUTION OF PRECIPITATION ASSOCIATED WITH A WINTERTIME EAST COATT.. (U) AIR FORCE INST OF TECH WRIGHT-PATTERSON AFB OH R D BIEVINS 1985 1/2

UNCLASSIFIED AFIT/CI/NR-86-17T F/G 4/2 NL

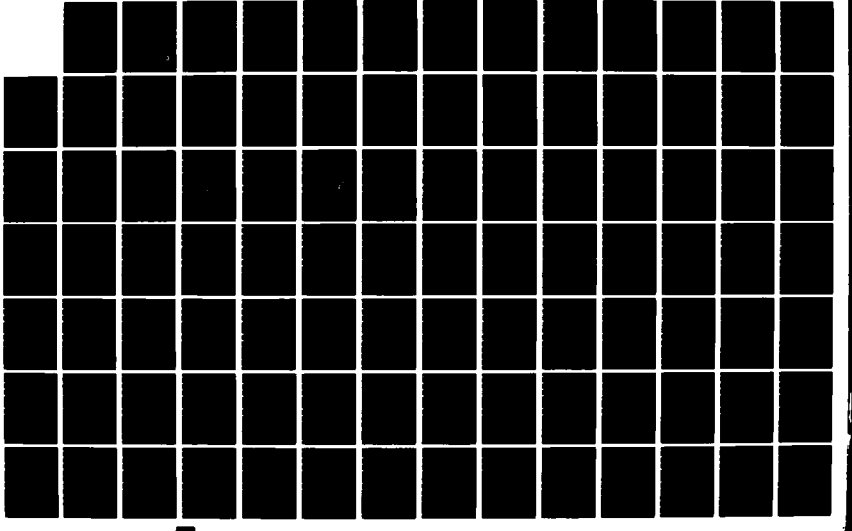

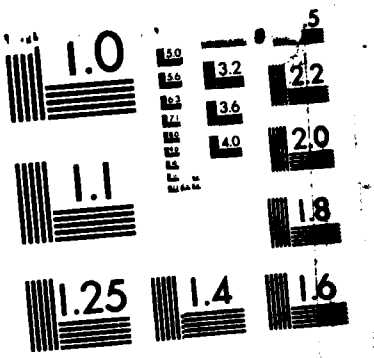

AD-A166 375

SECURITY CLASSIFICATION OF THIS PAGE *(When Data Entered)*

## REPORT DOCUMENTATION PAGE

READ INSTRUCTIONS BEFORE COMPLETING FORM

1. REPORT NUMBER: AFIT/CI/NR 86- 17T
2. GOVT ACCESSION NO.
3. RECIPIENT'S CATALOG NUMBER

4. TITLE *(and Subtitle)*: On the Evolution of Precipitation Associated with a Wintertime East Coast Cyclone: A GALE Preliminary Study

5. TYPE OF REPORT & PERIOD COVERED: THESIS/DISSERTATION
6. PERFORMING ORG. REPORT NUMBER

7. AUTHOR(s): Robert D. Bievins

8. CONTRACT OR GRANT NUMBER(s)

9. PERFORMING ORGANIZATION NAME AND ADDRESS: AFIT STUDENT AT: North Carolina University

10. PROGRAM ELEMENT, PROJECT, TASK AREA & WORK UNIT NUMBERS

11. CONTROLLING OFFICE NAME AND ADDRESS: AFIT/NR, WPAFB OH 45433-6583

12. REPORT DATE: 1985
13. NUMBER OF PAGES: 104

14. MONITORING AGENCY NAME & ADDRESS *(if different from Controlling Office)*

15. SECURITY CLASS. *(of this report)*: UNCLASS
15a. DECLASSIFICATION/DOWNGRADING SCHEDULE

16. DISTRIBUTION STATEMENT *(of this Report)*

APPROVED FOR PUBLIC RELEASE; DISTRIBUTION UNLIMITED

17. DISTRIBUTION STATEMENT *(of the abstract entered in Block 20, if different from Report)*

18. SUPPLEMENTARY NOTES

APPROVED FOR PUBLIC RELEASE: IAW AFR 190-1

Lynn Wolaver 24 April 86
LYNN E. WOLAVER
Dean for Research and Professional Development
AFIT/NR, WPAFB OH 45433-6583

19. KEY WORDS *(Continue on reverse side if necessary and identify by block number)*

20. ABSTRACT *(Continue on reverse side if necessary and identify by block number)*



DD FORM 1 JAN 73 1473 EDITION OF 1 NOV 65 IS OBSOLETE

86 4 8

SECURITY CLASSIFICATION OF THIS PAGE *(When Data Entered)*

# ON THE EVOLUTION OF PRECIPITATION ASSOCIATED WITH A WINTERTIME EAST COAST CYCLONE - A GALE PRELIMINARY STUDY



by

**ROBERT D. BLEVINS**



A thesis submitted to the Graduate Faculty of
North Carolina State University
in partial fulfillment of the
requirements for the Degree of
Masters of Science

**Department of**
**Marine, Earth and Atmospheric Sciences**

Raleigh

1985



APPROVED BY:

L. A. Nelson — Daniel A. Barker

W. J. Saucier — G. D. Watson

Chairman of Advisory Committee

# ABSTRACT

BLEVINS, ROBERT DAVID. On the Evolution of Precipitation Associated with a Wintertime East Coast Cyclone - A GALE Preliminary Study. (Under the direction of Gerald Watson and David Barber.

This research was initiated with the overall objective to analyze and then explain the precipitation structure of the 10-12 February 1983 east coast cyclone, of type A according to Miller (1946), which is typical of the type the GALE 1986 field project hopes to study. Careful hourly analysis of surface weather and precipitation were conducted using all available data obtained from the National Climatic Data Center at Asheville, N.C. Surface kinematic calculations were accomplished and compared to the observed precipitation pattern. Vorticity and divergence patterns were found to correlate well with the cold-air damming and the coastal front associated with the cyclone studied, but failed to correlate well with the observed precipitation structure.

Adiabatic and kinematic vertical motion profiles were better correlated with the observed precipitation, but failed to adequately explain the observed movement of precipitation. Subsequent isentropic analysis, similiar to that of the British researchers, allowed for the three dimensional analysis of air flow. Cross sections were analyzed for potential temperature, mixing ratio, and wind. These analyses revealed a warm conveyor belt and cold conveyor belt similiar to the Carlson (1980) model for midwest cyclones.

The unique setting of the east coast cyclone, which often develops in association with cold-air damming and the coastal front, was found to

increase the importance of the cold conveyor belt because of its fetch over the Gulf Stream and the greater lift it experiences movin over the cold wedge. The warm conveyor belt and cold conveyor belt were relabeled the Atlantic and the Gulf conveyor belt respectively due to the observed modifications.

The observed precipitation structure was well explained by the conveyor belt theory. Precipitation developed early in South Carolina, apparently as the conveyor belts became vertically stacked over the region, allowing the seeder-feeder process to develop. The mixed precipitation observed at Greensboro, N.C. was satisfactorily explained through the analyses of cold-air damming and the conveyor belts.

# BIOGRAPHY

Robert D. Blevins was born in Cleveland, Ohio on May 6, 1954. He was reared in Johnson City, Tennessee and graduated from Daniel Boone High School, Jonesboro, Tennessee in 1972. He attended The Pennsylvania State University, State College, Pennsylvania, where he received a Bachelor of Science degree in Meteorology in 1976. After attending Officer Training School, he was commissioned a second lieutenant in the United States Air Force.

The author held the positions of wing weather officer at F.E. Warren AFB, Wyoming and weather instructor for Navigation Training School, Mather AFB, California. Then, in August of 1983 he entered the Graduate School at North Carolina State University, Raleigh, North Carolina and began studies toward a Master of Science degree in Meteorology.

He is married to the former Kathi Irene Cook and has a daughter, Robbi, and a son, Ryan. The author's parents, Mr. and Mrs. Gomer Blevins, live in Johnson City, Tennessee.

ACKNOWLEDGEMENTS

The author wishes to express his appreciation to the United States Air Force and, in particular, the Air Force Institute of Technology and Air Weather Service for their financial and moral support. He also extends his appreciation to Dr. Gerald Watson, Chairman of his Advisory Committee, and Dr. David Barber for their guidance and advice in the preparation of this thesis. Appreciation is also extended to Dr. Walter Saucier and Dr. Larry Nelson for their helpful suggestions and assistance.

Particular thanks are also given to Dewey Harms and Jim Kroll for their aid and consultation concerning computer programming and for their moral support. Finally, the author would like to express his deepest appreciation and gratitude to his wife, Kathi, and to his parents and family for their prayers and continued support, without which this study would not have been possible.

TABLE OF CONTENTS

# 1. INTRODUCTION

## 1.1 General Comments

A major problem confronting local weather forecasters is the prediction of the onset, distribution, and amount of precipitation. Of concern here is the east coast of the United States in the wintertime. Synoptic patterns characteristic of this region and discussed by Miller (1946) include coastal cyclones which produce a mixture of rain, snow, sleet, and freezing rain as they move northeastward toward the heavily populated northeast portion of the country. The disruption of human activity caused by these often poorly forecast storms is enormous.

Mesoscale effects have long been known to have an important influence on the distribution and amount of precipitation associated with synoptic-scale disturbances. In 1949 Bergeron showed that low-level convergence due to differential friction in coastal zones can produce considerable local enhancement of precipitation. The fact that orography affects precipitation has been recognized for a much longer time. In addition to these physiographic factors, physical processes within large scale cyclones impose spacial and temporal variability in precipitation of importance to local forecast accuracy.

More recently researchers in Washington state and the British Isles have employed a variety of instruments such as weather radar, doppler radar, a dense network of autographic raingages, serial rawinsondes, aircraft, and satellite to the study of precipitation structures. They have found a wide range of space and time scales embedded within the broad

precipitation area revealed by routine meteorological charts.

Two mesoscale features, namely cold air damming (Richwein, 1980) and the coastal front (Bosart, 1975), unique to the east coast of the United States, have received much attention over the past decade. These features often act to enhance local precipitation and affect the rain, snow, freezing rain demarcation zone (Marks and Austin, 1979).

Accumulated evidence (e.g., Charba and Klein, 1980) suggests that while there has been an improvement of large-scale circulation prognosis over the past 10-15 years, there has been only slight improvement in the quantitative precipitation forecast. This disparity is a consequence of the sensitivity of precipitation amounts to several mesoscale factors which interact with the general cyclone scale during the evolution of clouds and precipitation.

Project GALE will be a concentrated effort to study the mesoscale dynamics and processes associated with wintertime east coast cyclones in an effort to better model and forecast this phenomena and its assoicated weather. This thesis will serve as a preliminary study for GALE and concentrate on the analysis of precipitation assoicated with a wintertime east coast cyclone.

## 1.2 Literature Review

### 1.2.1 Southeast United States Cyclone Climatology

The southeast Atlantic coastal region has been identified as an area of considerable wintertime cyclone activity and a preferred area for cyclone

deepening. Reitan (1974), using 20 years of January data, found a maximum of cyclone frequency and cyclogenesis on the eastern seaboard of the United States. In a similar study, Colucci (1976) focused on wintertime cyclone frequencies along the eastern United States and adjacent western Atlantic during the cool season of November to May. He used 10 years of data; a finer grid network enabled more detail.

Colucci's results broadly agree with those of Reitan. He found a maximum cyclone frequency in a narrow band from Cape Hatteras to New England, along the western edge of the Gulf Stream. A distinct minimum of cyclone frequency was found over the Appalachian mountains. Furthermore, cyclogenesis was most favorable over the southern Appalachians, the coastal Carolinas, and the adjacent western edge of the Gulf Stream. More than 70 percent of all cyclones moving along the coast of North and South Carolina deepened. Typical deepening rates in this area exceeded 1.5 mb/hr.

### 1.2.2 Synoptic Scale Cyclone Model

The introduction of daily synoptic maps over a century ago permitted analysis of the structure and behavior of extratropical cyclones. Since then considerable literature has accumulated concerning cloud and precipitation distribution associated with these larger scale circulation systems.

Two general categories of precipitation, stratiform and convective, are associated with extratropical cyclones. Houghton (1968) clearly distinquishes between the two basic precipitation mechanisms in terms of the time necessary for the growth of precipitation particles and the magnitudes of vertical motion in the precipitating clouds. Convective

precipitation develops more quickly than stratiform precipitation due to the stronger vertical motions associated with convective development. Stratiform precipitation will be the focus of this literature review.

Fitzroy (1863), based on analyses of the meager surface data then available, proposed a remarkably realistic picture of the structure of air currents associated with an extratropical cyclone. He recognized that cyclones form at the zone of interaction between air masses with different properties of temperature, moisture, and motion, which originate in the subtropical and polar regions. Shaw (1911) introduced an accurate schematic model based upon temperature, air trajectories, and precipitation distribution associated with moving cyclones.

Bjerknes (1918) investigated the structure of a number of cyclones in Europe using a special dense network of stations. Detailed analysis of the these data resulted in the first clear-cut description of the structure of extratropical cyclones and their role in the general circulation. The basic cyclone model (Fig. 1.1) developed by Bjerknes (1919), and slightly modified by Bjerknes and Solberg (1921,1922), first introduced the concept of warm, cold, and occluded fronts and went far toward indicating the underlying dynamical processes.

The meticulous analysis by Bergeron (1951; also for a summary see Palmen and Newton,1969) depicted in more detail the main features associated with mature cyclones and their attendant frontal systems; such features as comma-shaped cloud masses, clear slots, and extensive cold air showers were clearly shown. Bergeron's model was based on surface and upper air observations of quantity and quality not available in the earlier studies. Later satellite studies of mature cyclones by Widger (1964) agreed

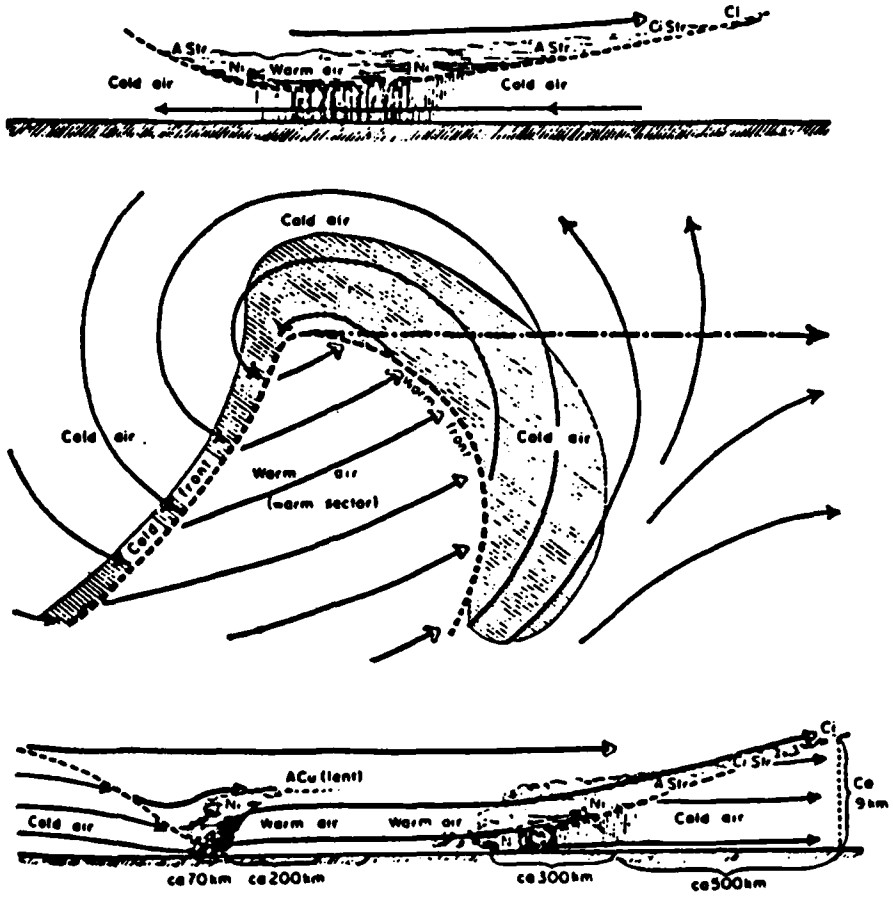


Fig. 1.1. Idealized cyclone, from J. Bjerknes and Solberg (1921). In middle diagram, dash-dotted shows direction of motion of cyclone; other arrows are streamlines of air flow at earth's surface. Top and bottom diagrams show cloud systems and air motions in vertical sections along direction of cyclone movement north of its center and across the warm sector south of its center.

remarkably well with Bergeron's model. Carlson (1980) explained the characteristic comma-shaped cloud mass by means of air trajectories along potential temperature and equivalent potential temperature surfaces for unsaturated and saturated air, respectively.

### 1.2.3 Pre-Frontal Precipitation

The first attempts to explain the occurrence of pre-frontal precipitation in the United states appear to be Holtzman (1936) and Lichitblau (1936). They introduced the concept of the upper cold front which, in advance of the surface front, accounts for mid-level precipitation in a manner similar to that of the surface cold front in Bjerknes' model. Sawyer (1952) concluded that precipitation distribution in cyclones can be attributed to a combination of three effects: (1) dynamically induced large-scale ascent; (2) small-scale overturning due to vertical instability; and (3) orography. Theoretical limits to stratiform precipitation variation caused by vertical instability were discussed by Miller (1955).

Petterssen *et al.* (1963), utilizing specially collected aircraft observations, concluded that the Norwegian cyclone model developed earlier for the North Atlantic and Europe (Fig. 1.1) could not be applied directly to the continental United States. The latter cyclones exhibit more vertical structure variation than typical of cyclones that have crossed the Atlantic. A similar study by Omoto (1965) confirmed the existence of pre-frontal rainbands with most cyclones crossing the United States. These features developed along low-level tongues of moisture in association with low-level convergence, a characteristic structure of the warm sector,

which supplies ample moisture into the precipitation system. Radar analysis by Nozumi and Arakawa (1968) showed warm sector mesoscale precipitation in 82 percent of cyclones studied.

In a series of studies of North Atlantic cyclones by British meteorologists, synoptic-scale trajectories on constant wet-bulb potential temperature surfaces, combined with radar and autographic raingage records, have considerably refined our understanding of the process leading to precipitation in extratropical cyclones (Browning and Harrold, 1969, 1970). Harrold (1973) introduced the concept of the "conveyor belt", a narrow jet of warm, moist air found near the top of the boundary layer in the warm sector. The "conveyor belt" is known to develop vertical instability and enhance the "seeder-feeder" process described by Bergeron (1950). The precipitation within the cyclones examined was found to be much more closely related to the position and behavior of the conveyor belt than to the frontal system. The importance of the conveyor belt is further stressed in work by Browning and Pardoe (1973) and Browning (1974). Browning (1984) found that the conveyor belt, when combined with orographic lifting, can enhance snowfall considerably. In this situation, the conveyor belt was recognized as producing the feeder cloud and orographic lifting the seeder cloud.

### 1.2.4 Mesoscale Precipitation

Mesoscale precipitation literature is extensive and emphasizes that processes on this scale must be considered when forecasting precipitation. Studies employing radar and serial radiosondes (e.g., Nagle and Serebreny,

1962; Elliott and Hovind, 1964, 1965) deduced that organized bands of precipitation are characteristic of cyclones moving onto the west coast of the United States.

The CYCLES (CYCLone Extratropical Storms project), a more elaborate study of precipitation structure, has been carried out by Hobbs and his collaborators along the Washington coast. Serial rawinsonde ascents, doppler radar, conventional surface and upper air data, and aircraft data were brought to bear by Hobbs *et al.* (1975) on the structure of an occluded frontal system. For the first time, mesoscale precipitation bands were related to cloud and microphysical processes. This study was continued and expanded by Hobbs *et al.*(1980), Herzegh and Hobbs, (1980,1981), Houze *et al.* (1981), Wang *et al.* (1983), and Parsons and Hobbs (1983).

Research by Kreitzberg (1968), Kreitzberg and Brown (1970), Austin and Houze (1972), and Bosart (1973) suggest that mesoscale precipitation features associated with west coast cyclones also accompany cyclones over the eastern United States. Storms over the east coast described by Bosart exhibit substantial mesoscale precipitation. Explicit classification and description of mesoscale precipitation associated with cyclones was first provided by Houze *et al.* (1976) and elaborated upon by Hobbs (1978). Houze (1981) summarized the structure of rainbands (Fig. 1.2) found by numerous researchers. Virtually all the types of rainbands described here have been identified in many parts of the world.

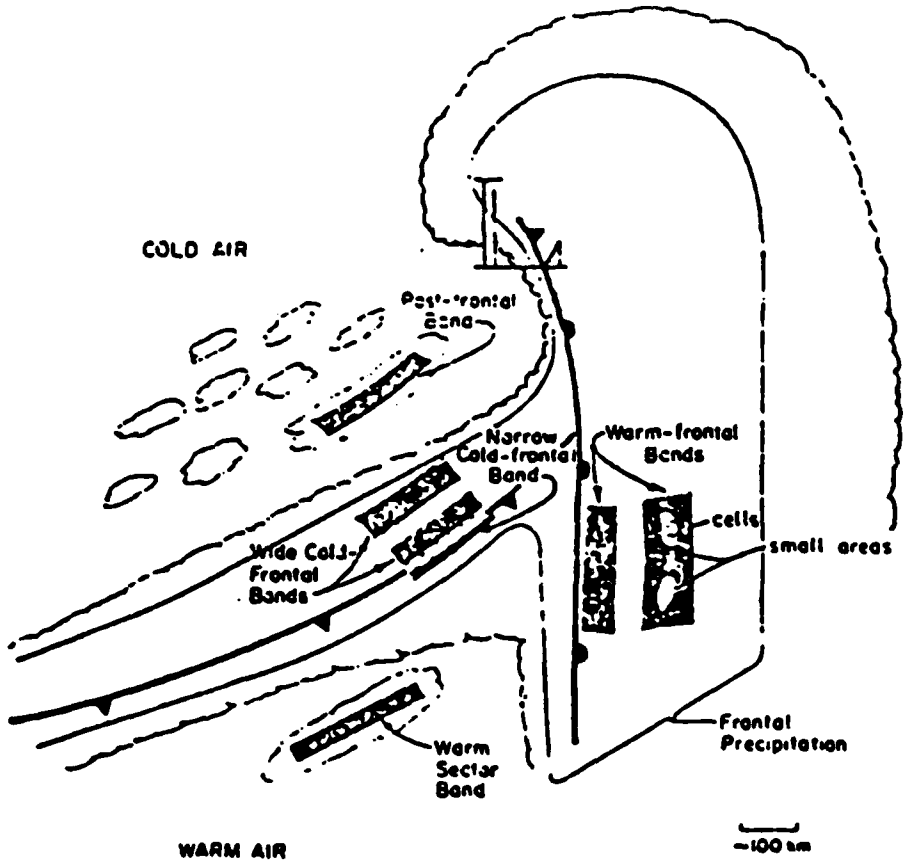


Fig. 1.2. Schematic of typical features of the cloud (scalloped boundary) and precipitation pattern of an extratropical cyclone from Houze (1976). Low pressure center is indicated by an L. Fronts are indicated by standard symbols.

## 1.3 Data and Methodology

### 1.3.1 Surface and Upper Air Data

Data for the east coast cyclone to be studied here were obtained from the National Climatic Data Center in Asheville, NC. Surface data were acquired for the Atlantic coastal states from Georgia to New Jersey, as well as Tennessee, Kentucky, and West Virginia. Hourly and special observations from civilian and military reporting stations, for the period 0000 GMT 10 February 1983 to 0000 GMT 12 February 1983, were used to construct surface analyses. In addition, wind and temperature information from offshore buoys and ships-of-opportunity were used to depict offshore weather during storm development.

Above-surface analyses for the same period were constructed from radiosonde observations from the upper air station network that included Dayton, Ohio; Nashville, Tennessee; Centreville, Alabama and stations to the east.

Precipitation analyses were constructed using six-hourly precipitation observations from airways stations and from the extensive hourly recording station network. Unfortunately, the reporting of precipitation amount to the nearest tenth of an inch at many locations introduced some problems to be described later. All these data were stored on computer disk and then checked for quality.

### 1.3.2 Objecitve Analysis Scheme and Grid Construction

The generation of fields of kinematic variables required the execution of numerous finite difference calculations. To simplify the process, the Barnes (1973) objective analysis scheme was employed to create gridded fields of raw data. This particular scheme was selected for its simplicity, accuracy, and cost effectiveness. It is an accepted objective analysis method in meteorology.

Briefly, the Barnes scheme uses gaussian weight functions to generate the gridded values. Weights are assigned to the raw data based solely upon the distance between the observation site and a particular grid point. Outside of a specified critical radius, a weight of zero is assigned to the observation. This effectively lessens the cost of computation without adversely affecting interpolated gridded data. A weight parameter is externally chosen which determines to what extent the scheme "smooths" the analyzed field.

The computer program of the Barnes analysis was produced by Harms (1985) of the atmospheric science program (North Carolina State University) as part of the preliminary studies for the upcoming GALE project. As part of this work, Harms conducted several tests of the Barnes scheme. His analysis of data from a midwest cyclone case study indicated that a weight parameter between 250km$^2$ and 500km$^2$ provided the minimum Root-Mean-Square Error values for most meteorological parameters. From this result, Harms determined the total response function, a measure of closeness of fit between interpolated values and observed values, to be 0.936 (a value of 1 indicates an exact agreement) for

a wavelenght of twice the station spacing.

Based on this information, and guidelines from Koch *et al.* (1980), a grid region for surface and upper air analyses was developed for the purposes of the present study. Koch and fellow authors suggested that grid point spacing should be between one-half and one times the average spacing of the observation network. The nearest-neighbor concept indicated a surface station spacing of about 85km. A value of 60km, was then selected for the surface grid. The total response function calculated by Harms, together with equations of the Barnes scheme, could then be solved for the optimum weight parameter. A value of $400km^2$ is appropriate to a the 60km spacing.

The same procedure was used to derive a weight parameter appropriate for an upper air grid. A grid spacing of 150km was selected based upon a 280km station spacing, and a weight parameter of $4600km^2$ calculated. Fig. 1.3 shows the domain of the grids used for calculating surface and upper air kinematic variables. The surface grid was extended further to the east in order to incorporate the available buoy data and remove edge effects of the Barnes scheme from analyses along the coast.

The effectiveness of the Barnes scheme is dependent upon the station spacing, therefore, "artificial" data were included at 1x1 degree locations over the ocean where the data void would adversely affect the results of generated fields. The lack of the upper air observations over the ocean was much less of a problem due to upper air station spacing; one "artificial" sounding was added in the southeast sector to satisfy station spacing requirements of the grid. No conclusions in this thesis are based on the artifical data offshore. The sole purpose of the artifical data is to reduce the edge effect of the Barnes scheme along the coast.

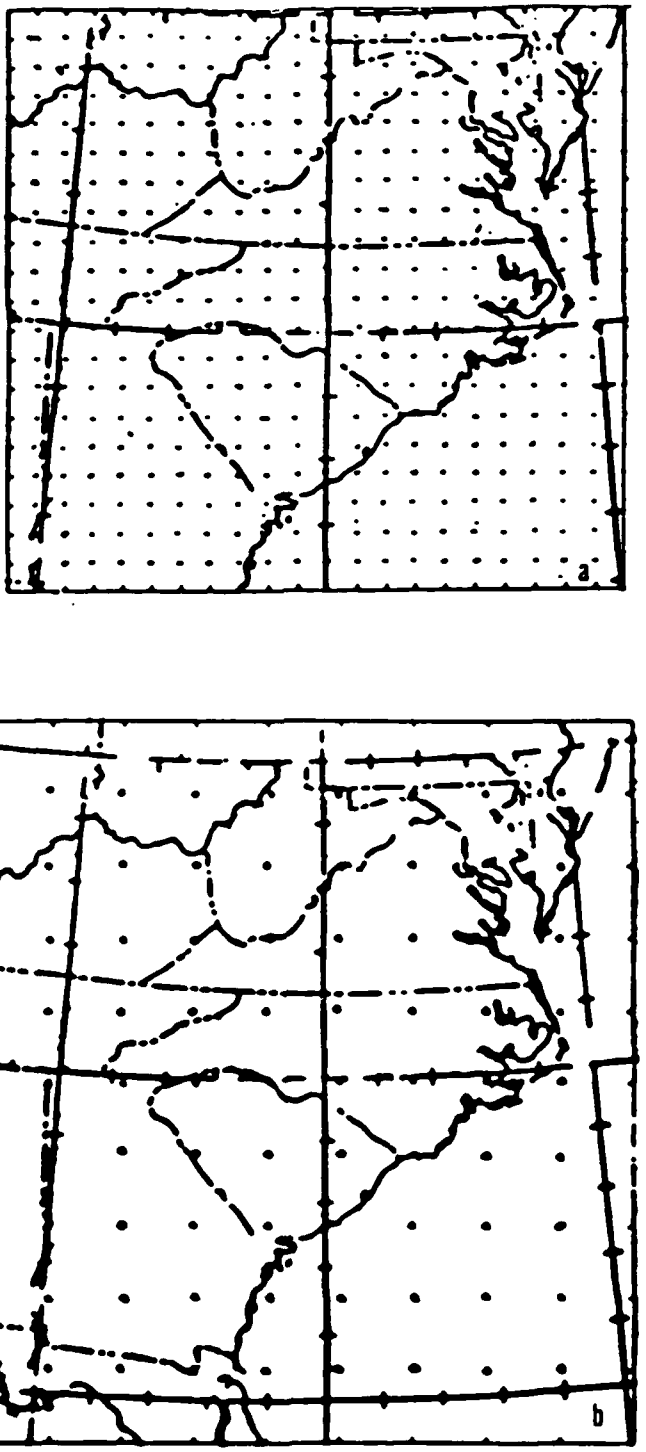


Fig. 1.3. a. Surface grid used for finite differencing. b. Upper air grid used for finite differencing.

The Barnes scheme was also used to analyze hourly precipitation. A grid spacing of 50km was adopted based upon an average station spacing of 60 km. A weight parameter of 60km$^2$ was calculated. Appropriate "artificial" precipitation data based on radar and satellite were included offshore to lessen the edge effect along the coast. The next chapter will present the synoptic overview of this case study and then examine the mesoscale aspects of precipitation evolution.

## 1.4 Objectives of this Study

This research presents a case study of the evolution of precipitation along the southeast Atlantic coast associated with a "classical" east coast cyclone. Efforts will concentrate on mapping hourly precipitation and then relating the precipitation pattern to pertinent kinematic meteorological fields of divergence, vorticity, and vertical motion. Cross sections of potential temperature, mixing ratio, and relative humidity are used to find adiabatic vertical motion fields, upper air moisture fields, and areas of potential instability. Isentropic analyses help depict the three-dimensional air motion.

An attempt is made to identify a 'conveyor belt' of the type described by Harrold (1973) which develops along with the large scale cyclogenesis.

Considered in the present study is an example of slow cyclogenesis (12 hour deepening rate less than 1mb/hr) of type 'A' according to the classification scheme of Miller (1946). The cyclone moves from the Florida peninsula to Cape Hatteras, North Carolina between 1800 GMT on the 10th of February and 1800 GMT on the 11th of February, 1983. Furthermore, this

case study is of the type participants of GALE[1] hope to study and falls into the proposed field experiment time frame of January 15 to March 15. It is hoped that the results of this thesis will serve as groundwork for further research based on the unique data obtained during GALE.

---

1. Genesis of Atlantic Lows Experiment (GALE) is a National Scientific Foundation funded project for the study of east coast cyclones. The field project is scheduled for January 15-March 15, 1986.

# 2. SYNOPTIC OVERVIEW

## 2.1 Large-Scale Overview

A well-defined, moderately intense 500mb trough with an $18 \times 10^{-5} s^{-1}$ absolute vorticity maximum has reached the lee of the Rocky Mountains by 0000 GMT on the 9th (Fig. 2.1a) The strong zonal flow at this latitude suggests continued eastward movement. The limited fine mesh (LFM) surface analysis in Fig. 2.1b shows a weak surface cyclone (1007mb) over southeastern New Mexico. The 10 knot southeasterly flow over the Texas to Mississippi region has surface temperatures in the mid 50 F to mid 60 F range. Cloud cover extends northward to Canada. Skies are clear to partly cloudy over the southeastern and mid-Atlantic states where temperatures are in the 30's and 40's. Cold air (~20 F) over the Great Lakes is associated with a polar high (1030mb) over south central Canada.

On crossing the Rocky Mountains, the 500mb trough (Fig. 2.2a) has extended southward into Mexico while undergoing some overall weakening. Positive vorticity advection (PVA) remains a prominent feature and movement over the Gulf coast seems certain. The surface analysis at 1200 GMT (Fig. 2.2b) shows a warm sector over eastern Texas with light southeasterly winds and temperatures in the 60's. North of the warm front temperatures are in the 30's and 40's. The surface based baroclinity and upper-level PVA seem favorable for further cyclone development. Fig. 2.3a shows a re-intensification of the PVA associated with the 500mb trough over the Texas gulf coast by 0000 GMT on the 10th. The surface low

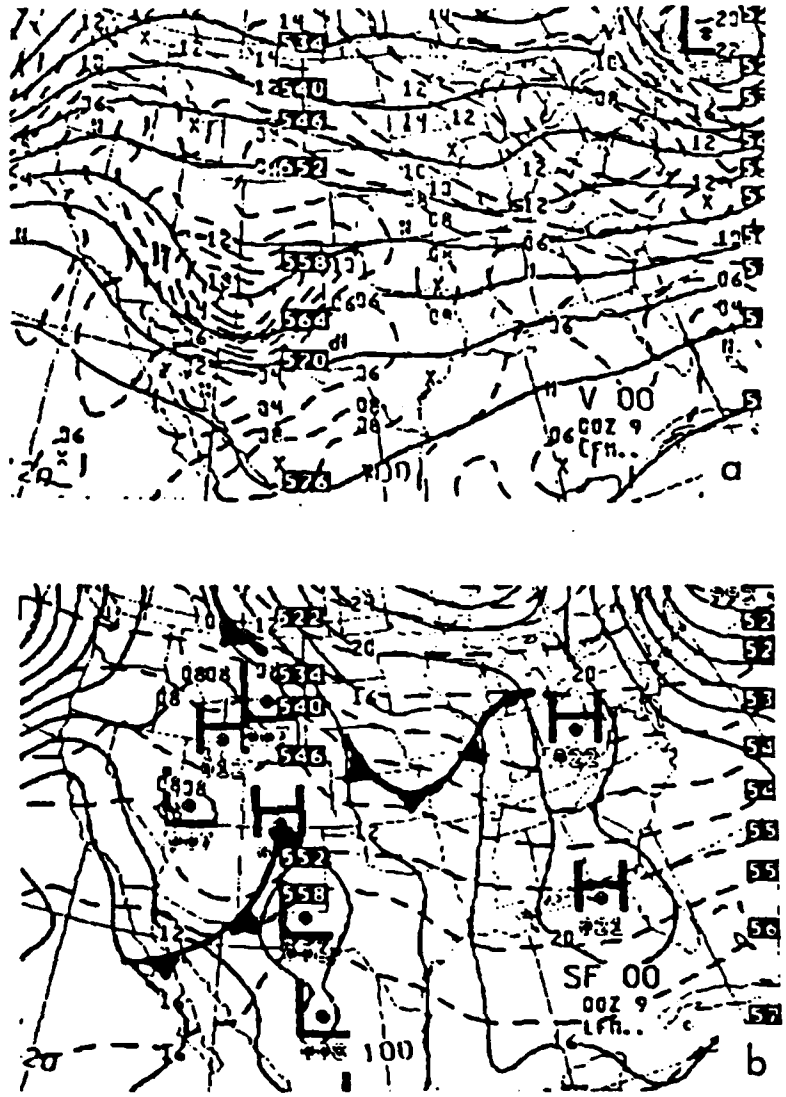


Fig. 2.1. a. LFM 500mb analysis with isohypses (solid,dam) and absolute vorticity (dashed, $10^{-5}s^{-1}$). b. LFM surface analysis with sea level isobars (solid,mb) and 500-1000mb thickness (dashed,dam). NMC surface frontal analysis is superimposed. 0000 GMT 9 February 1983.

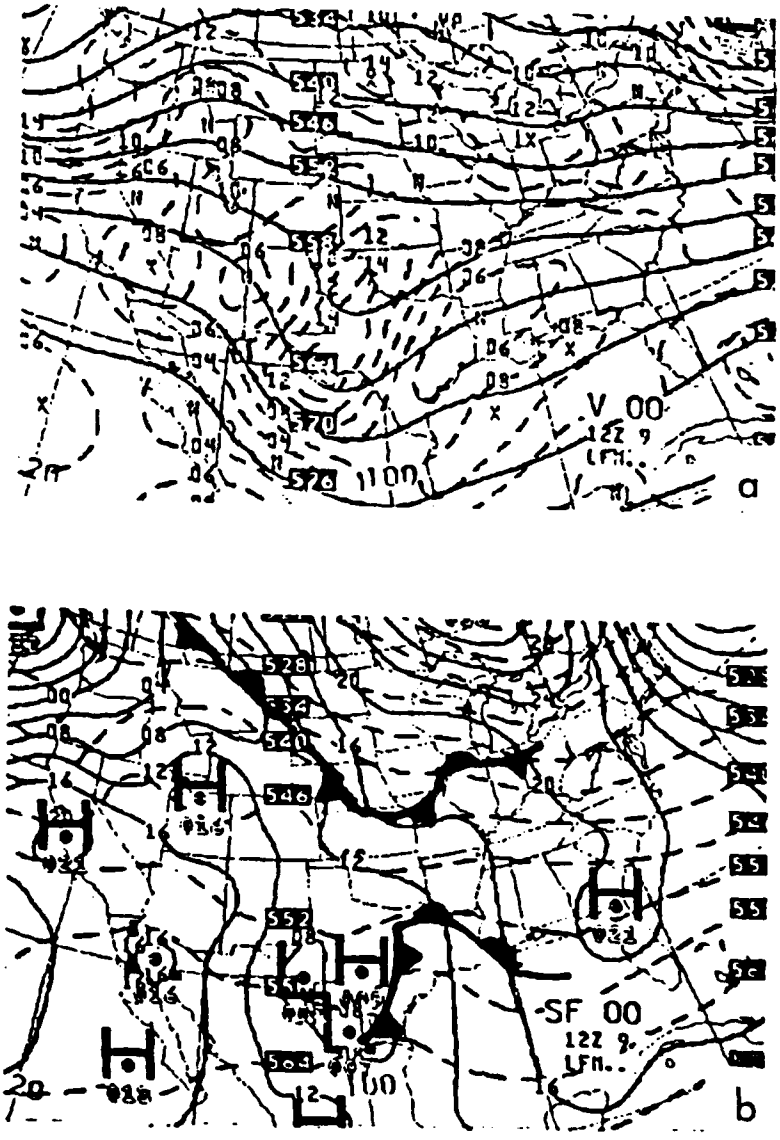


Fig. 2.2a,b. Same as Fig. 2.1a,b except for 1200 GMT 9 February 1983.

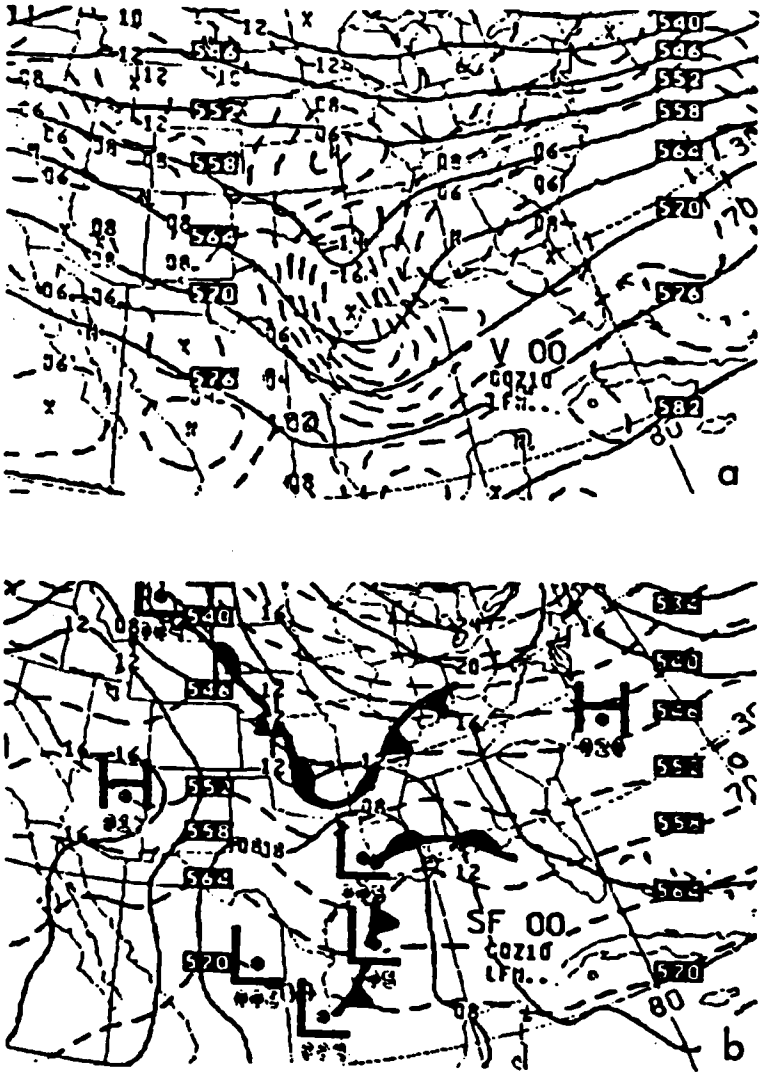


Fig. 2.3a,b. Same as Fig. 2.1a,b except for 0000 GMT 10 February 1983.

(1005mb) shown in Fig. 2.3b is vertically under the trough line. Evidently the rapid movement of the trough aloft (~30kn) maintains the PVA area east of the surface cyclone and contributes mainly to the latter's motion rather than to intensification. The warm advection over the Gulf coast, implied from surface geostrophic winds and 1000-500mb thickness pattern also contribute to the whole system's eastward movement. The baroclinic zone ahead of the surface low is maintained. Advanced high-level cloudiness has reached into the Carolinas while rain and drizzle are spreading into Kentucky and Tennessee.

By 1200 GMT on the 10th, the 500mb trough (Fig. 2.4a) is centered over the northern Gulf and continues to intensify. A disorganized surface low (Fig. 2.4b) directly beneath the upper trough has deepen. A mixture of light rain and snow has spread into the western Carolinas from Tennessee and Kentucky. The polar high centered near Hudson Bay builds a ridge southward along the east coast. Temperatures in central North Carolina are in the 30's with light north winds. NOAA buoys 44003 and 44006 have southeasterly winds with temperatures in the 60's. Appalachian damming and a coastal front, which appears as an extension of the warm front, are well-established.

At 0000 GMT on the 11th the 500mb trough (Fig. 2.5a) is moving northeastward over the southeastern states. Fig. 2.5b shows the surface low trails the trough aloft and has filled slightly over the past 12 hours. A warm front located just offshore extends northeast from the low. Precipitation has become widespread, but patchy, over the region during the last 6 hours. Light rain with embedded showers occurs in the eastern Carolinas, while light snow is falling in the western piedmont. Some

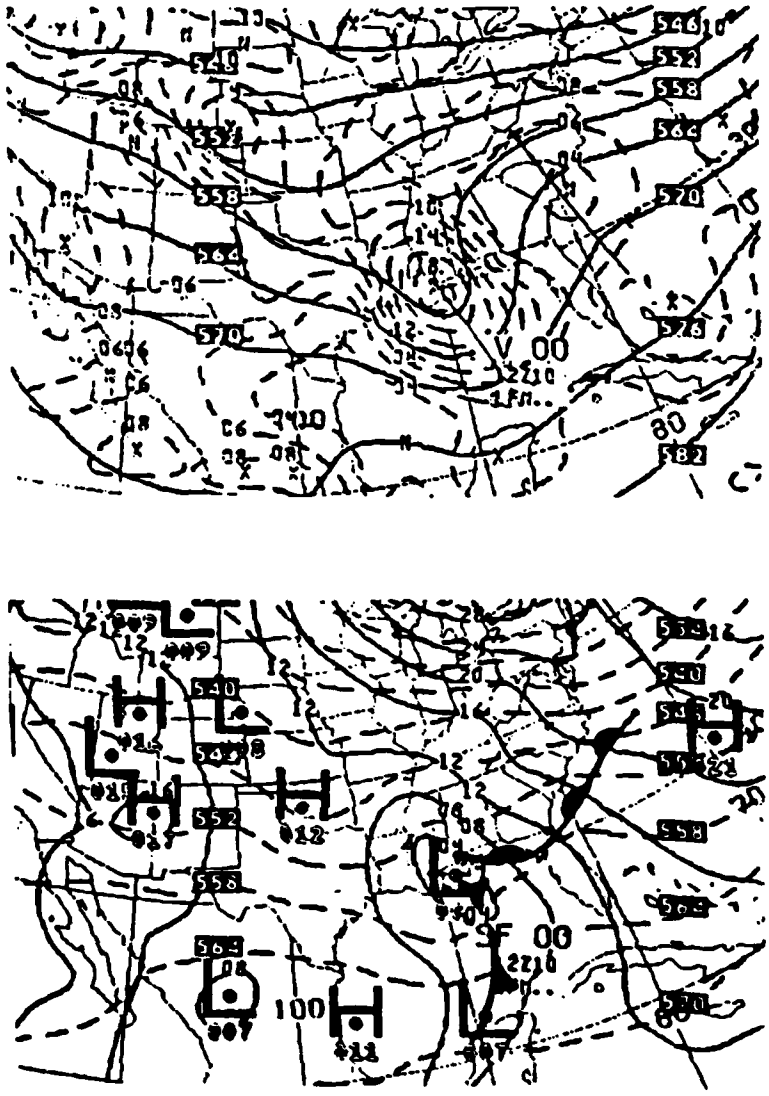

Fig. 2.4a,b. Same as Fig. 2.1a,b except for 1200 GMT 10 February 1983.

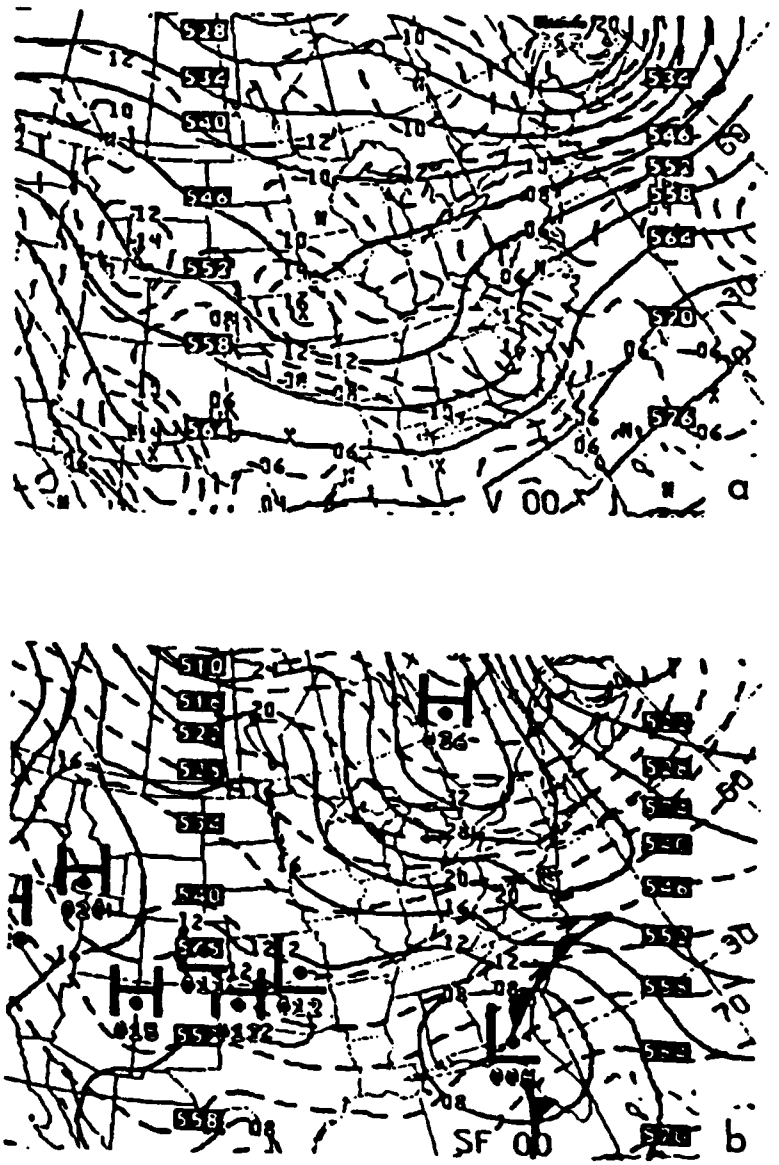


Fig. 2.5a,b. Same as Fig. 2.1a,b except for 0000 GMT 11 February 1983.

freezing rain has been observed in the transistion zone between these two areas of precipitation. Thunderstorms have been detected by radar and reported by station observations along the South Carolina coast in the vicinity of the coastal front.

A northwest-southeast 500mb trough (Fig. 2.6a) lies across North Carolina at 1200 GMT on the 11th. Fig. 2.6b shows the surface low (1002mb) just off the coast near Wilmington, NC. is deepening and continuing to move northeast along the coastal front. Earlier, approximately 0600 GMT on the 11th, the coastal front, marked by a strong across-front temperature contrast, moved onshore near Cape Hatteras, NC. In the warm air Cape Hatteras, NC registered 54 F with southeast winds while Rocky Mount-Wilson some 200km to the west in the cold air registered 38 F with a northeast wind. Both stations observed rainfall. By 0000 GMT on the 12th the surface low is 200km off the Virginia coast and little change in central pressure or circulation is noted. Fig. 2.7 shows that twelve hours later, however, with the storm off the southern New England coast, pronounced deepening and intensification occurred.

Storm precipitation totals (Fig. 2.8) show that considerable amounts of precipitaton fell across much of the Carolinas and Virginia with a noticeable increase in precipitation just inland and parallel to the coast and along the crest of the Applachians. Snowfall accumulations from this storm (Fig. 2.9) are impressive. Several locations, including Washington, Philadelphia, and New York, received more than 18 inches of snow. Enhancement of snowfall by the Appalachain mountains is evident. Two factors account for this: (1) increased precipitation due to upslope flow and (2) better accumulation of snowfall due to the colder conditions

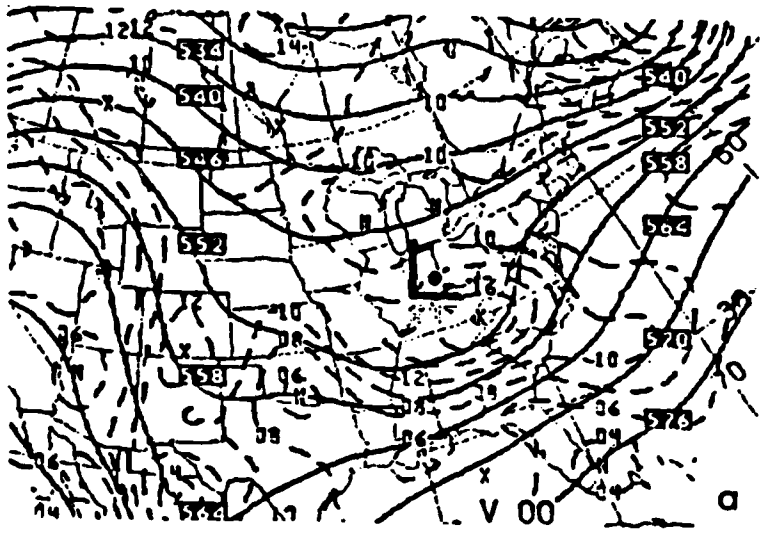


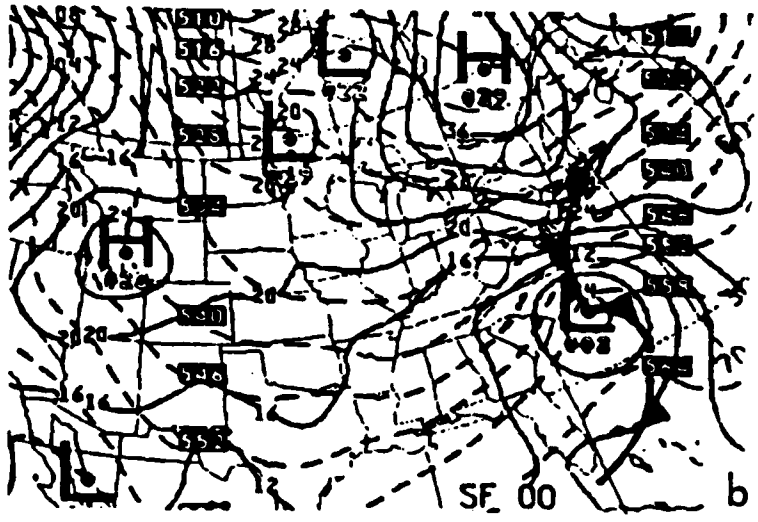


Fig. 2.6a,b. Same as Fig. 2.1a,b except for 1200 GMT 11 February 1983.

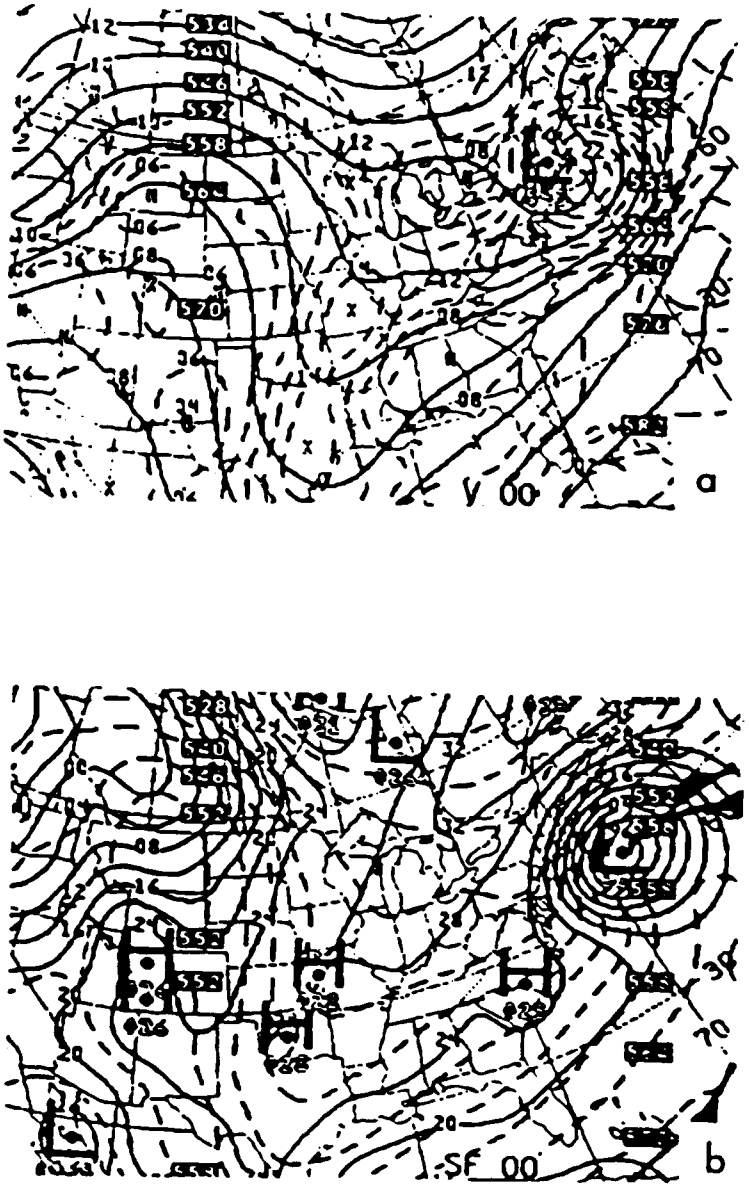


Fig. 2.7a,b. Same as Fig. 2.1a,b except for 1200 GMT 12 February 1983.

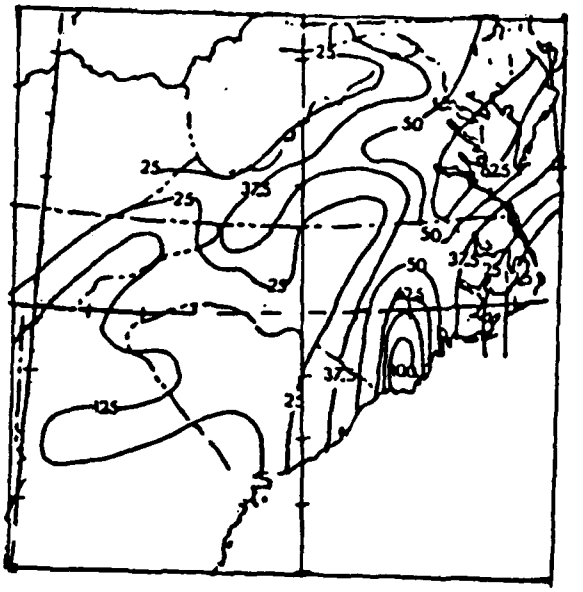

Fig. 2.8. Total storm precipitation (mm) for 10-12 February 1983.

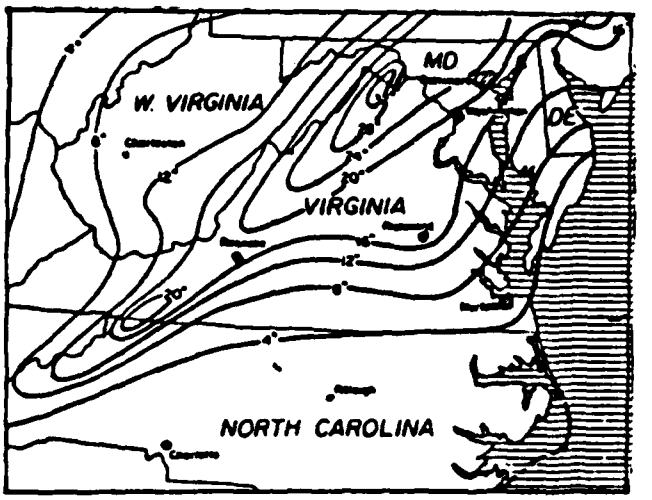


Fig. 2.9. Total storm snowfall (inches) for 10 - 12 February 1983. Data from February 1983 Storm Data.

associated with increased elevation.

## 2.2 Mesoscale Precipitation Analysis

Hourly precipitation was analyzed for the mid-Atlantic coastal region. Subjective analysis was accomplished using hourly precipitation reports, satellite imagery, and hourly weather plots. The Barnes objective analysis scheme was also applied. Several difficulties were encountered during this task, the most significant problem being the nature of the hourly precipitation data. Table 2.1 shows that approximately 78 percent of the total available hourly reporting stations were operative during this precipitation episode. Less than 22 percent of the hourly reporting stations reported precipitation to the nearest hundredth of an inch; all remaining stations reported precipitation only to the nearest tenth of an inch.

Table 2.1 Percentage of hourly precipitation stations operating and percentage of stations reporting to the nearest hundrendth of an inch.

| STATE | # OF RAINGAGES | # OF RAINGAGES OPERATING | #OF HUNDREDTHS RAINGAGES |
|---|---|---|---|
| North Carolina | 43 | 35 (81.4%) | 9 (21.0%) |
| Virginia | 49 | 36 (73.5%) | 12 (24.5%) |
| South Carolina | 27 | 22 (81.5%) | 6 (22.2%) |
| Georgia | 62 | 53 (85.5%) | 15 (24.2%) |
| West Virginia | 45 | 24 (53.3%) | 9 (20.0%) |
| Tennessee | 40 | 35 (87.5%) | 7 (17.5%) |
| Kentucky | 52 | 44 (84.6%) | 11 (21.2%) |
| TOTALS | 318 | 249 (78.3%) | 69 (21.7%) |

The stations reporting in tenths use a Fischer-Porter raingage. This device is a tipping bucket which tips and marks a chart strip when .10 inches of rain has fallen into the gage. In a situation of light rain this accumulation may take several hours. For example, if .02 inches of rain fell the first hour, .03 the second hour, .04 the third hour, and .02 the fourth hour; then .10 inches of rain would be recorded the fourth hour, and no precipitation indicated in the other hourly intervals. If less than .10 inches of rain fell, no precipitation would be recorded at all.

Because of this procedure, the Fischer-Porter raingages cannot portray an accurate picture at all of light precipitation distribution. This problem was deemphasized due to the significant amount of precipitation that fell for this case study and through the use of the Barnes objective analysis scheme.

Hourly reporting stations are located as shown in Fig. 2.10. Average station spacing is about 60km. Effectively it is a little larger because of inoperative stations and irregular station spacing. In addition, some stations are presumably not representative of the local area, and later in the period strong winds probably altered precipitation totals as measured by gages. These problems are largely deemphasized because the pattern of precipitation, not its absolute value, is the objective of this analysis.

## 2.3 Mesoscale Precipitation Pattern

A complete hourly series of weather and precipitation amounts for the period 1800 GMT on the 10th to 1200 GMT on the 11th and every two hours between 1200 GMT on the 10th and 1800 GMT on the 10th can be found in

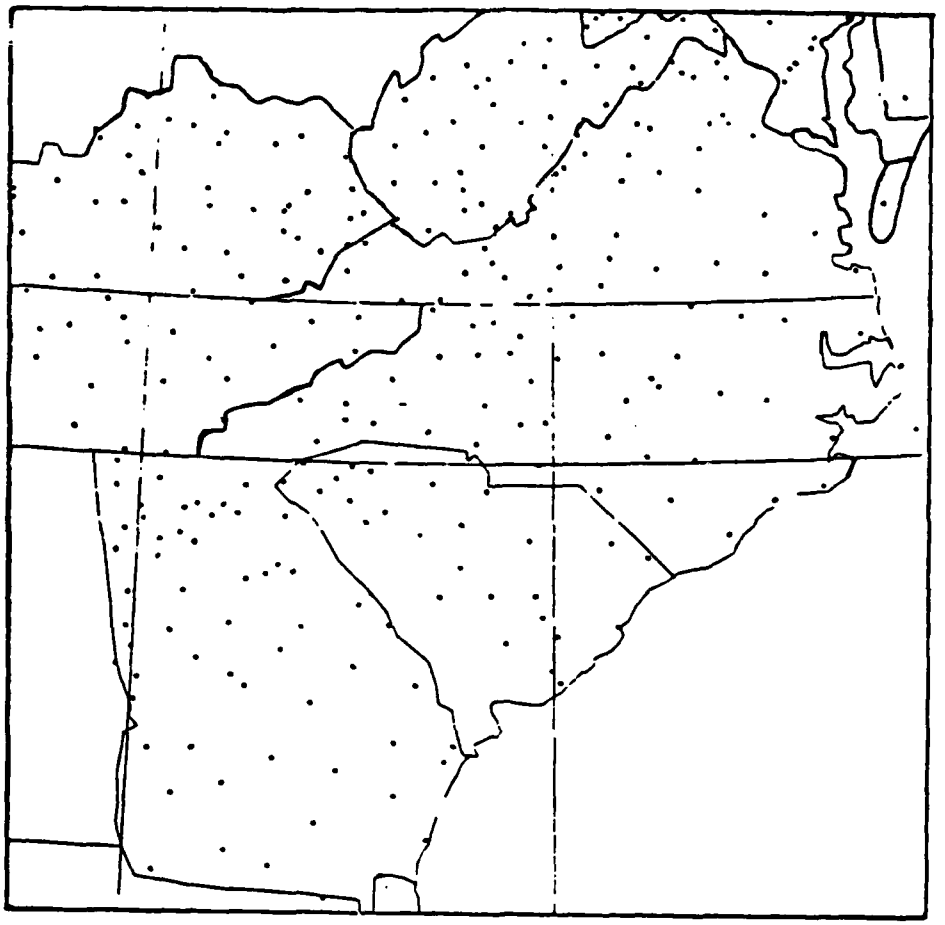

Fig. 2.10. Network of hourly reporting raingages.

Appendix A. Selected charts to follow show that by 1200 GMT on the 10th an area of significant rain (Fig. 2.11b) was located over north central Tennessee and south central Kentucky. Lighter and more scattered precipitation occurred east of this area covering extreme northwest South Carolina and western North Carolina. Precipitation in North Carolina (Fig. 2.11a) turned into a mixture of rain, freezing rain, ice pellets, and finally to snow.

During the next several hours, the precipitation gradually moved northeast into southern West Virginia, western and west central Virginia with precipitation becoming widely scattered in western North Carolina and ending in South Carolina. Significant amounts (~10 mm) of precipitation fell only in central Tennessee and south central Kentucky and infrequently in the mountainous areas of North Carolina and Virginia in the form of mixed precipitation and snow. Until 1600 GMT on the 10th no precipitation associated with the cold front moving from the southwest had been observed in Georgia or South Carolina.

Precipitation analysis for 1800 GMT on the 10th (Fig. 2.11d) shows rainfall of more than 2.5 mm occurring in southeast Kentucky and southwest Georgia. Fig. 2.11c shows the development of the mixed precipitation zone eastward across northern North Carolina. The precipitation area in southeast Georgia moves northeastward the next several hours and merges with the precipitation in South Carolina that breaks out rapidly between 1700 GMT and 1800 GMT. By 2000 GMT on the 10th (Fig. 2.12b), significant amounts of precipitation are occurring in South Carolina. Fig. 2.12a shows that showery precipitation, which is indicative of potential instability aloft, is occurring along coastal South Carolina at this time. A

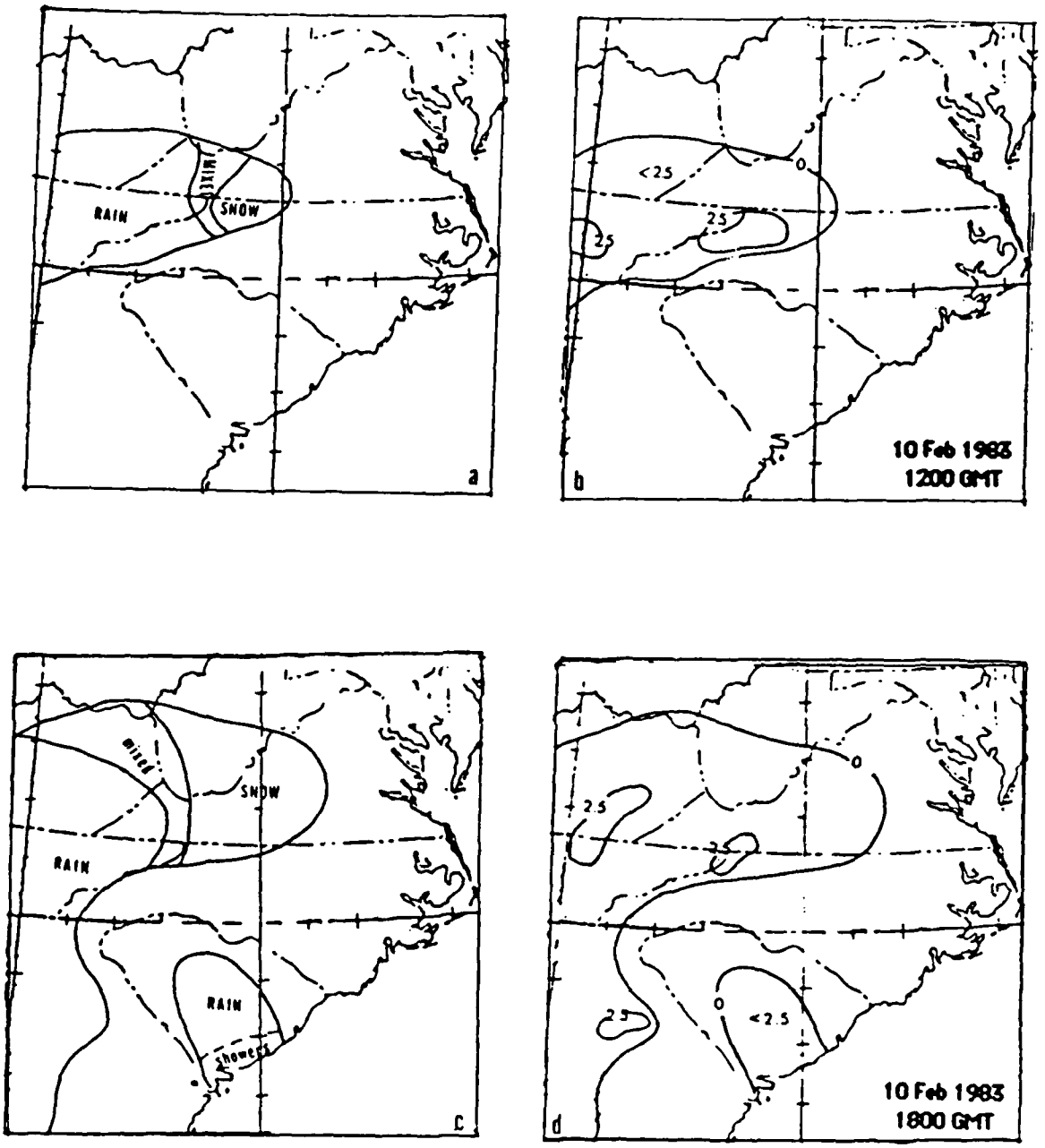


Fig. 2.11. Hourly precipitation (mm) amounts (a,c) and precipitation type (b,d) for date and time indicated.

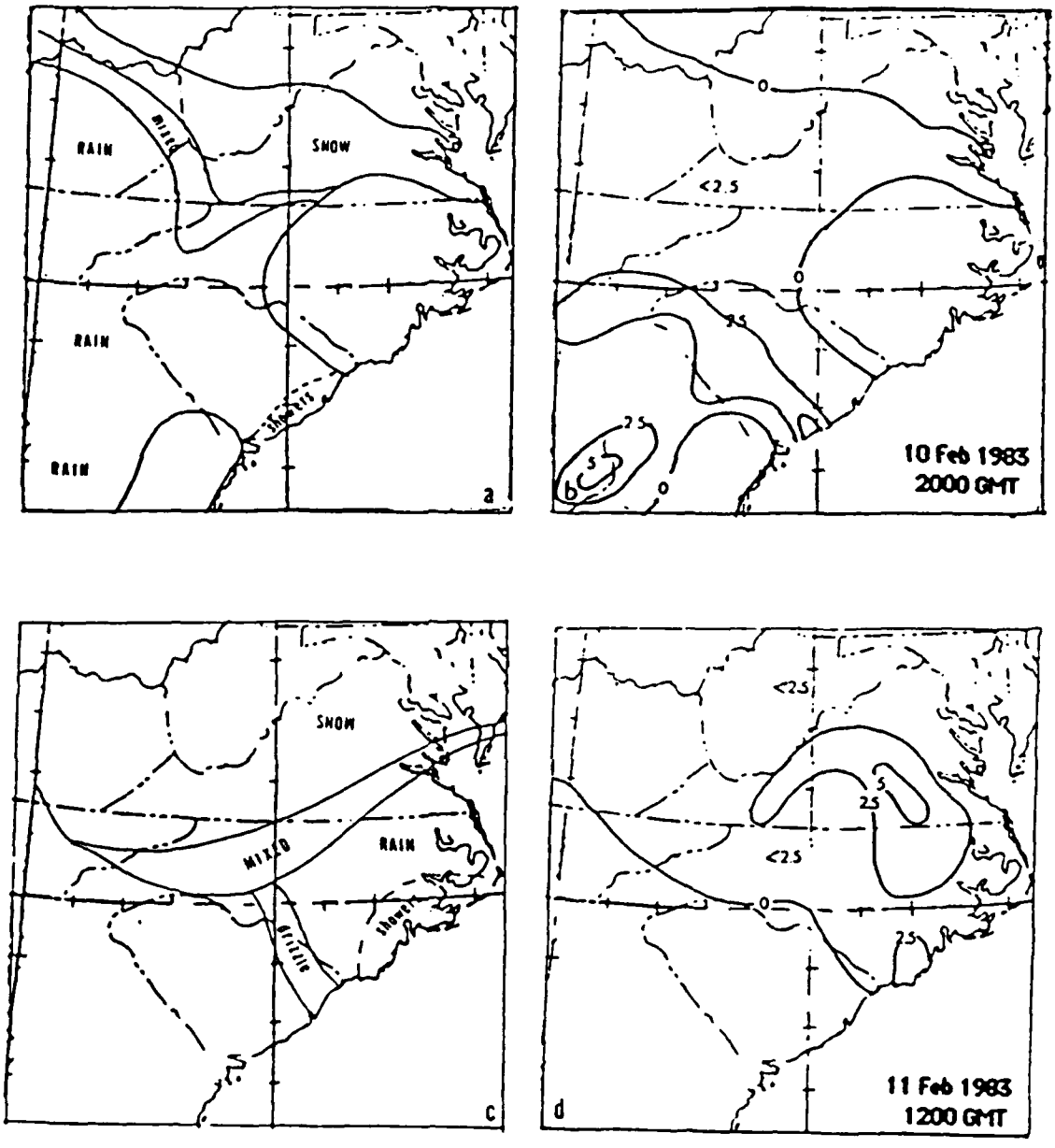


Fig. 2.12a,b,c,d. Same as Fig. 2.11a,b,c,d except for date and time indicated.

thunderstorm is reported at Myrtle Beach at 0000 GMT on the 11th. The precipitation band, which is oriented perpendicular to the coast and has the heaviest rate close to the coast, begins to move northward up the coast while maintaining its orientation.

After progressing up the coast the band of precipitation seems to stall just north of Wilmington, NC. for several hours. While the "base" of the precipitation remains anchored, the orientation changes from nearly perpendicular to the coast to one more oblique and nearly north to south in direction. Beginning approximately 1200 GMT on the 11th, this marked band of heavy precipitation begins to diminish (Fig. 2.12d) while a pronounced band of snow develops (Fig. 2.12c) from the central Virginia coast through interior Virginia. Later (not shown) a heavy band of snow with a melted liquid equivalent in excess of 50 mm per hour developed in interior Virginia and moved slowly northward bringing record snowfall amounts to several northeast cities. Refer to Fig. 2.9 for storm snowfall totals.

Fig. 2.13 clearly shows the slow re-orientation of the precipitation band, as well as the precipitation developing through central and eastern Virginia. This occurs well before the precipitation from the south reached the area. Cape Hatteras, NC. did not experience precipitation until after 0300 GMT; some 7 hours after Norfolk, VA. and 5 hours after Wilmington, NC.

A persistent feature in the precipitation analysis is a probable enhancement of precipitation just to the east of the Appalachians in the Carolinas and Virginia. Further evidence of this is seen from the storm total precipitation analysis shown in Fig. 2.8 . A first look at surface winds reveal that they are nearly parallel to the mountains and not conducive to the enhancement of precipitation through up-slope motion. Analysis of the

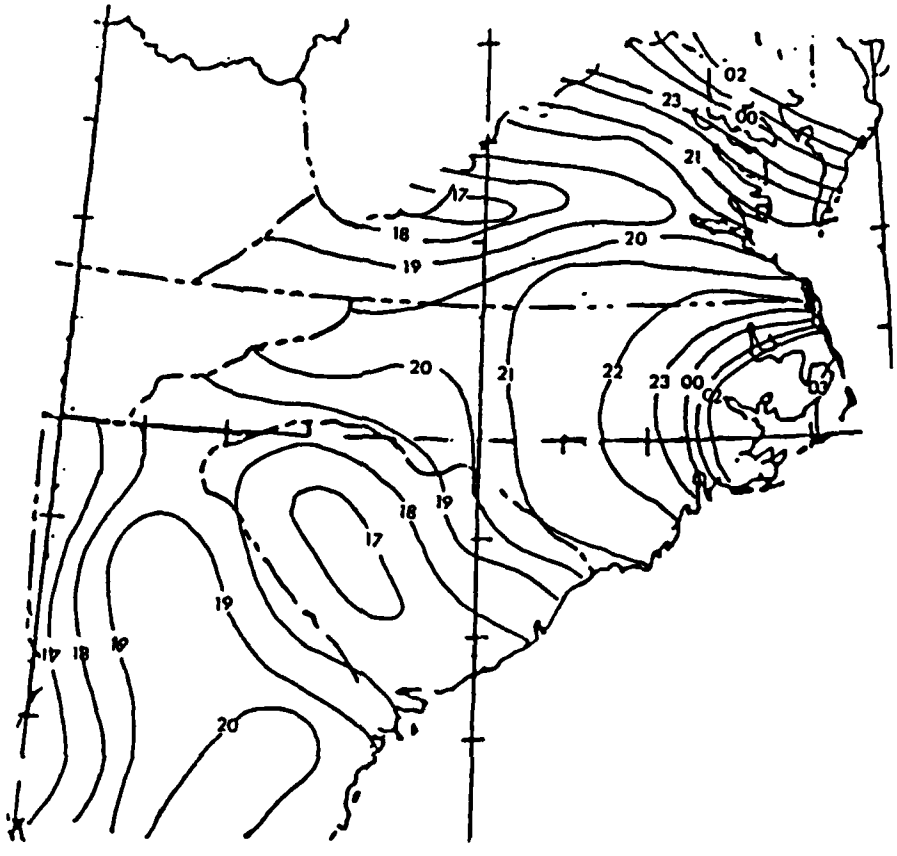


Fig. 2.13. Precipitation start times for 1700 GMT 10 February 1983 (17) to 0300 GMT 11 February 1983 (03).

upper-air winds from Greensboro, NC and Athens, GA reveals that winds just above the sufrace increased in speed and veered westward to become nearly perpendicular to the mountains; this is favorable for enhanced precipitation. Winds at Greensboro are more favorable for enhanced precipitation than at Athens, and this is indicated in the total precipitation analysis.

The series of weather plots presented in Appendix A show a band of mixed precipitation moving from Tennessee and Kentucky into Virginia. This mixed precipitation remains nearly stationary for several hours and then edges westward as strong cold air advection developed in association with the developing cyclone off the Carolina coast. As the band of heavier precipitation moves from South Carolina into North Carolina, a mixed band of precipitation approximately 60km to 100km wide develops west-east across north central North Carolina. This band seems to be wider across the mountains in western North Carolina and narrower along the North Carolina and Virginia coast. Significant narrowing and northward movement of this band near the coast occurs after 0200 GMT on the 11th when rapid baroclinic development occurs off coastal North Carolina.

The precipitation which began as light snow in southeast Virginia rapidly mixes and changes over to rain. A very distinct boundary between snow and rain oriented northeast to southwest later develops between Richmond, VA. and Norfolk, VA. Richmond briefly experiences mixed precipitation before changing back to all snow. The mixed precipitation along the Appalachians gradually moves south and west into the northern mountains of South Carolina. The 'pivot point' of this rotation seems to be Greensboro, NC. which began, and continued, as mixed precipitation as the heavier precipitation moved northward from South Carolina. Chapter four describes

the Greensboro precipitation in detail and relates it to the observed weather phenomena.

## 2.4 Cyclone Motion in Relation to Precipitation

The surface cyclone motion (Fig. 2.14 ), central pressure (Fig. 2.15), and geostrophic vorticity (Fig. 2.16) are interesting in relation to the aforementioned precipitation development. The vorticity was caluculated at the cyclone center with an NMC grid distance of 190 km. The cyclone moves into western Mississippi by 0600 GMT on the 10th and is weakening. Re-development occurs in the Florida panhandle at 1800 GMT on the 10th along a cold front moving across Florida. Satellite imagery (not shown) reveal very little cloudiness associated with this re-development.

The cyclone, moving steadily eastward at approximately 25kn, continues to weaken until it moves off the coast near Brunswick, GA. at 0300 GMT on the 11th. During this time significant precipitation has developed over South Carolina and moved at approximately 47kn to the northeast. National Weather Service radar at Charleston, SC. and Cape Hatteras, NC. indicate the individual cells moving at 20 to 25 knots from the south. This indicates a developing area of precipitation several hundred kilometers ahead of the weakening cyclone. Even though steady progress is made by the cyclone across southern Georgia between 2300 GMT on the 10th and 0200 GMT on the 11th, the precipitation, which moved steadily up the coast between 1800 GMT and 2300 GMT on the 10th, noticeably slowed just north of Wilmington between 2300 GMT on the 10th and 0200 GMT on the 11th.

Between 0300 GMT and 0800 GMT the cyclone moved rapidly (at

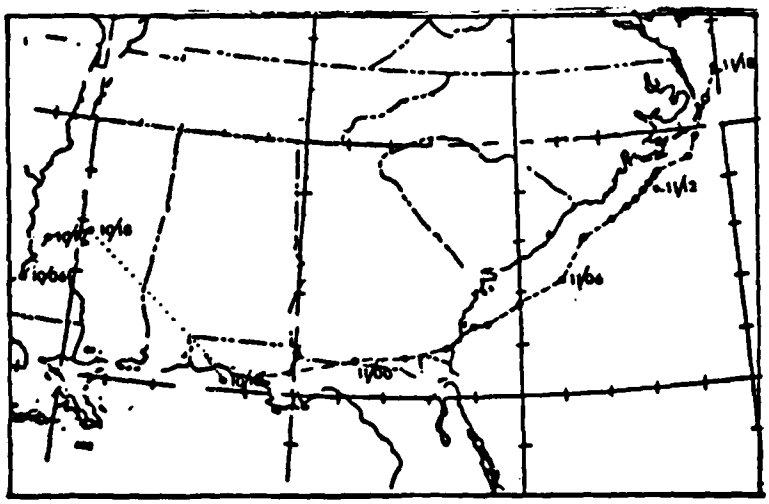

Fig. 2.14. Cyclone position every six hours from 0600 GMT 10 February 1983 (10/06) to 1800 GMT 10 February 1983 (10/18). Hourly cyclone position from 0000 GMT 11 February 1983 (11/00) to 1800 GMT 11 February 1983 (11/18).

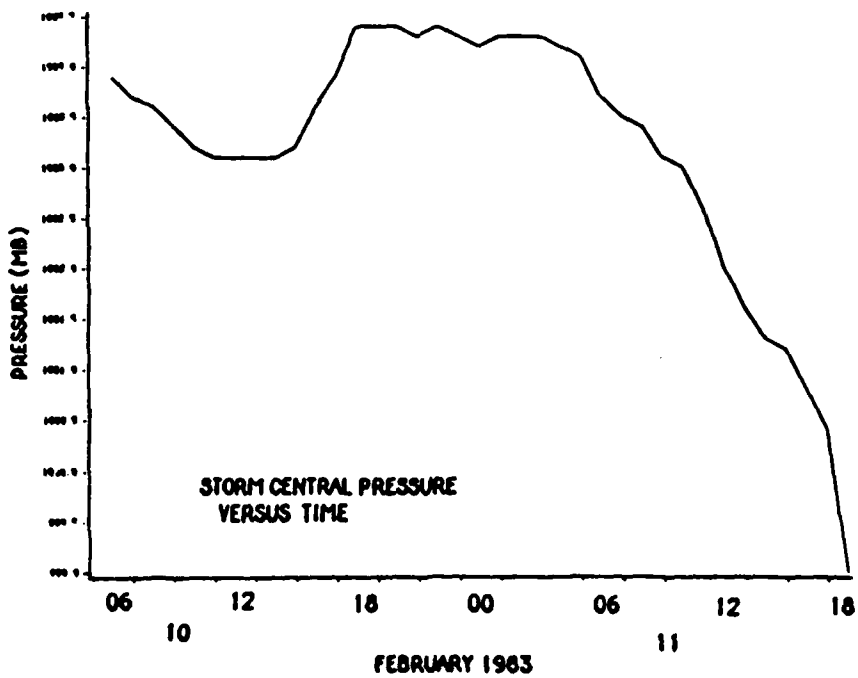


Fig. 2.15. Hourly central pressure (mb) for the cyclone. All times are GMT. Values are derived from hourly surface analysis and are uncorrected for the semidiurnal pressure oscillation.

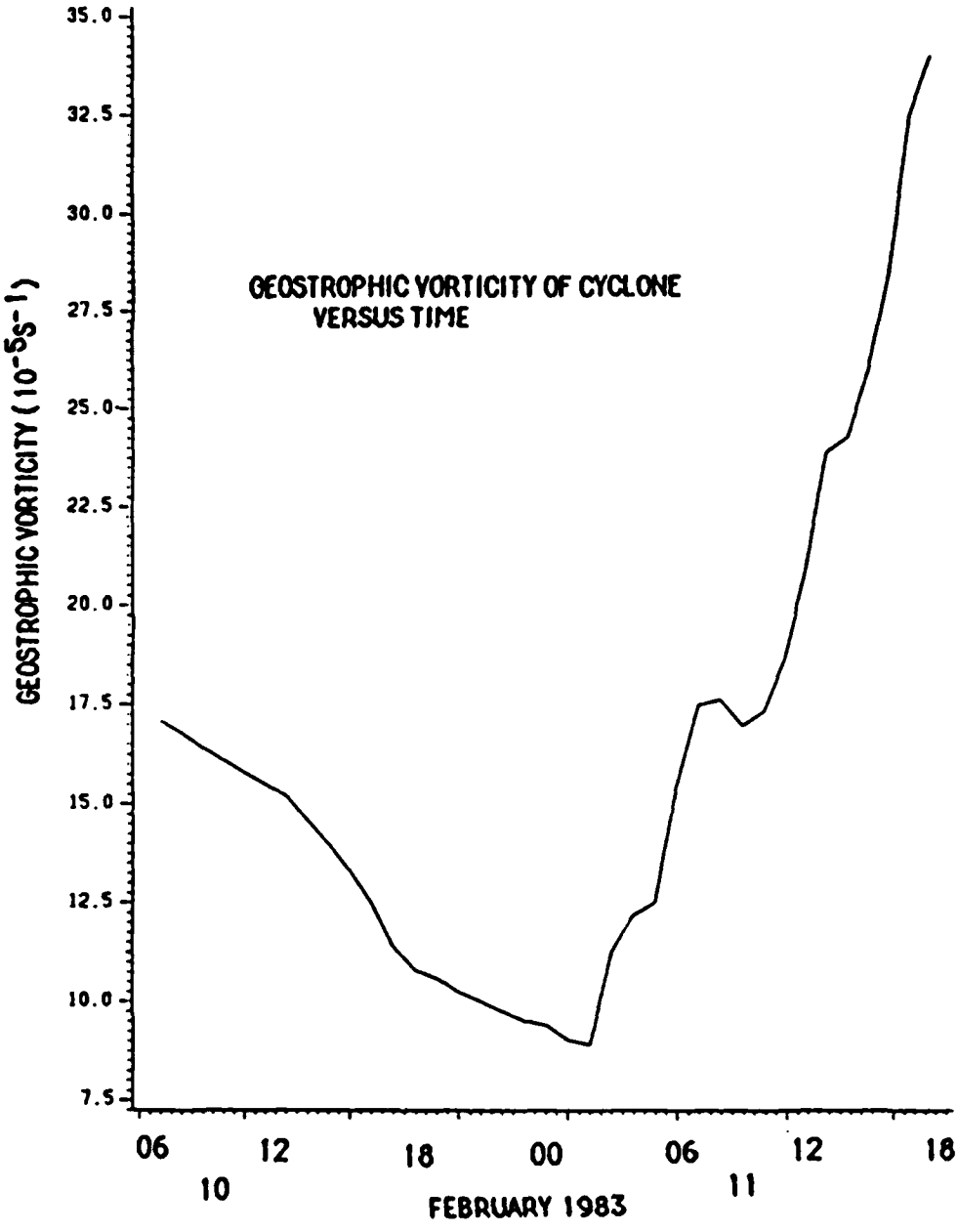


Fig 2.16. Hourly geostrophic vorticity for the cyclone center. All times are GMT. Values are derived from hourly surface analysis.

approximately 40kn) to the northeast along the northern fringe of the Gulf Stream and strengthens from 11 to 18 x $10^{-5}s^{-1}$ in terms of geostrophic vorticity. Central pressure remains above 1000mb. Noticeable slowing, to approximately 10kn,and continued strengthening to 24 x $10^{-5}s^{-1}$ occurs between 0900 GMT and 1400 GMT on the 11th as the cyclone moves to a position just off the coast near Wilmington, NC. It is during this time that the coastal precipitation band changes from a north-south orientation in eastern North Carolina to east-west across interior Virginia. The cyclone, maintaining its current heading, accelerates and strengthens to 34 x $10^{-5}s^{-1}$ by 1800 GMT on the 11th. The heavy snow in interior Virginia moves northward with the cyclone.

Of particular interest in the present study is the development of significant precipitation over the Carolinas well ahead of the cyclone even as the circulation weakened. A probable cause of this precipitation evolution is the warm conveyor belt, a feature first described by Harrold (1973).

Chapter three will relate the kinematics of the wind field to the precipitation development and movement in an attempt to confirm the conveyor belt hypothesis.

# 3. KINEMATICS OF WIND FIELD IN RELATION TO PRECIPITATION

## 3.1 Surface Divergence and Vorticity Calculations.

Divergence and vorticity of surface winds were calculated hourly from all available surface wind information over land and from offshore buoys. Additionally, hourly offshore winds were estimated every 1 degree of latitude and longitude from 75 degrees longitude westward to the coast and between 30 degrees and 40 degrees latitude using the 6 hour NMC surface analysis, careful hourly analysis, and time continuity. These subjective winds were necessary in order to lessen the edge effects the Barnes objective analysis scheme would encounter in the vicinity of the coast. Offshore values of vorticity and divergence should be observed with caution. No findings in this thesis were stricitly based upon offshore data.

The Barnes objective analysis scheme was used to obtain gridded data over a 22 x 22 grid centered at 35.5 degrees north latitude and 80 degrees west longitude. The grid spacing is 60km. Following the guidance provided by Harms (1985) and using the equations of Barnes (1973), a weight parameter of $400km^2$ was selected. For ease of computation, the wind information was gridded as U and V components relative to the grid. Once the U and V values were obtained the equations used for divergence and vorticity, respectively, are:

$$\partial u/\partial x + \partial v/\partial y \text{ and } \partial v/\partial x - \partial u/\partial y.$$

The derivatives are approximated by centered finite-differences over 120km. Hourly divergence and vorticity fields will be compared to hourly

precipitation to find any relationship that may exist. The patterns of divergence and vorticity, not their absolute values, will be stressed, as the parameter values are sensitive to the weight chosen and grid spacing used. Some results are next described.

Initially (1200 GMT on the 10th) the divergence field (Fig. 3.1b) shows a relatively weak pattern with a slight zone of convergence (negative divergence) just offshore from South Carolina to Cape Hatteras, NC., and then more weakly up the coast to Wallops Island, VA. A divergence maximum is located in the vicinity of western North Carolina, eastern Tennessee, and southwest Virginia. Light precipitation at 1200 GMT on the 10th (Fig. 2.11a) is surprisingly better correlated with the surface divergence area than the convergence area. In the area of light precipitation, the atmosphere is stable and the surface may not actively participate in the development of precipitation.

A trough is developing off the southeast coast during this time, separating stronger southeast flow offshore from weaker northeast flow just onshore. The weak divergence is probably associated with the effects of the Appalchian mountains which act to dam the cold air along the eastward slopes.

Like the divergence pattern, the vorticity pattern (Fig. 3.1a) is weak. The only notable feature is an area of weak negative vorticity centered in eastern Tennessee.

The magnitude of divergence and vorticity gradually intensify over the next 6 hours, while the general pattern remains the same. The maximum value of divergence at 1800 GMT on the 10th (Fig. 3.1d) has increased to 2.2 $\times 10^{-5} s^{-1}$ as it moves a little closer to the shore. It is well aligned with

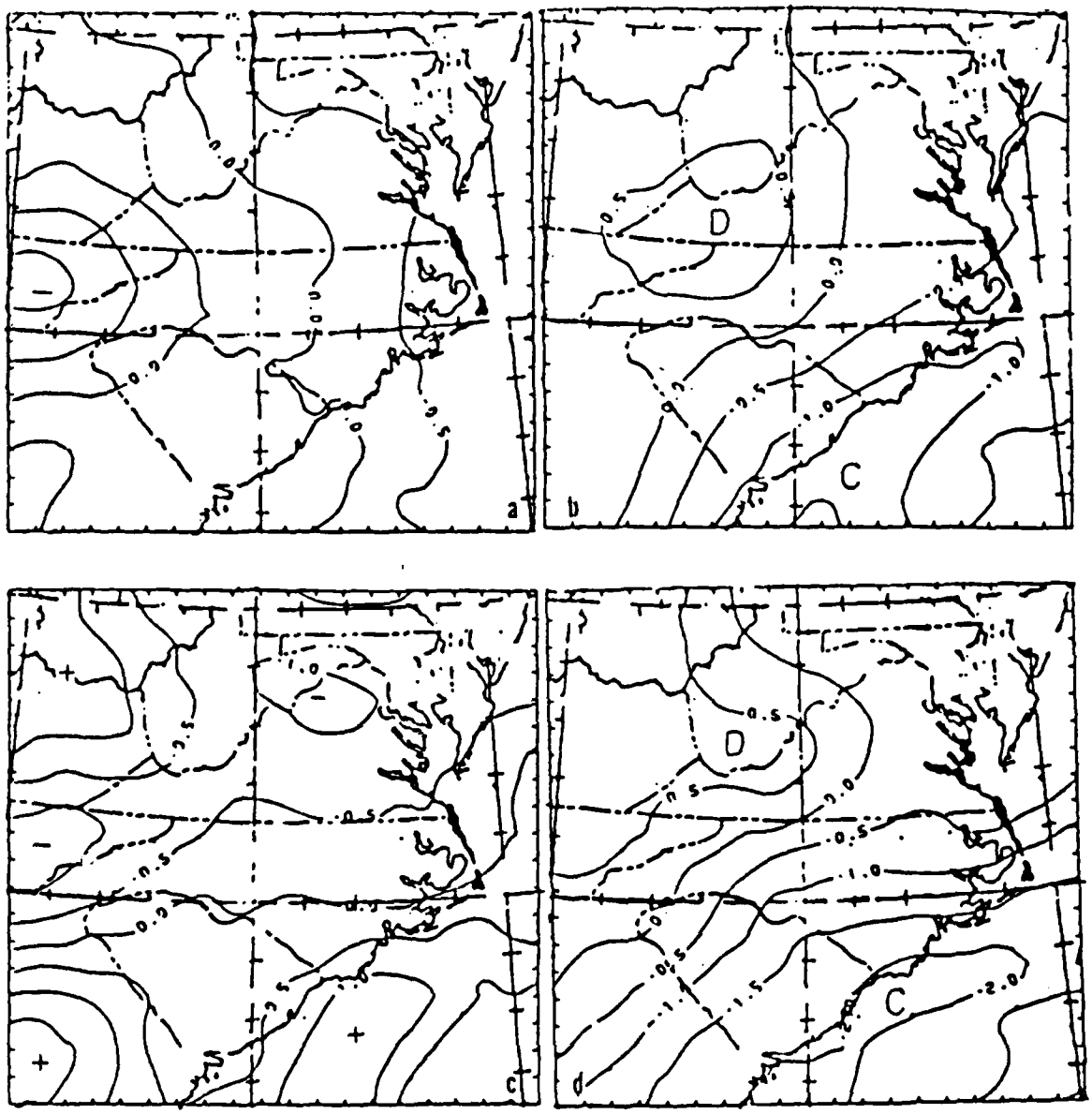


Fig. 3.1. a. Surface relative vorticity. b. Surface divergence. Units are $10^{-5}s^{-1}$. Postive vorticity (+) and negative vorticity centers (-) are indicated. Divergence (C) and convergence (D) centers are indicated. 1200 GMT 10 February 1983. c,d. Same as a,b except for 1800 GMT 10 February 1983.

the surface warm front that has developed just offshore. At 1800 GMT on the 10th, the vorticity pattern (Fig. 3.1c) has somewhat intensified and become better defined. A definite elongated zone of positive vorticity lies just offshore probably associated with the warm frontal zone, and negative vorticity lies across northern Virginia. The latter feature extends into eastern Tennessee and is associated with a well-defined ridge of surface pressure associated with the cold-air damming. The hourly precipitation and current weather do not agree very well with these patterns of vorticity and divergence. Evidentally, the surface layer is not dominant in the weather production at this time.

Significant precipitation develops in South Carolina by 1900 GMT on the 10th and moves northeastward as previously described. Between 1800 GMT on the 10th and 0000 GMT on the 11th the divergence field (Fig. 3.2b) and the vorticity field (Fig. 3.2a) continue their along-shore orientation, which correlates well with the warm frontal zone. The maximum vorticity and convergence areas remain just offshore, and their centers move northeastward in good agreement with the maximum in precipitation. The vorticity has increased to $1.7 \times 10^{-5} s^{-1}$ and divergence to $-5.3 \times 10^{-5} s^{-1}$. The vorticity maximum seems to lag behind the convergence maximum.

Just as the northward moving precipitation maximum seems to stall, both the divergence and vorticity fields (not shown) also stall just south of Cape Hatteras, NC. between 2300 GMT on the 10th and 0200 GMT on the 11th. Since both divergence and vorticity are calculated from the wind field, the halt in movement of these fields must be related to some important feature of the winds. This "feature" will be described shortly.

Neither pattern of surface divergence nor vorticity correlate well with

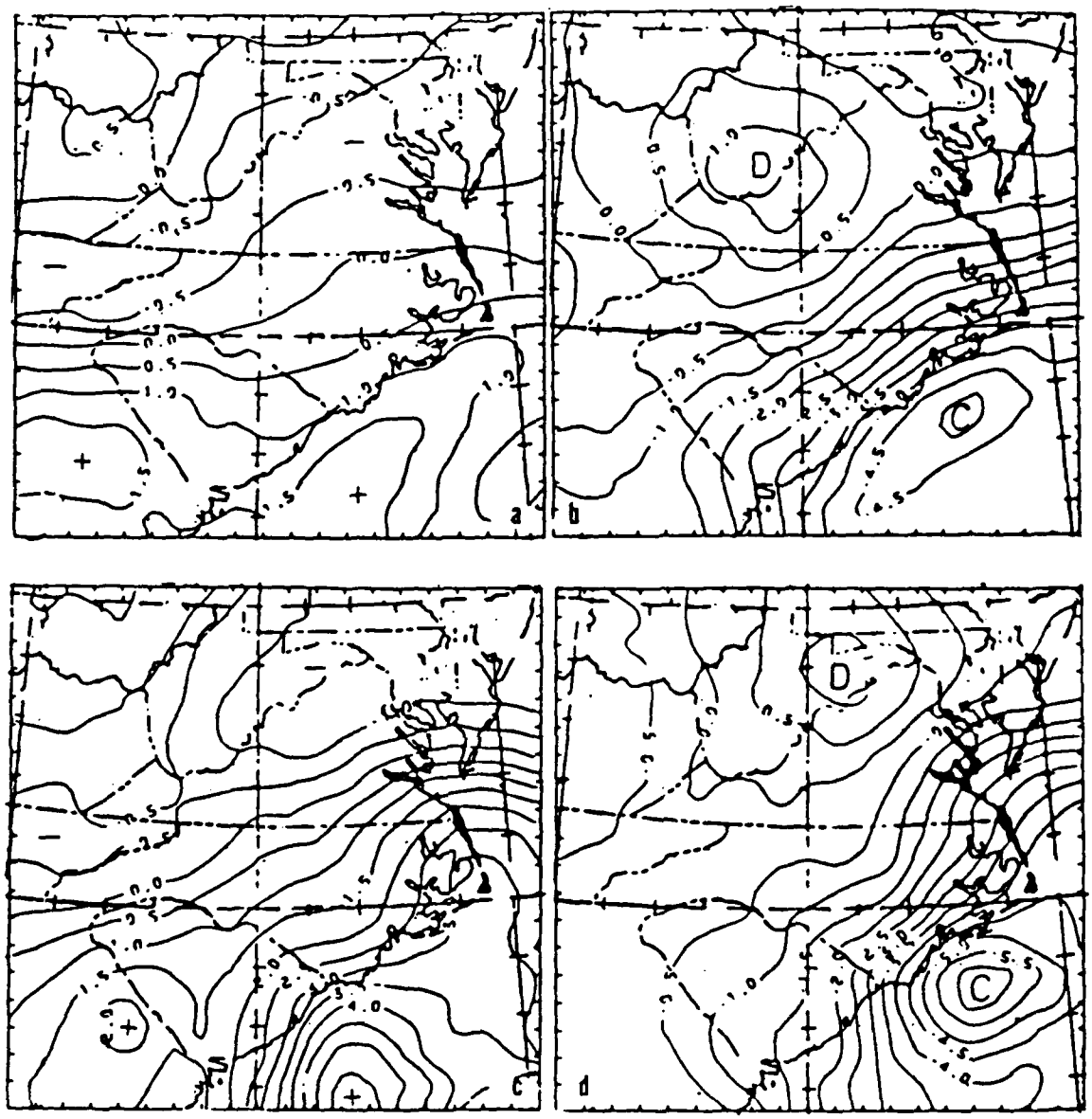


Fig. 3.2. a,b. Same as Fig. 3.1a,b except for 0000 GMT 11 February 1983. c,d. Same as Fig. 3.1c,d except for 0600 GMT 11 February 1983.

the light precipitation that develops early in Virginia. At 0600 GMT on the 11th, both the divergence and vorticity maximum are well ahead of the surface cyclone. The divergence (Fig. 3.2d) and vorticity (Fig. 3.2c) patterns continue to intensify to $-6.2 \times 10^{-5} s^{-1}$ and $5.6 \times 10^{-5} s^{-1}$, respectively, and have become less well-defined. The surface cyclone, which is deepening, has become much better associated with the vorticity center. A good correlation still exists between the precipitation and the convergence area just offshore.

A dramatic change in the divergence (Fig. 3.3b) and vorticity (Fig. 3.3a) is observed at 1200 GMT on the 11th. While continuing to intensify, the orientation of the divergence and vorticity pattern has become oriented nearly east-west across southern Virginia. This orientation change agrees remarkably well with the change in the significant precipitation pattern observed at 1200 GMT on the 11th.

## 3.2 Divergence and Vorticity Patterns Related to Precipitation.

Both the surface divergence and vorticity pattern agree well with the initiation of moderate precipitation in South Carolina and its subsequent movement north along the coast. Neither pattern shows good correlation with the lighter snowfall that develops early in interior Virginia, but both patterns do agree with the heavier precipitation which begins around 1200 GMT on the 11th through interior Virginia. The more the convective instability exhibited by the precipitation, the better is the correlation due to the more active participation by the surface flow field in the production of precipitation.

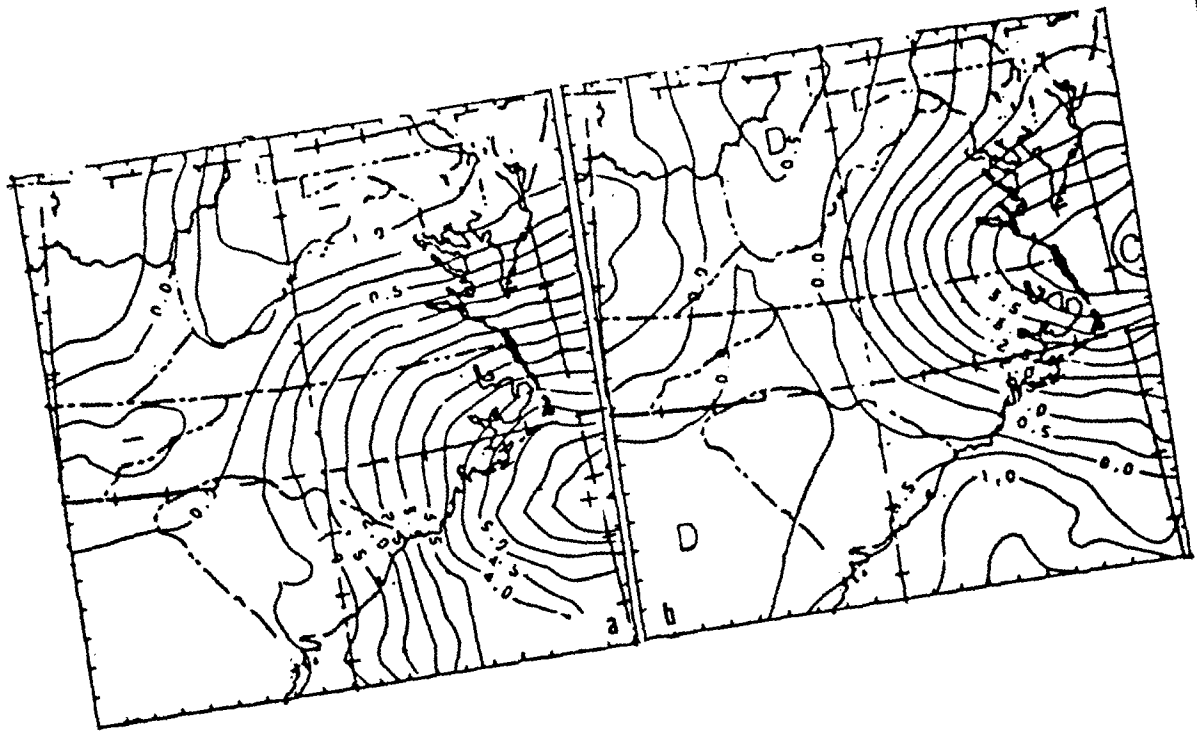


Fig. 3.3. a,b. Same as Fig. 3.1a,b except for 1200 GMT 11 February 1983.

The vorticity and divergence pattern initially correlate well, in both orientation and location, with the developing offshore warm (coastal) front well ahead of the surface cyclone. That is, low-level convergence is accompanied by cyclonic relative vorticity. Later in the period, after the cyclone has become better developed, the vorticity and divergence are more strongly correlated to the surface cyclone position. Vorticity, divergence, and surface baroclinity were all favorable for continued cyclone development off the southeast coast.

The significant precipitation which developed in the Carolinas clearly related to the surface warm front and its associated surface divergence and vorticity fields. This happened well ahead of the surface cyclone. One is led to believe that the warm (coastal) front initiated upslope flow on a potential temperature surface which is then coupled with the "Atlantic conveyor belt" orginating over the Atlantic ocean. The latter feature will be described shortly.

## 3.3 Offshore Divergence and Vorticity Values.

The vorticity and divergence fields are suspect in their patterns offshore, due to the weakeness in application of the Barnes analysis scheme described above. To test the previous results, the triangle method was employed to evaluate vorticity and divergence. The values were calculated hourly using the station triangles of Charleston, SC., with buoys 44003-44006 and Cape Hatteras, NC. with buoys 44002-44003. Assumptions involved in these calculations are (1) that reported winds are representative of the actual wind field; (2) there is a linear variation of

winds between observation points; and (3) the calculated values represent area averages.

The triangle method for divergence involves calculating the initial area of the triangle formed by the three observation points, then adding the appropriate vector representing the surface wind to the end points of the triangle and recomputing the area of the triangle once the vectors are added. The formula for divergence is:

$$\nabla\cdot\vec{V}=(1/A)\,\Delta A/\Delta t,$$

where A is the area of the original triangle, $\Delta A$ is the area difference between the original triangle and the triangle computed from adding the wind vectors to the end points, and $\Delta t$ is the time increment used. Vorticity calculated from this method, uses the following formula:

$$\nabla\cdot\vec{V}_{rot.} = \vec{V}\times\vec{V} = (1/A)\,\Delta A/\Delta t.$$

The terms are as before, but before the triangle is recomputed using the wind vectors; the wind vectors are rotated 90 degrees, making a cross-product instead of a dot-product.

Both Charleston-44003-44006 (Fig. 3.4a) and Hatteras-44002-44003 (Fig. 3.4b) show the same general pattern with the latter displaced later in time and more pronounced, as one would expect with a developing cyclone moving north along the coast.

Fig. 3.4a depicts the convergence area developing at 1800 GMT on the 10th, which agrees with the onset of precipitation in South Carolina; likewise Fig. 3.4b depicts an area of convergence that correlates well with precipitation as it moves northward. The time change of surface vorticity

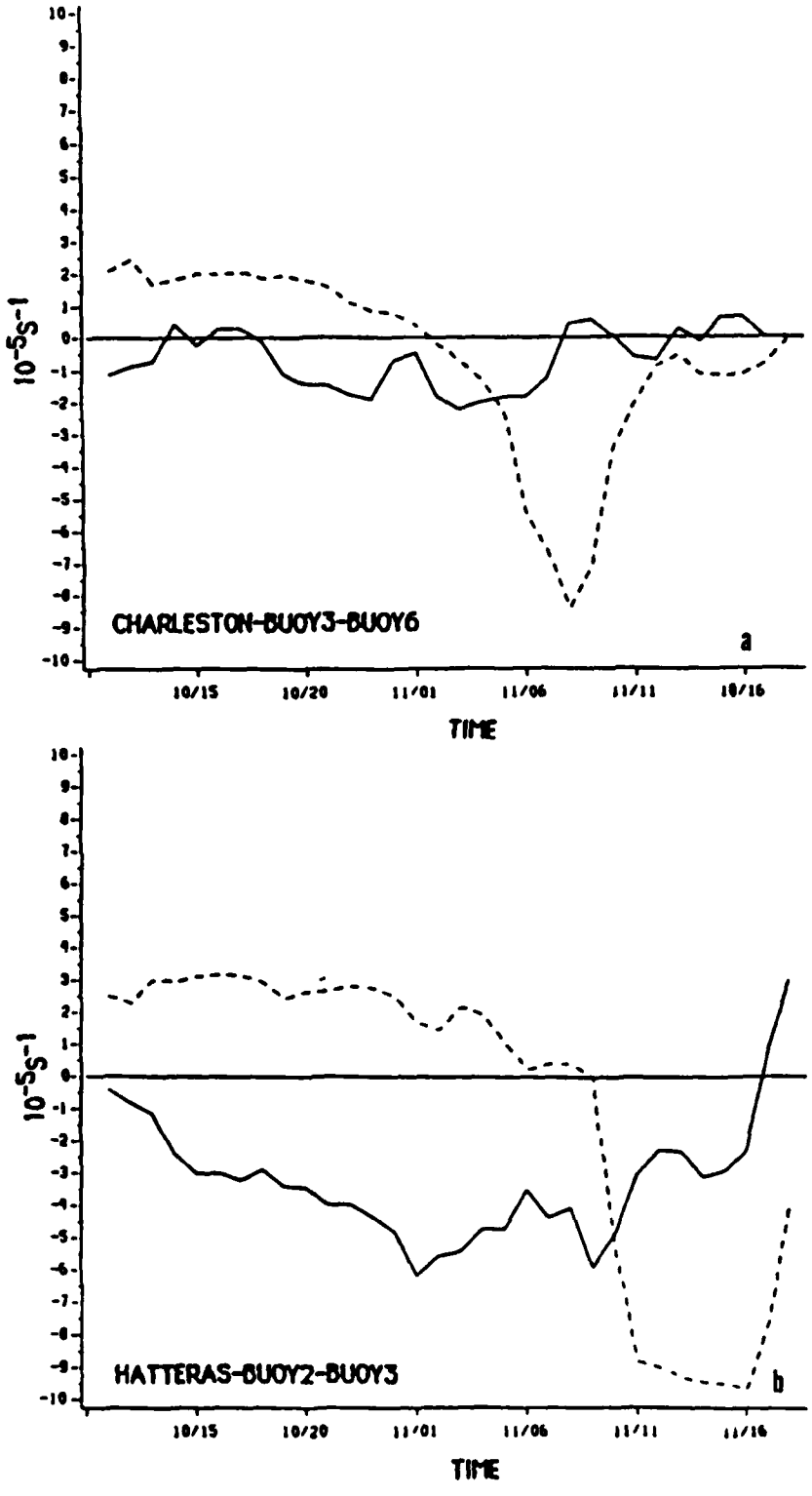


Fig. 3.4. a. Time plot of surface divergence (solid, $10^{-5}s^{-1}$) and surface relative vorticity (dashed, $10^{-5}s^{-1}$) for Charleston, S.C.-Buoy 3-Buoy 6 triangle. Times are GMT. b. Hatteras, N.C.-Buoy 2-Buoy 3 triangle.

at both locations is slightly positive but declining early in the period, and then becoming sharply negative at 0400 GMT on the 11th in the Charleston-44003-44006 triangle and 0900 GMT on the 11th in the Hatteras-44002-44003 triangle. This sequence agrees closely with the cessation of precipitation and the rapid clearing in both areas evident in satellite imagery.

The major discrepancy when comparing the triangle and kinematic computation methods is the failure of the kinematic method to reveal the rapid change to negative vorticity; although, this method does develop a strong gradient of decreasing positive vorticity. The author feels that the triangle method is more correct in this instance because of the better agreement with the cloud patterns and cyclone evolution over the near-shore waters.

## 3.4 Kinematic Vertical Motion

Researchers (e.g., Omoto, 1965) have found that significant precipitation develops in association with vertical motion fields not necessarily related to baroclinic zones. Omoto showed that precipitation develops where low-level vertical motion is strongest and moisture abundant. Two methods are used to derive vertical motion in the present study; the kinematic and adiabatic methods.

Kinematic vertical motion, obtained by vertically integrating the equation of continuity, is computed for 1200 GMT on the 10th, 0000 GMT on the 11th, and 1200 GMT on the 11th. Upper-air wind data over the eastern United States were gridded to a 10 x 8 grid centered at 35.5 N and 80 W. A

grid spacing of 150km was used to be consistent with a station spacing of 280km (Koch *et al.*,1980). Guidance from the study by Harms (1985) suggested a weight of 4600km$^2$ to be used in the Barnes scheme. Experiments based on this weight "smoothed" the data too much; the weight parameter then was reduced to 1000km$^2$. The latter value produces a wavelength pattern twice the grid size.

The integration of the continuity equation was accomplished by dividing the atmosphere into pressure layers. The first layer extended from the surface to 950mb in an attempt to account for vertical motion caused by the sloping terrain east of the Applachians. Above that 50mb layers were used from 950mb to 700mb, and beyond that were 100mb divisions to 200mb. Following accepted meteorological practice, the vertical velocity over flat terrain and at 200mb were considered to be zero.

The kinematic method of vertical motion computation requires accurate wind information if it is to be successful. It is well known that upper-level winds possess sufficient error to hinder meaningful results without application of a correction system. Therefore, kinematic vertical velocities were altered using the O'Brien (1970) correction scheme. In each layer a linear increase in wind measurement error with height is assumed.

The corrected and uncorrected profiles of kinematic vertical motion calculated at Greensboro, NC. are shown in Fig. 3.5. One can readily see that there is a large discrepency in the middle and upper levels, especially for the first two time periods. At 1200 GMT on the 10th (Fig. 3.5a) there is a reversal of sign near the expected level of non-divergence. Therefore values and patterns should be interpreted with care. In relating these calculations to the precipitation, the corrected kinematic vertical motion is used.

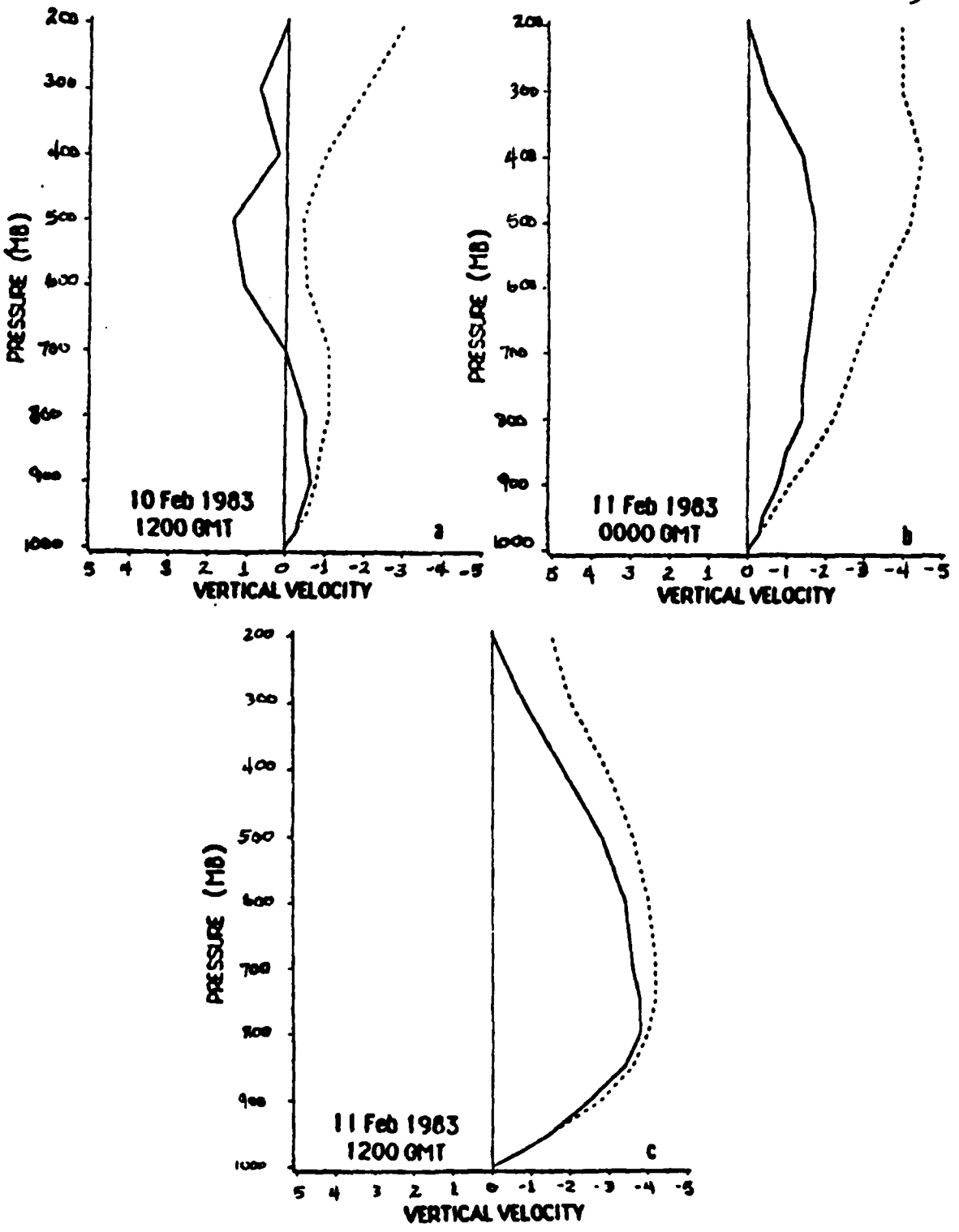


Fig. 3.5. Corrected (solid) and uncorrected (dashed) vertical motion ($10^{-3}$mbs$^{-1}$) at Greensboro, N.C. for date and time indicated.

## 3.5 Adiabatic Vertical Motion

Adiabatic vertical motion is based on the assumption that air experiences only dry adiabatic temperature changes; that is, potential temperature, $\theta$, is conserved. There are certain situations in which the adiabatic assumption is not valid. Close to the surface ,eddy heat conduction is significant. Radiative processes are another diabatic source (sink) of heat, but are relatively unimportant above the surface. Also, when air becomes saturated the release of latent heat causes a change in potential temperature. In this case, the wet-bulb potential temperature, $\theta_w$, or equivalent potential temperature, $\theta_e$, are conserved. Determining the air motion on $\theta_e$ surfaces is difficult, however, so that dry adiabatic motion will be accepted as providing reasonable estimates of the vertical velocity even in the areas of precipitation. Green *et al.* (1966) pointed out the adiabatic assumption is reasonably valid for most large-scale systems.

Adiabatic vertical motion is found by expanding:

$$d\theta/dt = \partial\theta/\partial t + \vec{V}\cdot\nabla_p\theta + \omega\partial\theta/\partial p.$$

where $\partial\theta/\partial t$ is the local tendency of 0, $\vec{V}\cdot\nabla_p\theta$ is the horizontal advection, $\partial\theta/\partial p$ is the stability, and $\omega$ the vertical velocity. By setting $d\theta/dt = 0$ by making the adiabatic assumption, the equation becomes:

$$\omega = (-\partial 0/\partial t - \vec{V}\cdot\nabla_p\theta)/(\partial\theta/\partial p).$$

The local tendency, $\partial\theta/\partial t$, was calculated using a $\Delta t$ of 24 hours. The stability was calculated using a pressure increment of 50mb. The advection

term was calculated in component form every 50mb; the u and v components are relative to each cross section orientation shown in Fig. 3.11. These u and v advective component fields were then plotted onto a map and graphically added. Values of the tendency adiabatic vertical motion were then calculated and added to the advective component of adiabatic vertical motion to obtain the total adiabatic vertical motion. The contribution of the former term to vertical velocity was generally between 10 and 30 percent of latter, the advective contribution.

## 3.6 Vertical Motion Related to Precipitation

Results of the adiabatic vertical motion calculations broadly agree with the kinematic vertical motion and correlates well with the observed significant precipitation. The adiabatic vertical motion at 850mb (Fig. 3.6b) for 1200 GMT on the 10th is generally comparable to the kinematic vertical motion (Fig. 3.6a). The adiabatic values seem somewhat larger and the pattern aligns better with the precipitation that develops by 1800 GMT on the 10th in South Carolina. One noticeable difference is the larger ascent indicated by the kinematic computations over Georgia. Satellite imagery show cloudiness in this region, but precipitation is scattered and very light at 1200 GMT on the 10th. For these reasons, the adiabatic vertical motion appears to be more correct.

Significant differences between adiabatic vertical motion (Fig. 3.6d) and kinematic vertical motion are evident at 700mb. The adiabatic vertical motion appears better related to precipitation, but neither pattern agrees particularly well. The descending motion across Georgia is suspect in the

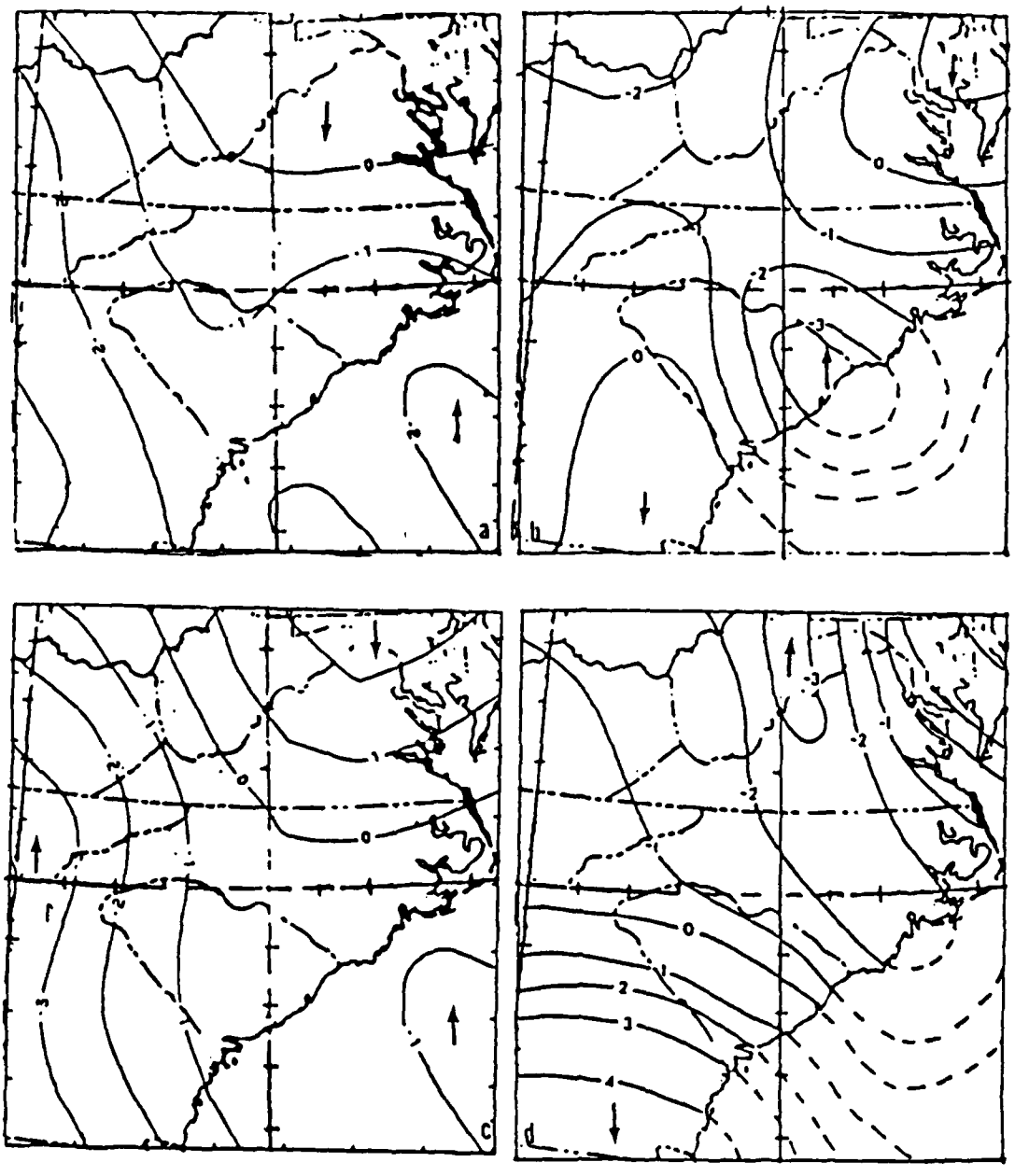


Fig. 3.6. a. 850mb kinematic vertical motion ($10^{-3}$mbS$^{-1}$) field b. 850mb adiabatic vertical motion ($10^{-3}$mbS$^{-1}$) field. Arrows give the sense of the vertical motion. 1200 GMT 10 February 1983. c. Same as a except for 700mb. d. same as c. except for 700mb.

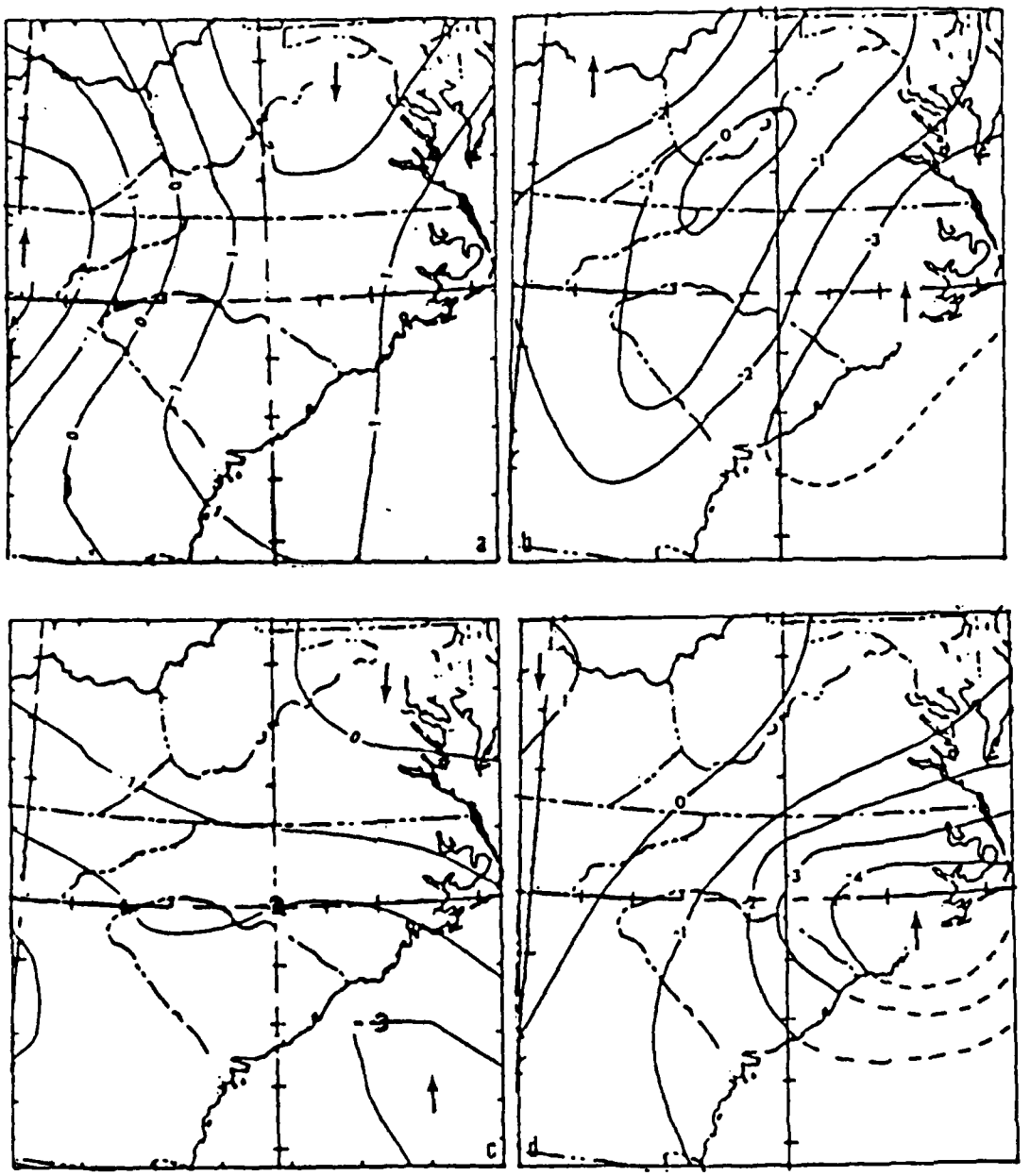


Fig. 3.7. a,b. same as Fig. 3.6a,b except for 500mb. c,d. same as 3.6c,d except for 850mb 0000 GMT 11 February 1983.

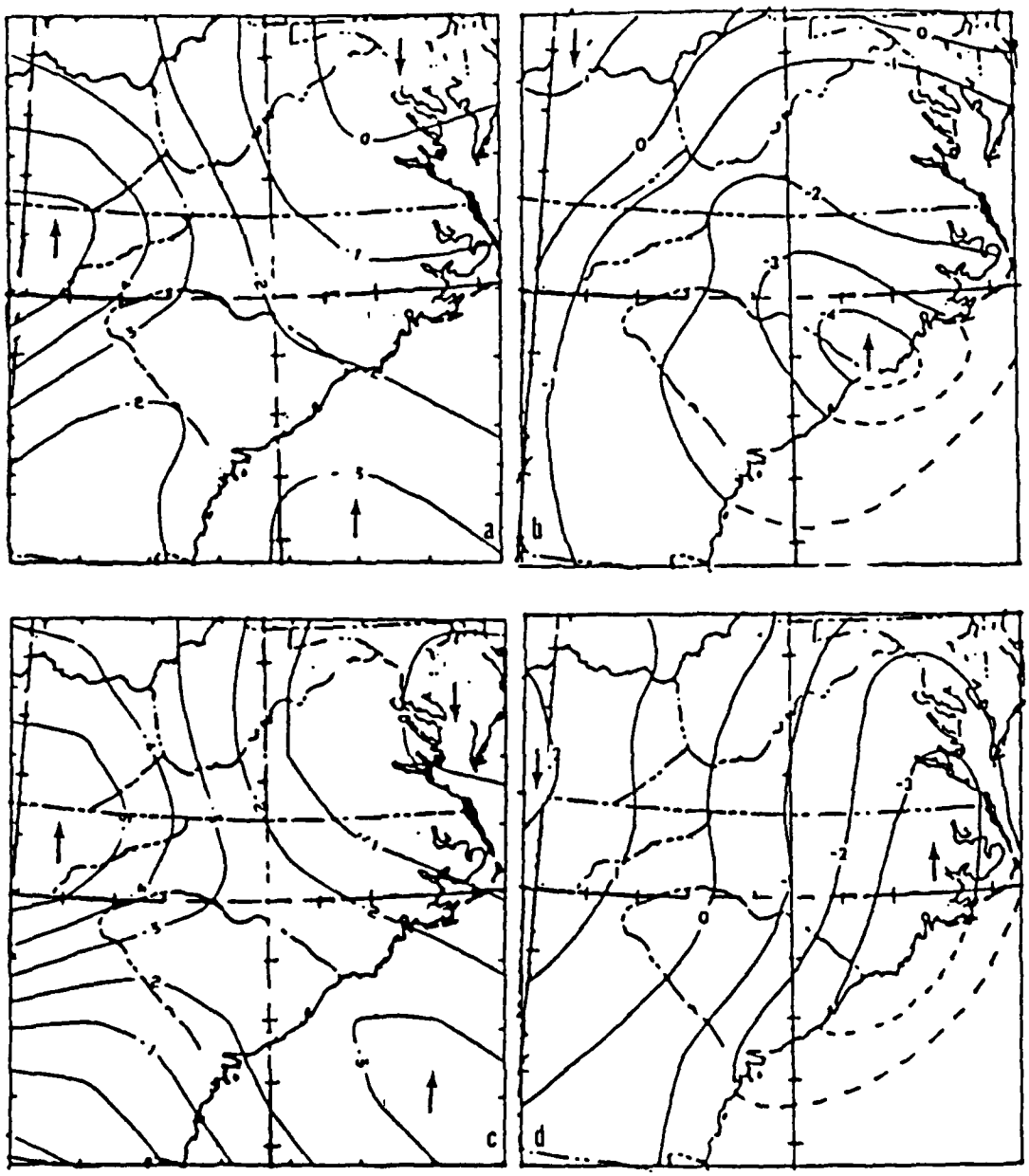


Fig. 3.8. a,b. Same as Fig. 3.6a,b except for 700mb 0000 GMT 11 February 1983. c,d. Same as Fig. 3.6c,d except for 500mb 0000 GMT 11 February 1983.

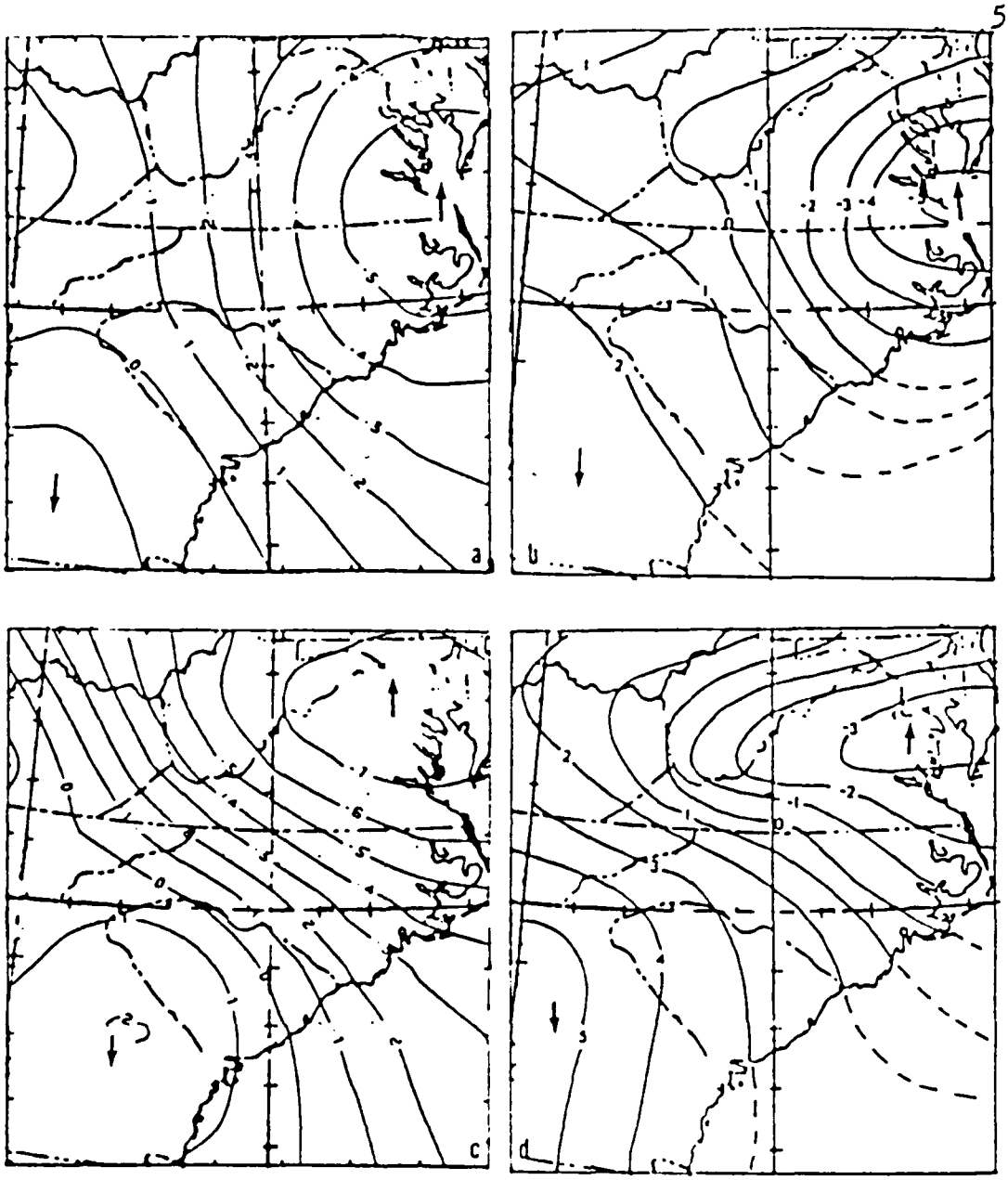


Fig. 3.9. a,b. Same as Fig. 3.6a,b except for 850mb 1200 GMT 11 February 1983. c,d. Same as Fig. 3.6c,d except for 700mb 1200 GMT 1200 11 February 1983

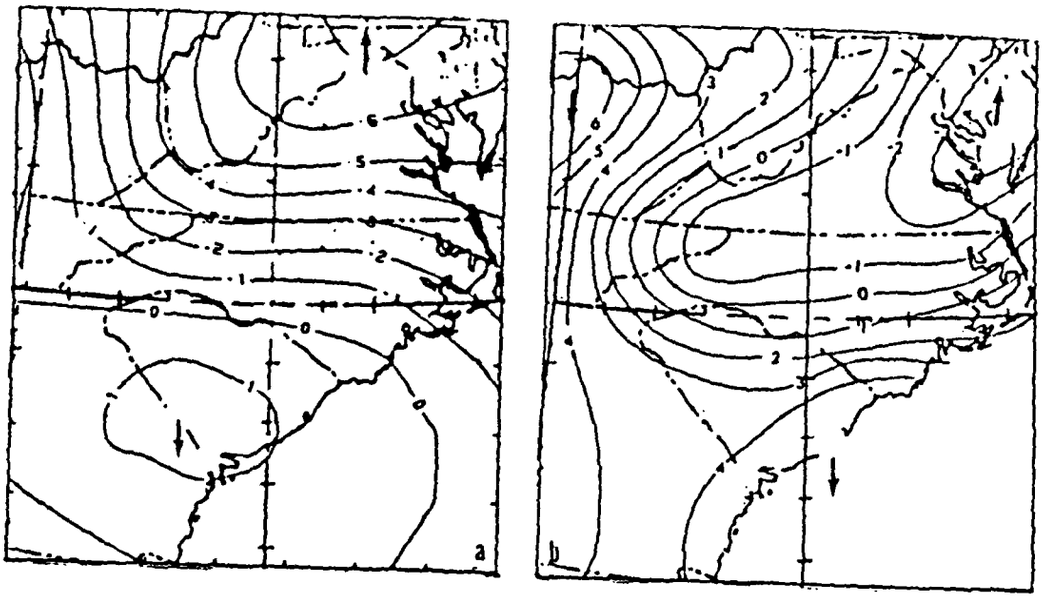


Fig. 3.10. a,b. Same as Fig. 3.6a,b except for 500mb 1200 GMT 11 February 1983.

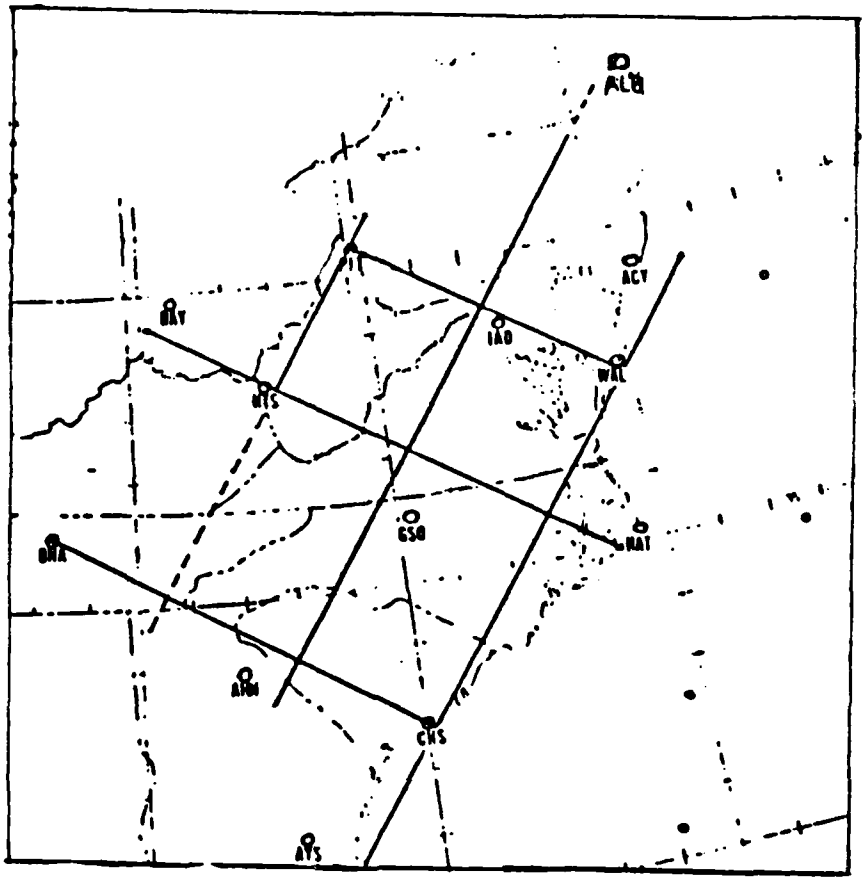


Fig. 3.11. Cross section grid used for adiabatic vertical motion calculations and isentropic analysis. Stations are Albany, NY. (ALB), Atlantic City, NJ. (ACY), Wallops Island, VA. (WAL), Washington (Dulles), DC. (IAD), Pittsburgh, PA. (PIT), Dayton, OH. (DAY), Huntington, WV. (HTS), Greensboro, NC. (GSO), Cape Hatteras, NC. (HAT), Nashville, TN. (BNA), Athens, GA. (AHN), Charleston, SC. (CHS), and Waycross, GA. (AYS).

face of increasing clouds, even though they are for the most part higher level clouds. At 500mb the adiabatic vertical motion (Fig. 3.7b) appears to be more acceptable as suggested by the better correlation with the precipitation that starts around 1800 GMT across South Carolina.

The adiabatic vertical motion pattern (Fig. 3.7d) for 850mb at 0000 GMT on the 11th agrees very well in orientation and magnitude with the kinematic vertical motion (Fig. 3.7c). Both agree remarkably well with the precipitation area that has developed across eastern South and North Carolina. The adiabatic vertical motion correlates better with the clearing occurring across Georgia. At 700mb (Fig. 3.8b), the adiabatic vertical motion pattern appears to be more reliable than the kinematic vertical motion pattern (Fig. 3.8a). The strong ascending motion across Tennessee in the kinematic field disagrees with the scattered, light precipitation that is falling there.

The adiabatic vertical motion pattern (Fig. 3.8d) at 500mb appears to slightly better aligned with the precipitation regions and much better in Georgia and South Carolina where descending motion coincides with clearing skies. The kinematic method (Fig. 3.8c) fails to depict the descending motion.

Excellent agreement in location and intensity between the adiabatic (Fig. 3.9b) and kinematic (Fig. 3.9a) vertical velocities is observed at 850mb at 1200 GMT on the 11th. Both depict a distinct east-west ascending motion axis across northern Virginia, with a rapid shift to descending motion to the south. The adiabatic vertical motion displays a stronger gradient and is believed to be the more valid based on satellite imagery and precipitation analysis. This excellent agreement between adiabatic (Fig. 3.9d) and

kinematic (Fig. 3.9c) vertical motion fields continues at 700mb. Both display a more definite east-west axis of enhanced vertical motion which agrees with the significant precipitation. The adiabatic vertical motion field once again better depicts the strong gradient to descending motion. The kinematic vertical motion (Fig. 3.10a) seems slightly better than the adiabatic vertical motion (Fig. 3.10b) at 500mb in relation to the significant precipitation, although the adiabatic vertical motion better depicts the ascending motion causing the clearing skies across South Carolina and Georgia.

## 3.7 Precipitation Rate Calculation

A more objective comparison between the adiabatic and kinematic vertical motion profiles is now made. Precipitation calculations based on the two vertical velocities (Fig. 3.12) are made for 0000 GMT and 1200 GMT on the 11th at Greensboro, NC. and 1200 GMT on the 11th at Washington, D.C. The results will be a 2-hour precipitation total centered at the appropriate time. These will be compared to the actual precipitation reported.

Methods of forecasting large-scale precipitation from large-scale vertical motion fields have been reasonably successful. Fulks (1935) developed a method of calculating hourly precipitation from moist adiabatically ascending air. He was able to construct a table of precipitation rate versus vertical velocity value. Estoque (1957) used the 500mb height tendency forecast to derive a parabolic vertical motion profile to forecast the large-scale precipitation. Smebye (1958) employed the vorticity equation and first law of thermodynamics to construct a model

to account for precipitation. He established large-scale vertical motion similar to Estoque by indirectly obtaining vertical motion through 500mb height changes.

Precipitation rate in the present study will employ vertical motion profiles obtained from the two methods illustrated in the preceding figure. The equation used to calculate the amount of precipitation is:

$$P = \omega(\Delta p/g)(\partial r_s/\partial p)$$

Here P is the amount of precipitation, $\omega$ is the vertical motion, p is the pressure, and g is gravity.

Results of the calculations are given in Table 3. below:

Table 3. Observed precipitation versus calculated precipitation over a two-hour period based on the kinematic and adiabatic vertical motion profiles.

| Precipitation(mm) | GSO (00Z/11) | GSO (12Z/11) | IAD (12Z/11) |
|---|---|---|---|
| Actual | 1.78 | 2.29 | 3.56 |
| Kinematic profile | 0.68 | 1.72 | 2.82 |
| Adiabatic profile | 0.73 | 0.55 | 1.27 |

This test proved inconclusive for determining which is the better method to compute vertical motion. The test did, however, point out that when using the adiabatic method, effects of saturation must be accounted for. The systematic underestimation of precipitation when using the adiabatic vertical motion profiles is a least partly due to the assumption of

non-condensing, rather than condensing, adiabatic motion. Future studies using GALE data should incorporate equivalent potential temperature analysis where the air is saturated.

Better agreement between the amount of precipitation calculated and observed was achieved with the kinematic vertical motion profile. The underestimation of actual rates in this case is likely due to actual measurements being compared to vertical velocities representative of an area 300Km$^2$ surrounding the station. Both profiles found that approximately 75 percent of the total precipitation was produced between 850mb and 550mb.

Fig. 3.12 shows that even though the adiabatic vertical motion is smaller overall than the kinematic vertical motion, the former does seem to show more detail in the vertical motion profile than does the kinematic. These details appear related to important vertical structure in the moisture transport. This will be discussed shortly.

## 3.8 Isentropic Analysis

Isentropic analysis has been used, most commonly by the British researchers (eg. Green *et al.*, 1966; Browning and Pardoe, 1973; Atkinson and Smithson, 1978; Browning, 1983) to describe the large-scale three-dimensional flow of air in the vicinity of cyclones. This analysis enables the three-dimensional tracking of air provided that: (1) the motion of air is adiabatic and (2) the system is basically steady-state for the period it takes air to travel through it (Green *et al.*, 1966). "Conveyor belts", as these authors have called them, transport great amounts of

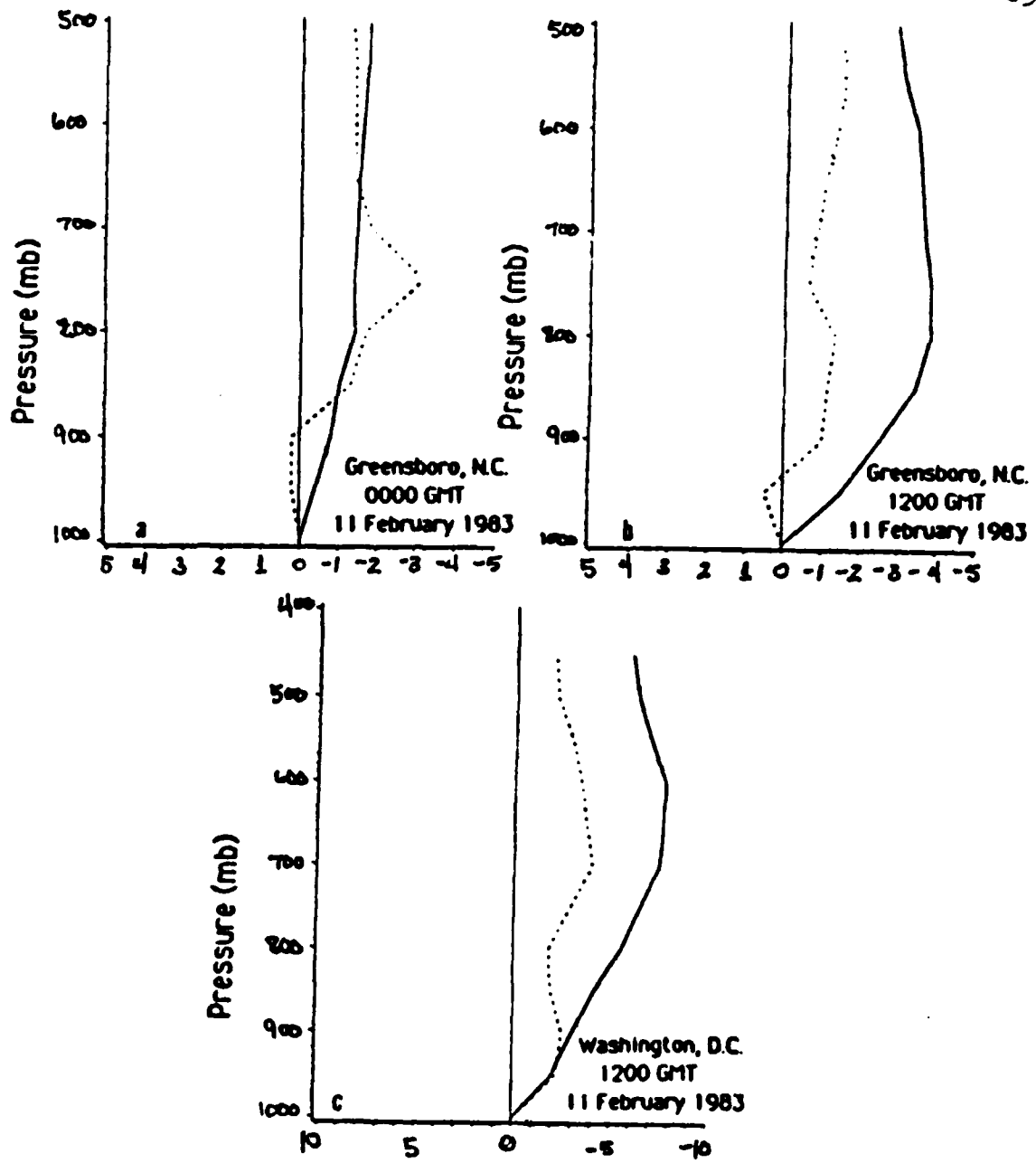


Fig. 3.12. Comparsion of kinematic (solid) and adiabatic (dashed) vertical motion ($10^{-3}$mb$^{s-1}$) profiles for location, time, and date indicated.

moisture. Water vapor mixing ratio analysis will be useful in depicting the structure and evolution of these features.

Isentropic were completed for 1200 GMT on the 10th, 0000 GMT and 1200 GMT on the 11th. Additionally, cross sections were constructed along the lines shown in Fig. 3.11 . Through the careful analysis of mixing ratio and winds in the upper air, two conveyor belts were identified. One conveyor belt liess nearly along the $\theta$=286 K surface and the other along the $\theta$=295 K surface.

Flow on these two $\theta$-surfaces for the three periods are shown in Fig. 3.13 to Fig 3.15, and appear similar to the model described by Carlson (1980) and depicted in Fig. 3.16. His model would label the flow from the Gulf as the "warm conveyor belt", and the lower-level flow from the Atlantic ocean; the "cold conveyor belt". Browning (1971) alludes to the cold conveyor belt as responsible for the re-distribution of moisture falling from the warm conveyor belt.

The model by Carlson is an idealized depiction of a midwestern cyclone in which the warm conveyor belt is dominant. Differences between his model and this case study are due to the unique geographical influence of the mid-Atlantic coast on the weather, that is, cold air damming. These differences can be made clearer by labeling the conveyor belts according to the origin. The warm conveyor belt in Carlson's model will be labeled the "Gulf conveyor belt" and the cold conveyor belt; the "Atlantic conveyor belt". Additionally, the cold wedge flow evident in this case study is not found in Carlson's model. This cold wedge flow appears to be more analogous to the cold conveyor belt in Carlson's model because the Atlantic conveyor belt is very warm. The conveyor belts with this case study may be dynamically

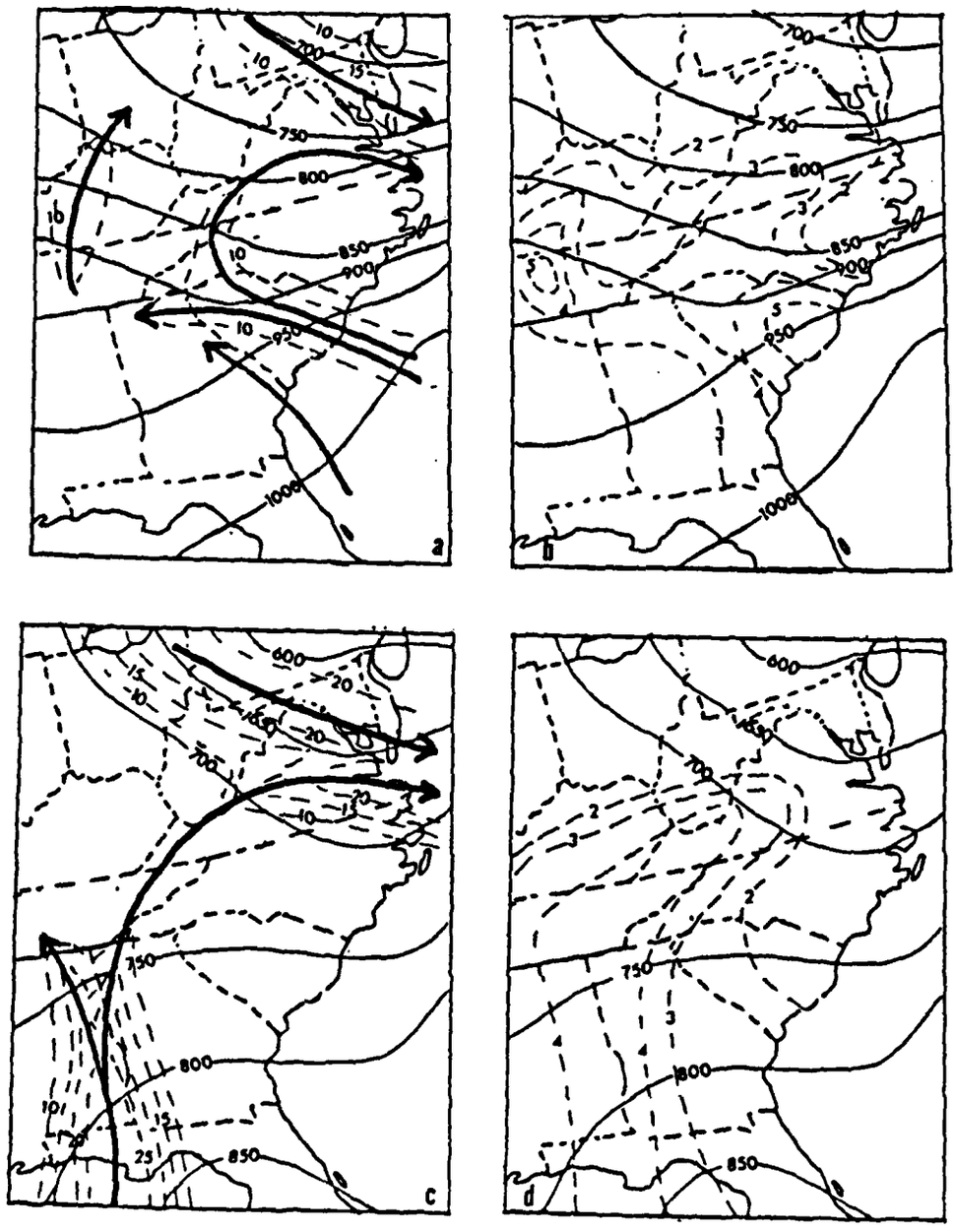


Fig. 3.13. a. Streamlines (heavy solid arrows) and isotachs (dashed,ms-1) plotted along pressure (solid, mb) for θ=286 K. b. mixing ratio (dashed, g/kg) and pressure (solid,mb) for θ=286 K. 1200 GMT 10 February 1983. c. Same as a except for θ=295 K. d. Same as c except for θ=295 K.

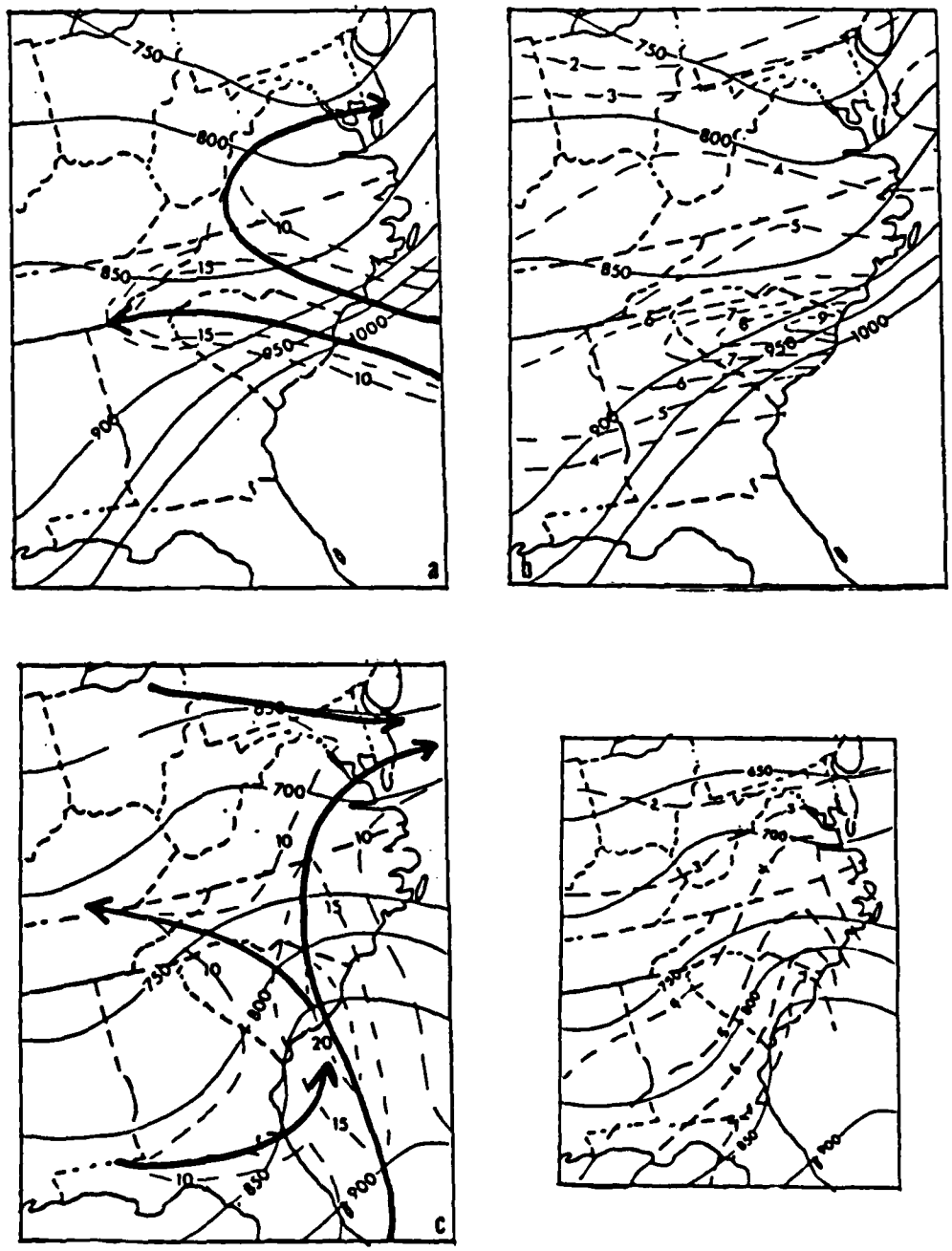


Fig. 3.14a,b,c,d. Same as Fig. 3.13a,b,c,d. except for 0000 GMT 11 February 1983.

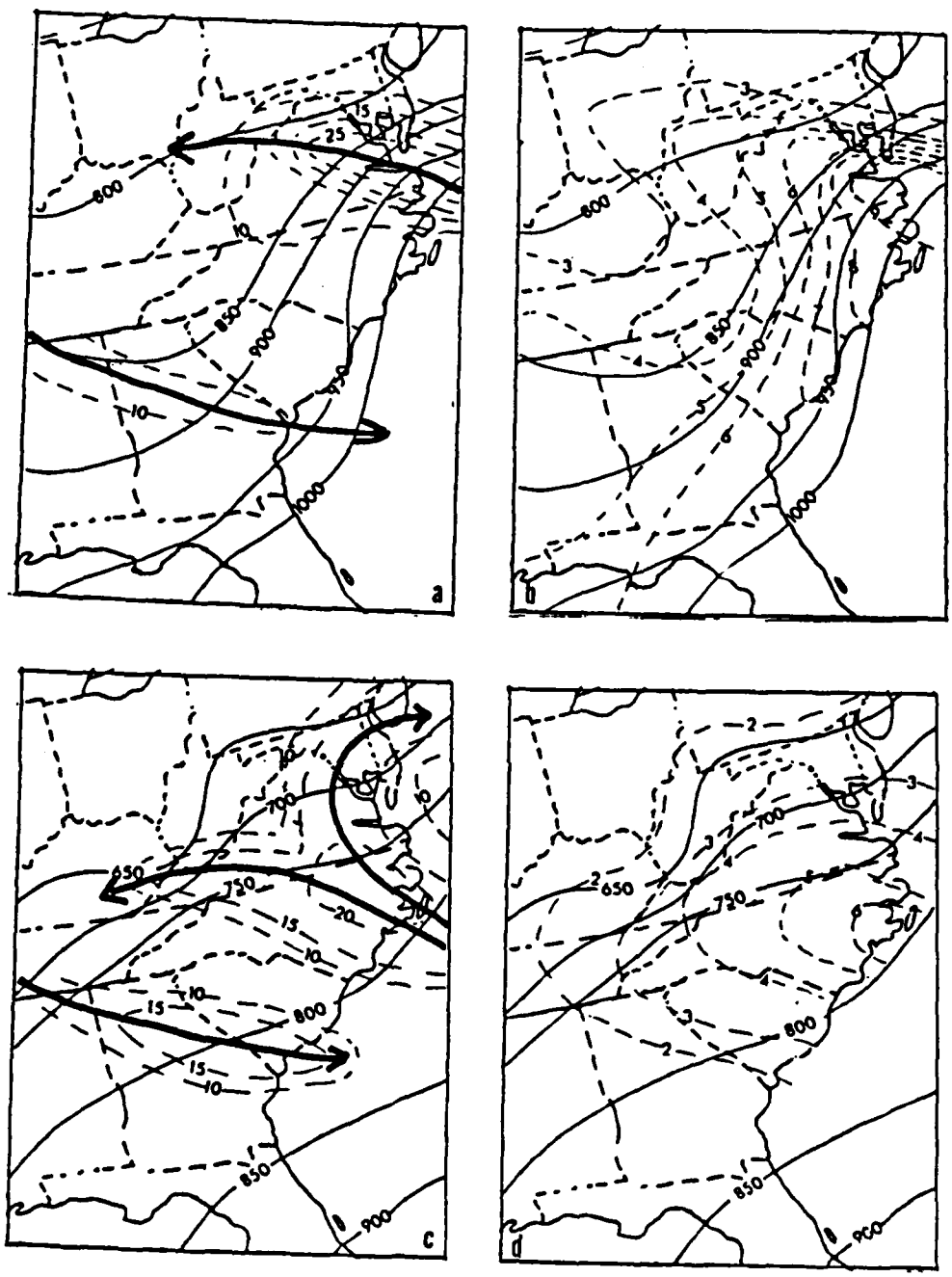


Fig. 3.15a,b,c,d. Same as Fig. 3.13a,b,c,d. except for 1200 GMT 11 February 1983.

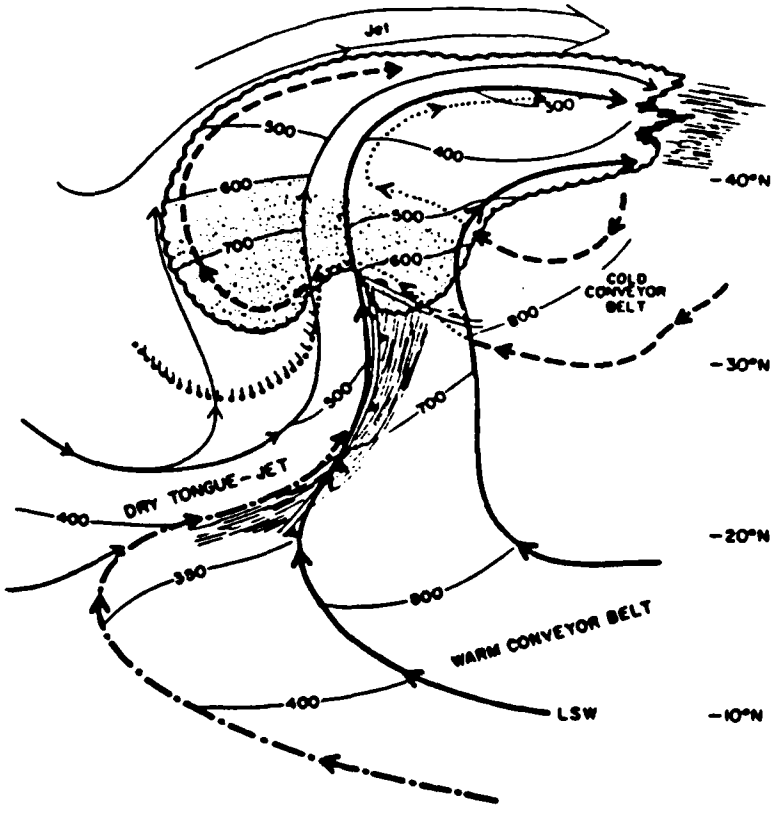


AIRFLOW THROUGH MID-LATITUDE WAVE CYCLONE

Fig. 3.16. Schematic composite of airflow through middle-latitude cyclone by Carlson (1980). Streamlines (heavy solid streamlines) depict airflow at top of the warm conveyor belt. Dashed flow represents cold conveyor belt (drawn dotted when it lies beneath the warm conveyor or dry air stream). Dot-dashed flow represents air originating at upper levels west of the trough. Thin solid lines denote the heights of the airstreams (mb) and are approximately normal to the direction of the respecitve air motion; (isobars are omitted for the cold conveyor belt where it lies beneath warm conveyor or beneath the jet stream flow). The region of dense upper-and middle-level layer cloud is represented by scalloping and sustained precipitation by stippling. Streaks denote thin cirrus. The edge of the low-level stratus is shown by the curved border of small dots with tails. The major upper tropospheric jet streams are labeled JET. The limiting streamline for the warm conveyor belt is labeled LSW.

different than those found in Carlson's model.

Figs. 3.13a,b depict a moderate easterly flow on the θ=286 K near the surface at Charleston, SC. lifting to 910mb over Athens, GA. This flow then curves northward and ascends to approximately 830mb before exiting to the east across North Carolina at a higher altitude (θ=295 K). Figs. 3.13c,d depict a southerly flow of moist, warm air from the tropics along the Alabama-Georgia border. Satellite imagery depicts a distinct cloud band associated with this flow, which is well ahead of the surface cold front.

Cross section analysis of mixing ratio (Fig. 3.17a) along the line BNA-AHN-CHS at 1200 GMT on the 10th depicts a mixing ratio maximum aligned with the Atlantic conveyor belt at CHS which slopes up over the cold air. The mixing ratio isopleths are more steeply sloped than the potential temperature surface, indicating that the air is saturated, therefore following an equivalent potential surface temperature. Another maximum, just west of AHN at approximately 700mb is in good agreement with the position of the Gulf conveyor belt that can be pictured as flowing into the page.

By 0000 GMT on the 11th, the Gulf conveyor belt has moved eastward to a position just west of HAT as indicated by the mixing ratio analysis for the cross section DAY-HTS-GSO-HAT (Fig.3.17b). This agrees with the position indicated by satellite imagery. The Atlantic conveyor belt axis has moved northward and increased its moisture content. Notice the rapid lifting of the Atlantic conveyor belt over the cold air centered over GSO and the apparent penetration to HTS.

The rapid lifting of the Atlantic conveyor belt over the cold air is releasing its potential instability depicted by the vertical profile of

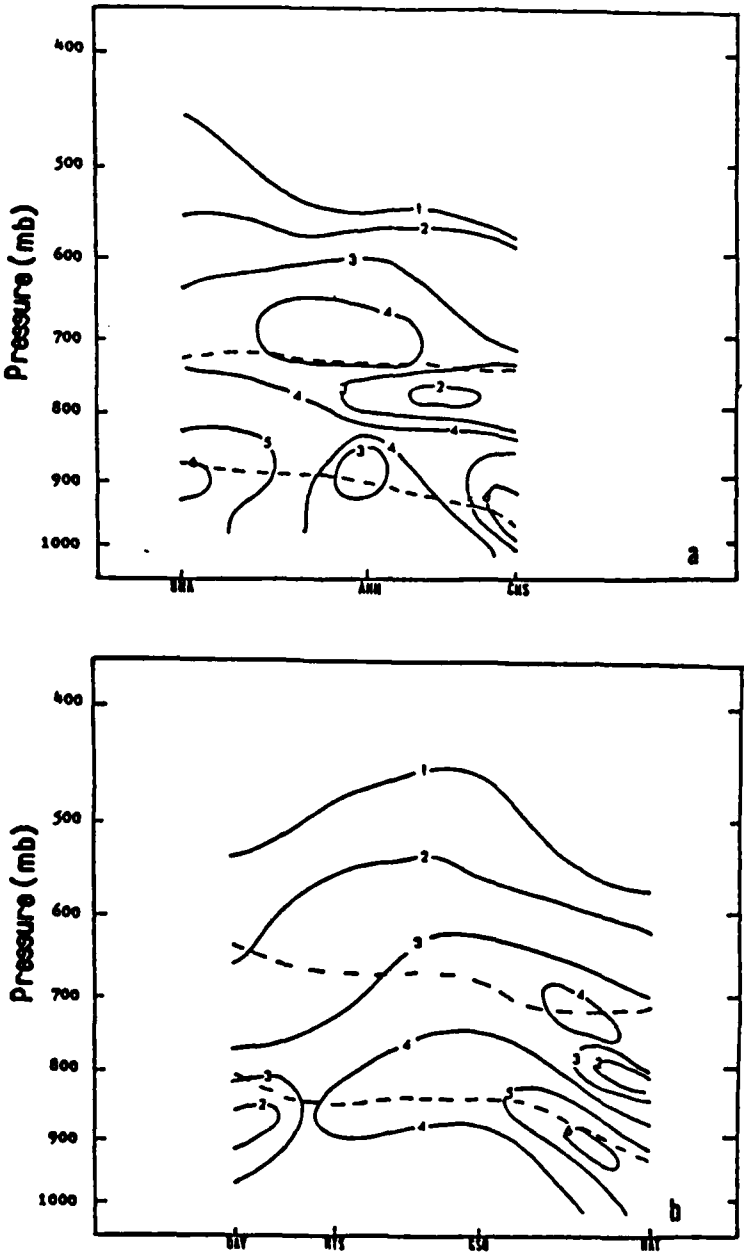


Fig. 3.17. a. Cross section of mixing ratio (solid, g/kg) and potential temperature (dashed, degrees kelvin) for BNA-AHN-CHS. Lower potential temperature is θ=286 K, Upper potential temperature is θ=295 K. 1200 GMT 10 February 1983. b. Same as a except for DAY-HTS-GSO-HAT 0000 GMT 11 February 1983.

potential and equivalent potential temperature at HAT (Fig. 3.18) This release of potential instability by large scale synoptic forcing is the cause of the observed mesoscale structure of the precipitation reported by Harrold (1973). The much stronger lift experienced by the Atlantic conveyor belt is due to cold air damming, and it seems to be more responsible for the production of precipitation than in Carlson's model of a mid-west cyclone. Some evidence of this is seen by the agreement between the axis of the Atlantic conveyor belt and the precipitation that developed near 1800 GMT over South Carolina. Interpolation of the location of the Gulf and Atlantic conveyor belts to 1800 GMT on the 10th (Fig. 3.20) suggests that the precipitation in South Carolina developed when the two conveyor belts became vertically stacked over South Carolina. This indicates that the Gulf conveyor belt still has important role in the production of precipitation.

At 1200 GMT on the 11th, the Gulf conveyor belt (Figs. 3.15a,b) has become oriented southeast-northwest across northern North Carolina and Virginia directly above the Atlantic conveyor belt (Figs 3.15c,d). Cross sections DAY-HTS-GSO-HAT (Fig. 3.19a) and PIT-IAD-WAL (Fig. 3.19b) depict the more steeply sloping Atlantic conveyor belt. The potential instability associated with the Atlantic and Gulf conveyor belts (see Fig. 3.19) results in mixing between the two conveyor belts so that they are now nearly indistinguishable in the mixing ratio analysis. The axis of heavier precipitation across Virginia quickly adjusts to the orientation of the conveyor belts which indicates their importance in the production of precipitation.

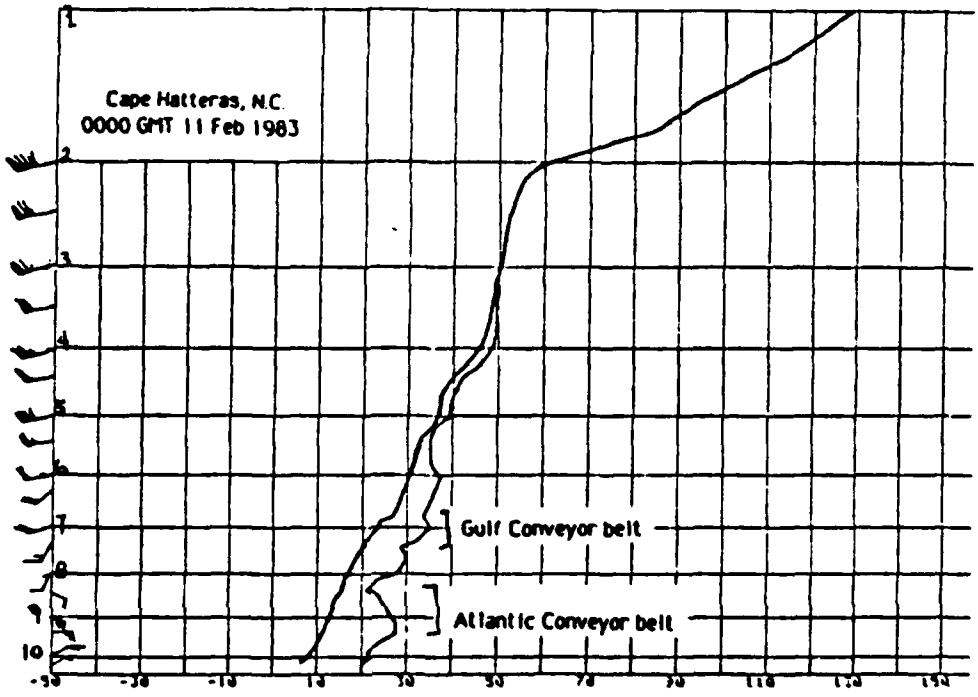


Fig. 3.18. Potential temperature and equivalent potential temperature profile for Cape Hatteras, North Carolina, 0000 GMT 11 February 1983. Abscissa is labelled degrees K minus 300 degrees. Ordinate is labelled in hundreds of millibars. Wind speed is plotted in $ms^{-1}$ with a full barb representing $5ms^{-1}$ and a half-barb representing $2.5ms^{-1}$. A flag represents $25ms^{-1}$. Wind direction is plotted as usual.

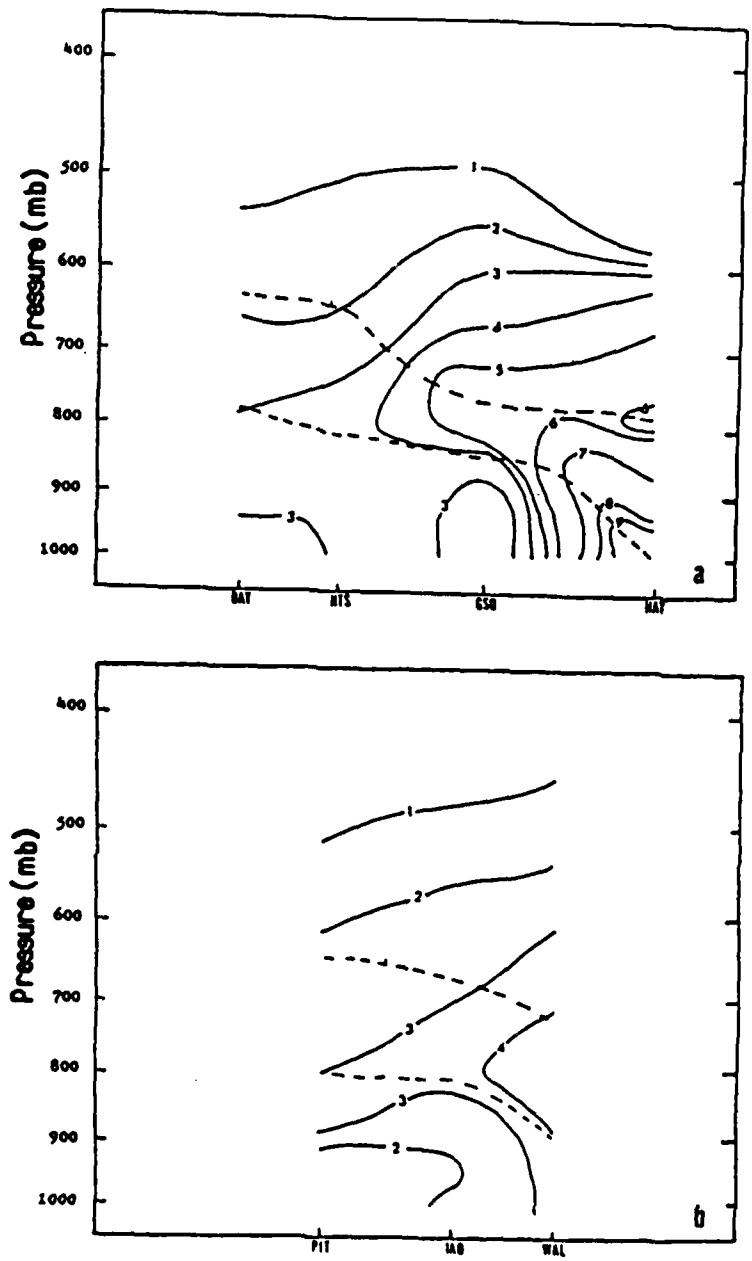


Fig. 3.19. a. Same as 3.17a except for DAY-HTS-GSO-HAT 1200 GMT 11 February 1983. b. Same as 3.17b except for PIT-IAD-WAL 1200 GMT 11 February 1983.

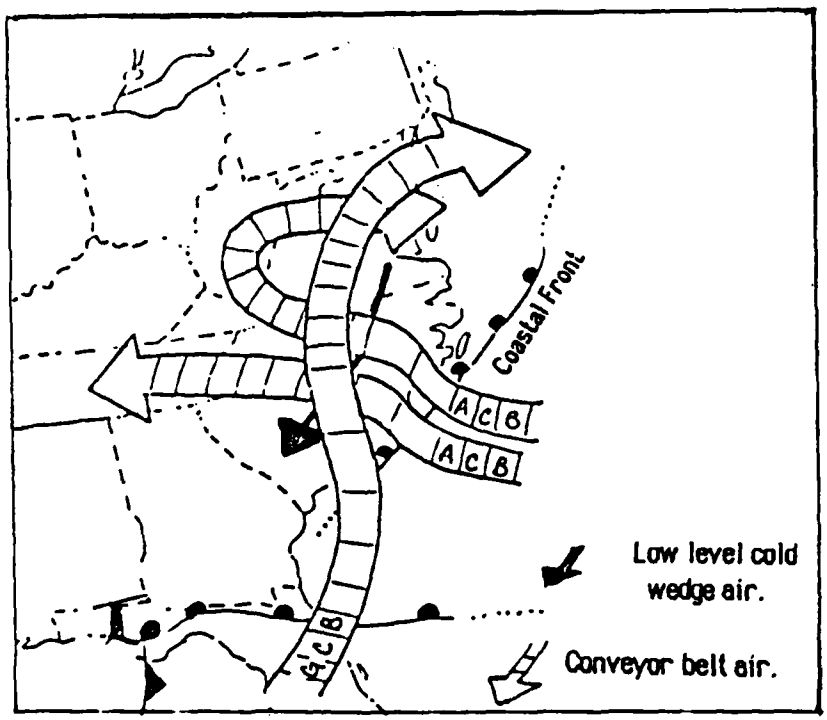


Fig. 3.20. Schematic of the Gulf Conveyor belt (GCB) and the Atlantic conveyor belt (ACB) at the time precipitation developed over South Carolina. Arrow indicates direction of air flow. Spacing of lines inside the arrows attempts to convey relative lift in the vertical as the air ascends the cold wedge. Frontal systems have usual meaning.

## 3.9 East Coast Cyclone Conveyor Belt Model

Fig. 3.20 depicts an idealized model of the conveyor belts at the time thatthe preciptation developed over South Carolina, approximatley 1800 GMT on the 10th. The conveyor belts have become vertically stacked over South Carolina; the Atlantic conveyor belt lies beneath the Gulf conveyor belt, allowing the seeder-feeder process to develop. A shallow surface layer of northeast flow maintains the cold wedge across central Virginia and North Carolina.

The cold wedge forces a substantial lift of the moist, warm conveyor belt air. This releases the potential instability associated with the Atlantic conveyor belt, which orginates in the boundary layer over the Gulf Stream. This upper-level instability is verified by the showery type of the precipitation reported along the coast. Additionally, evaporative cooling of the air just above the Atlantic conveyor belt by precipitation falling from the Gulf conveyor belt can also aid in the release of the potential instability.

# 4. MIXED PRECIPITATION AT GREENSBORO, NORTH CAROLINA

## 4.1 Introduction

As discussed in Section 2.3 and shown in Appendix A, a band of mixed rain, snow, sleet, and freezing rain precipitation 60-100km wide has developed across the northern portion of North Carolina, and remained nearly stationary for much of the time that precipitation fell across this region. Mesoscale analysis is employed to fine relationships of the precipitation type to atmospheric structure readily identifiable by the synoptic forecaster. In the previous chapters isentropic surface and cross-section analyses focused on the warm air overriding the cold dome associated with cold-air damming and entrenched across central North Carolina and Virginia to the east of the Appalachians. The precipitation developed principally in the conveyor belt which rose from the boundary-layer off the mid-Atlantic coast to several thousand meters altitude over Virginia. The zone of mixed precipitation defined the area where the precipitation developing aloft in this conveyor belt fell through the shallow cold air wedge before reaching the ground.

## 4.2 Detailed Description of Precipitation

Because of its optimal location in the mixed precipitation zone the Greensboro, NC. (GSO) radiosonde station will be used to focus on the atmospheric structure associated with the mixed precipitation. Very light

snow began at GSO just before 1200 GMT on the 10th, mixed briefly with ice pellets, and ended at 1500 GMT on the 10th. There was no accumulation on the ground and .25 mm of water equivalent was measured.

More significant precipitation, began as a light rainshower at approximately 2030 GMT, and after passing through a brief transistion of type changed to all snow by 2140 GMT. A combination of snow or snow and ice pellets continued until 0300 GMT on the 11th at which time 1 inch of snow and 48 mm of liquid equivalent precipitation were reported. The temperature was 37 F when precipitation began and had fallen to 31 F. At approximately, 0330 GMT on the 11th, the precipitation changed from light snow to freezing rain which continued until approximately 0600 GMT on the 11th before again mixing with snow. This precipitation then changed to ice pellets and light snow, occasionally mixed with freezing rain. This continued until approximately 1530 GMT on the 11th, when the precipitation diminshed considerably and changed over to light snow before ending approximately 1900 GMT on the 11th.

Total snowfall was 3.1 inches with a maximum snow depth of 3 inches. During this period, 22.6 mm of liquid equivalent fell, and thus snow depth to liquid equivalent of just over 3.3 to one. An interesting point is that even as the temperature fell from 37 F to 25 F at 1500 GMT on the 11th, precipitation for the most part remained a mixture. After 1530 GMT, when the precipitation noticeably lightened and became all snow, the surface temperature was actually rising.

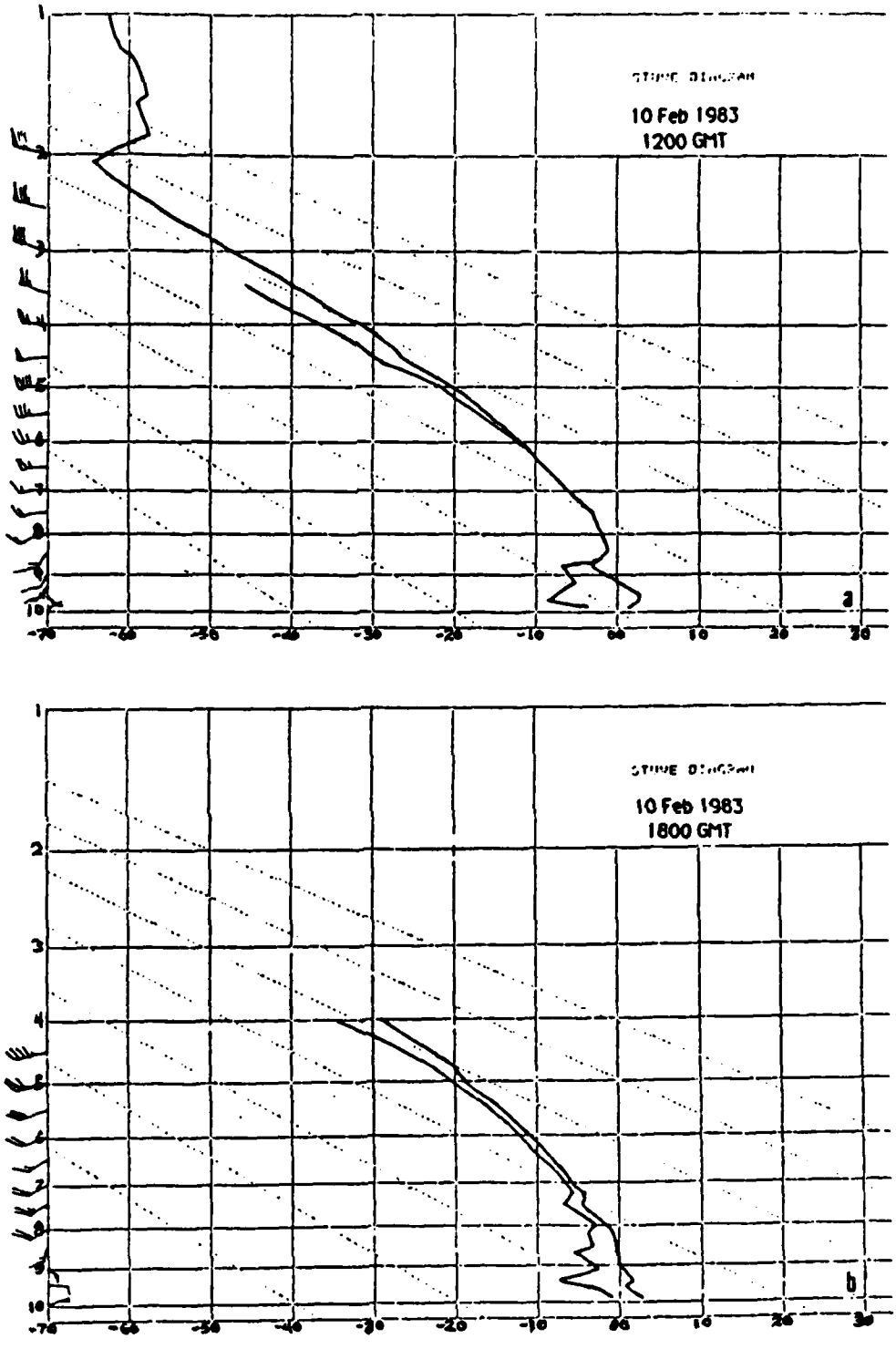


Fig. 4.1a,b. Profile of temperature and dewpoint on a Stuve diagram for date and time indicated. Wind barbs are plotted every 50mb with a full barb representing 5 $ms^{-1}$ and a half barb representing 2.5 $ms^{-1}$. Wind direction is in conventional notation.

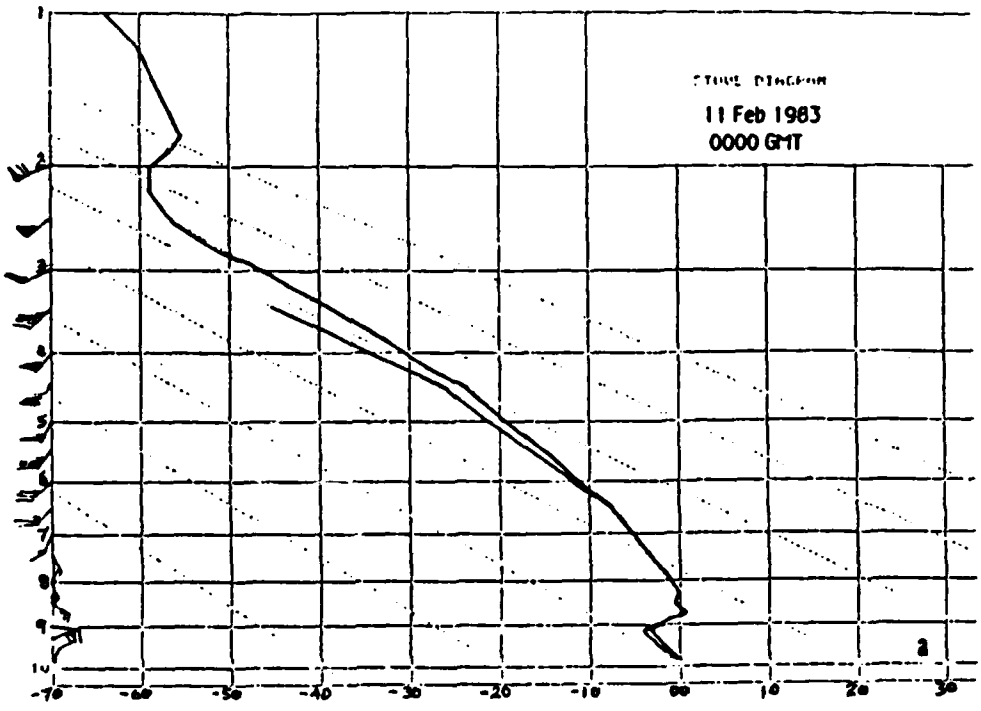


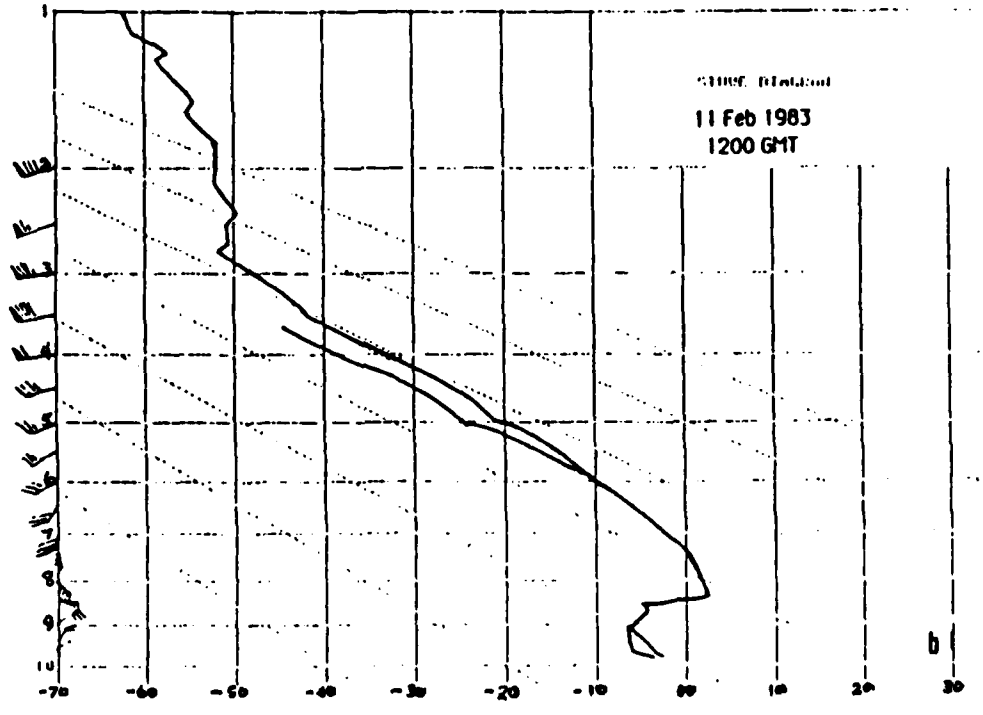


Fig. 4.2a,b. Same as Fig. 4.1a,b. except for date and time indicated.

## 4.3 Upper Air Analysis

Preesure-layer depth in meters for 1800 GMT on the 10th, 0000 GMT on the 11th, and 1200 GMT on the 11th are given below:

Table 3. Thickness in meters for isobaric layers at times indicated and total layer change.

| LAYER | 1800 GMT/10 | 0000 GMT/11 | 1200 GMT/11 | Net Change |
|---|---|---|---|---|
| 1000-500mb | 5425 | 5419 | 5435 | +10 |
| 1000-700mb | 2846 | 2839 | 2842 | -4 |
| 1000-850mb | 1306 | 1295 | 1281 | -25 |

Significant cooling occurred in the 1000-850mb layer through the precipitation period as indicated by the decreasing thickness. This is an indication that pool of cold air associated with the cold-air damming remained intact. Further evidence for this is shown by continued northeast winds and falling surface temperatures through the daylight hours while significant precipitation was falling. The continued cooling in the lowest layers probably prevented the precipitation from becoming freeing rain or rain after 0000 GMT on the 11th even though warming occurred in the 1000-700mb and 1000-500mb layers. This is evidence of the northward moving warm air overriding the surface cold wedge.

The upper-air soundings for GSO for 1200 GMT on the 10th to 1200 GMT on the 11th are shown in Figs. 4.1 to 4.2. The special sounding at the intermediate time (1800 GMT) was taken because of the threat of mixed

precipitation. Fig. 4.1a shows that at 1200 GMT on the 10th, the layer below approximately 860mb is relatively dry, but nearly saturated above. The production of precipitation aloft is at temperatures below freezing, which is consistent with the light snow observed at GSO at 1200 GMT on the 10th, even though surface temperatures are slightly above freezing. Fig. 4.1b shows that by 1800 GMT on the 11th some moistening has occurred from the surface to 860mb, and southeast winds of 15kn have developed around 900mb, which may be indicating the intrusion of the Atlantic conveyor belt. Fig. 4.2a shows significant cooling from the surface to around 900mb and significant warming from there to 750mb. A layer of air has warmed to above freezing around 870mb, while the surface has cooled to freezing. The most significant warming coincided with the strongest southeast winds with speed now approaching 25kn. The upper air structure is now becoming favorable for freezing rain. The 0000 GMT observation on the 11th indicated ice pellets, light snow, and fog.

Over the next twelve hours, dramatic cooling occurred from the surface to 850mb and dramatic warming from 850 to 600mb (Fig. 4.2b). The temperature at 900mb cooled 4 C, while at 750mb the temperature warmed 3.5 C. Again, strongest warming coincided with the strongest southeast winds of the Atlantic conveyor belt. The dramatic cooling was probably due to a combination of evaporational cooling, diurnal cooling, and advection of colder air from the northeast at the surface. The 1200 GMT observation on the 11th indicates 25 F with ice pellets and light snow.

As the precipitation, even with warming temperatures at the surface, turned to all snow at GSO after 1530 GMT, the strong south-southeast winds

aloft associated with the warm conveyor belt have most likely begun to decrease. The associated warm air advection subsided over GSO as the conveyor belt air and other ingredients necessary for mixed precipitation shifted to the east. The 0000 GMT sounding on the 12th (not shown) indicates no distinct warm wedge of air aloft and no south-southeast winds.

Points to be made from this discussion are:

(1) The earlier snow changed to mixed precipitation even as surface temperatures dropped, because of the arrival of warm Atlantic conveyor belt air just above the cold-wedge air.

(2) It is thus important for forecasters to identify, and if possible to track the Atlantic conveyor belt.

(3) Cold-air damming in the lowest layers can maintain surface temperatures below freezing even as the Atlantic conveyor belt brings significant warming above. This vertical coincidence of air masses is ideal for the production of mixed precipitation.

# 5. Summary and Conclusions

Analyses of hourly precipitation associated with a developing east coast cyclone have revealed a complex pattern of structure and evolution. Precipitation was found to develop several hundred kilometers in advance of the surface cyclone even while it weakened as it moved eastward along the Gulf coast. This is significant to the weather forecaster concerned with the association of precipitation to the observable flow field.

Surface vorticity and divergence fields related well to the coastal front and cold-air damming, both of which are commonly associated with east coast cyclogenesis. In the early stages of precipitation development the surface kinematic fields had little of the expected relationship suggesting that the ascent and moisture are primarily aloft. Areas of heavier rainfall which form as the cyclone moves northeastward along the Atlantic coast, are related to the surface flow field. Conditions near the surface were found to respond to the precipitation rather than participing in the production of precipitation, due to the low-level stability associated with the cold-air damming.

Two vertical motion fields, calculated by the kinematic and adiabatic methods, agreed well with the position of the heavier precipitation; the adiabatic vertical motion was in somewhat better agreement. As expected there was a systematic underestimation of the adiabatic vertical motion strength in regions of precipitating clouds where latent heat release would enhance ascent.

Isentropic analyses led to the identification of two conveyor belts related to similar flow features in a midwest cyclone model. However,

there are significant differences between the midwest model and the east coast cyclone of interest here. These differences arise from the different geographical settings. A model for conveyor belt structure associated with east coast cyclones was suggested. In this model, "the cold conveyor belt" is relabeled the "Atlantic conveyor belt" and the "warm conveyor belt" is relabeled the "Gulf conveyor belt". The low-level cold wedge flow east to the Appalachians was found to reinforce the cold wedge and function as the cold conveyor belt in Carlson's model. The Atlantic conveyor belt was found to be much stronger in this setting. The Gulf Stream provided more heat and moisture which increased the potential instability associated with the Atlantic conveyor belt. This potential instability was then released when the Atlantic conveyor belt moved inland and encountered the surface cold-wedge which forced the conveyor belt air aloft. The role these conveyor belts play in the evolution of precipitation is the most important result of the present research.

The analysis of the mixed precipitation which occurred at Greensboro, North Carolina revealed that the forecaster interested in anticipating this troublesome weather must identify the presence of cold-air damming and the Atlantic conveyor belt aloft. It was shown that snow changed to mixed precipitation, even in the face of falling surface temperatures, due to the combined presence of these two air masses.

Further studies of precipitation with east coast cyclones (as the GALE project) should analyze the formation and strength of the Atlantic conveyor belt through the use of statistics. Additionally, the question of what dynamical processes produce the conveyor belts should be addressed. A plausible hypothesis, supported by observations from this study, suggests

that the conveyor belts develop as part of the transverse circulation associated with the upper-level jet stream, although it is not clear from this study which develops first. Uccellini (1980) expounds on the dynamics between the upper-level jet streaks and the development of low-level jets.

## References

Atkinson, B.W., and P.A. Smithson, 1978: Mesoscale precipitation areas in a warm frontal wave. *Mon. Wea. Rev.*, **106**, 211-222.

Austin, P.M., and R.A. Houze, 1972: Analysis of the structure of precipitation patterns in New England. *J. Appl. Meteor.*, **11**, 926-935.

Beregeron,T., 1949: The problem of artificial control of rainfall on the globe. The coastal orographic maxima of precipitation in autumn and winter. *Tellus*, **1**, 15-32.

Bjerknes, J., 1919: On the structure of moving cyclones. *Geofys. Publ.*, Norske Videnskaps-Acad. Oslo, **1**, No. 1, 1-8.

Bosart, L.F., 1973: Detailed analyses of precipitation patterns associated with mesoscale features accompanying United States east coast cyclogenesis. *Mon. Wea. Rev.*, **101**, 1-12.

_____, 1975: New England coastal frontogenesis. *Quart. J. Roy. Meteor. Soc.*, **101**, 957-978.

Browning, K.A., and T.W. Harrold, 1969: Air motion and precipitation growth in a wave depression. *Quart J. Roy. Meteor. Soc.*, **95**, 288-309.

_____, and _____, 1970: Air motion and precipitation growth at a cold front. *Quart. J. Roy. Meteor. Soc.*, **96**, 369-389.

_____, 1971: Radar measurements of air motion near fronts. *Weather*, **26**, 320-340.

_____, and C.W. Pardoe, 1973: Structure of low-level jet streams ahead of mid-latitude cold fronts. *Quart. J. Roy. Meteor. Soc.*, **99**, 619-638.

_____, 1974: Mesoscale structure of rain systems in the British Isles. *J. Meteor. Soc. Japan*, **52**, 314-327.

_____, 1983: Air motion and precipitation growth in a major snowstorm. *Quart. J. Roy. Meteor. Soc.*, **109**, 225-242.

AD-A166 375 ON THE EVOLUTION OF PRECIPITATION ASSOCIATED WITH A WINTERTIME EAST COATT (U) AIR FORCE INST OF TECH WRIGHT-PATTERSON AFB OH R D BIEVINS 1985 2/2

UNCLASSIFIED AFIT/CI/NR-86-17T F/G 4/2 NL

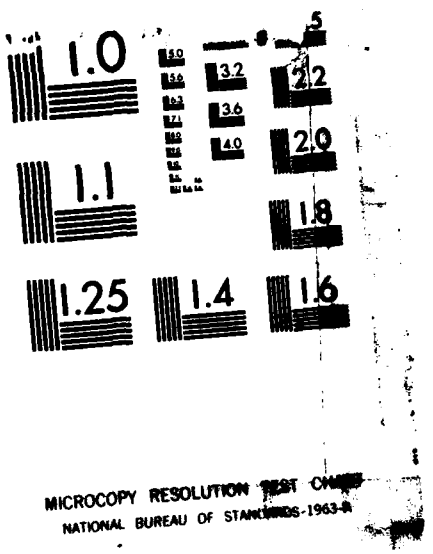
1.0
1.1
1.25
1.4
1.6
2.2
2.0
1.8
3.2
3.6
4.0
MICROCOPY RESOLUTION TEST CHART
NATIONAL BUREAU OF STANDARDS-1963-A

Bjerknes, J., and H. Solberg, 1921: Meteorological conditions for the formation of rain. *Geofys. Publ.*, Norske Videnskaps-Acad., Oslo, 2(3), 1-60.

_____, and _____, 1922: Life cycle of cyclones and the polar front theory of atmospheric circulation. *Geofys. Publ.*, Norske Videnskaps-Acad, Oslo, 3(1), 1-18.

Carlson, T.N., 1980: Airflow through midlatitude cyclones and the comma cloud pattern. *Mon. Wea. Rev.*, **108**, 1498-1509.

Charba, J.P., and W.H. Klein, 1980: Skill in precipitation forecasting in the National Weather Service. *Bull. Amer. Meteor. Soc.*, **61**, 1546-1555.

Colucci, S.J., 1976: Winter cyclone frequencies over the eastern Untied States and adjacent western Atlantic, 1964-1973. *Bull. Amer. Meteor. Soc.*, **57**, 548-553.

Elliot, R.D., and E.L. Hovind, 1964: On convection bands within Pacific coast storms and their relation to storm structure. *J. Appl. Meteor.*, **3**, 143-154.

_____, and _____, 1965: Heat, water, and vorticity balance in frontal zones. *J. Appl. Meteor.*, **4**, 196-211.

Estoque, M.A., 1957: An approach to quantitative precipitation forecasting. *J. Meteor.*, **14**, 50-54.

Fitzroy, R., 1863: *The weather book, A manual of practical meteorology.* London

Fulks, J.R., 1935: Rate of precipitation from adiabatically ascending air. *Mon. Wea. Rev.*, **63**, 291-293.

Green, J.A., F.H. Ludlam, and J.R. McIlveen, 1966: Isentropic relative-flow analysis and the parcel theory. *Quart. J. Roy. Meteor. Soc.*, **92**, 210-219.

Harms, D.E., 1985: Applications of an objective analysis scheme to mesoscale observation network design. Masters Thesis, North Carolina State Univ.- Raleigh, 91pp.

Harrold, T.W.,1973: Mechanisms influencing the distribution of precipitation with baroclinic disturbances. *Quart. J. Roy. Meteor. Soc*, **99**, 232-251.

Herzegh, P.H., and P.V. Hobbs, 1980: The mesoscale and microscale structure and organization of clouds and precipitation in midlatitude cyclones. II: Warm-frontal clouds. *J. Atmos. Sci.*, **37**, 597-611.

_____, and _____, 1981: The mesoscale and microscale structure and organization of clouds and precipitation in midlatitude cyclones. IV: Vertical air motions and microphysical structures of prefrontal surge clouds and cold-frontal clouds. *J. Atmos. Sci.*, **38**, 1771-1784.

Hobbs, P.V., and R.A. Houze, T.J. Matejka, 1975: The dynamical and microphysical structure of an occluded front and its modification by orography. *J. Atmos. Sci.*, **32**, 1542-1562.

_____, 1978: Organization and structure of clouds and precipitation on the mesoscale and microscale in cyclonic storms. *Rev. Geophys. Space. Phys.*, **16**, 741-755.

_____, T.J. Matejka, P.H. Herzegh, J.D. Locatelli, and R.A. Houze, 1980: The mesoscale and microscale structure and organization of clouds and precipitation in midlatitude cyclones. I: A case study of a cold front. *J. Atmos. Sci.*, **37**, 568-596.

Holtzman, B., 1936: Synoptic determination and forecasting significance of cold fronts aloft. *Mon. Wea. Rev.*, **64**, 400-414.

Houghton, H.G., 1968: On precipitation mechanisms and their artifical modifications. *J. Appl. Meteor.*, **7**, 851-859.

Houze, R.A., 1981: Structure of atmospheric precipitation systems: A global survey. *Radio Sci.*, **16**, 671-689.

_____, S.A. Rutledge, T.J. Matejka, and P.V. Hobbs, 1981: The mesoscale structure and organization of clouds and precipitation in midlatitude cyclones. III: Air motions and precipitation growth in a warm-frontal rainband. *J. Atmos. Sci.*, **38**, 639-648.

Koch, S.E., M. des Jardins, and P.J. Kocin, 1981: The gempack barnes analysis scheme. *NASA Technical Memorandum* 83851, NASA/GLAS, Greenbelt, MD. 20771, 56pp.

Kreitzburg, C.W., 1968: The mesoscale wind field in an occlusion. *J. Appl. Meteor.*, **7**, 53-67.

_____, and H.A. Brown, 1970: Mesoscale weather systems within an occlusion. *J. Appl. Meteor.*, **9**, 417-432.

Lichitblau, S., 1936: Upper air cold front in North America. *Mon. Wea. Rev.*, **64**, 414-425.

Marks, F.D., and P.M. Austin, 1979: Effects of the New England coastal front on the distribution of precipitation. *Mon. Wea. Rev.*, **107**, 53-67.

Miller, J.E., 1946: Cyclogenesis in the Atlantic coast region of the United States. *J. Meteor.*, **3**, 31-44.

_____, 1955: Intensification of precipitation by differential advection. *J. Meteor.*, **12**, 472-477.

Nagle, R.E., and S.M. Serebreny, 1962: Radar precipitation echo and satellite observations of a maritime cyclone. *J. Appl. Meteor.*, **1**, 279-295.

Nozumi, Y., and H. Arakawa, 1968: Prefrontal rainbands located in the warm sector of subtropical cyclones over the ocean. *J. Geophys. Rev.*, **73**, 487-492.

O'Brien, J.J., 1970: Alternative solutions to the classical vertical velocity problem. *J. Appl. Meteor.*, **9**, 197-203.

Omoto, Y., 1965: On prefrontal precipitation zones in the United States. *J. Meteor. Soc. Japan*, **43**, 310-330.

Palmen, E., and C.W. Newton, 1969: *Atmospheric circulation systems. Their structure and physical interpretations.* Academic Press, New York.

Parsons, D.B., and P.V. Hobbs, 1983: The mesoscale and microscale structure and organization of clouds and precipitation in midlatitude cyclones. VII: Formation, development, interaction, and dissipation of rainbands. *J. Atmos. Sci.*, **40**, 559-579.

Petterssen, S., D.L. Bradbury, E.P. McClain, Y. Omoto, G.V. Rao, E.R. Ternes, and G.F. Watson, 1963: An investigation of the structure of cloud and weather systems associated with cyclones in the United States. Final Rept. , AF 19(604)-7230, Article H. Dept. Geophys. Sci., Univ. Chicago.

Reitan, C.H., 1974: Frequencies of cyclones and cyclogenesis for North America, 1951-1970. *Mon. Wea. Rev.*, **102**, 861-868.

Sawyer, J.S., 1952: A study of the rainfall of two synoptic situations. *Quart. J. Roy. Meteor. Soc.*, **78**, 231-246.

Shaw, W.N., 1911: *Forecasting Weather*, 3rd ed. Constable, London.

Smebye, S.J., 1958: Computation of precipitation from large-scale vertical motion. *J. Meteor.*, **15**, 547-560.

Uccellini, L.W., 1980: On the role of upper tropospheric jet streaks and leeside cyclogenesis in the developement of low-level jets in the Great Plains. *Mon. wea. Rev.*, **108**, 1689-1696.

Widger, W.K., 1964: A synthesis of interpretation of extratropical vortex patterns as seen by TIROS. *Mon. wea. Rev.*, **92**, 263-282.

# Appendix A

Hourly objective precipitation type and amount analysis.

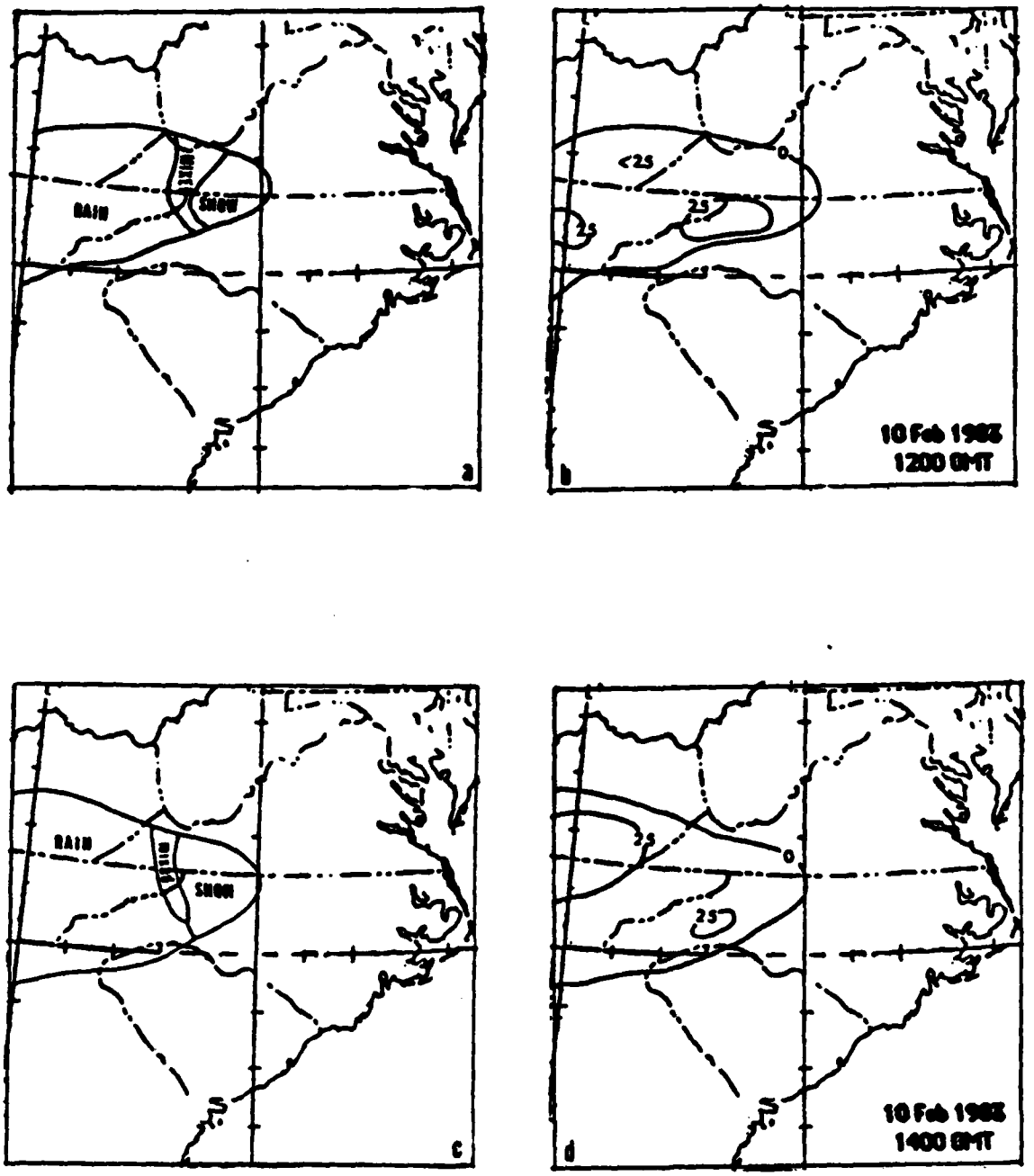


Fig. 1. Hourly precipitation (mm) amounts (a,c) and precipitation type (b,d) for date and time indicated.

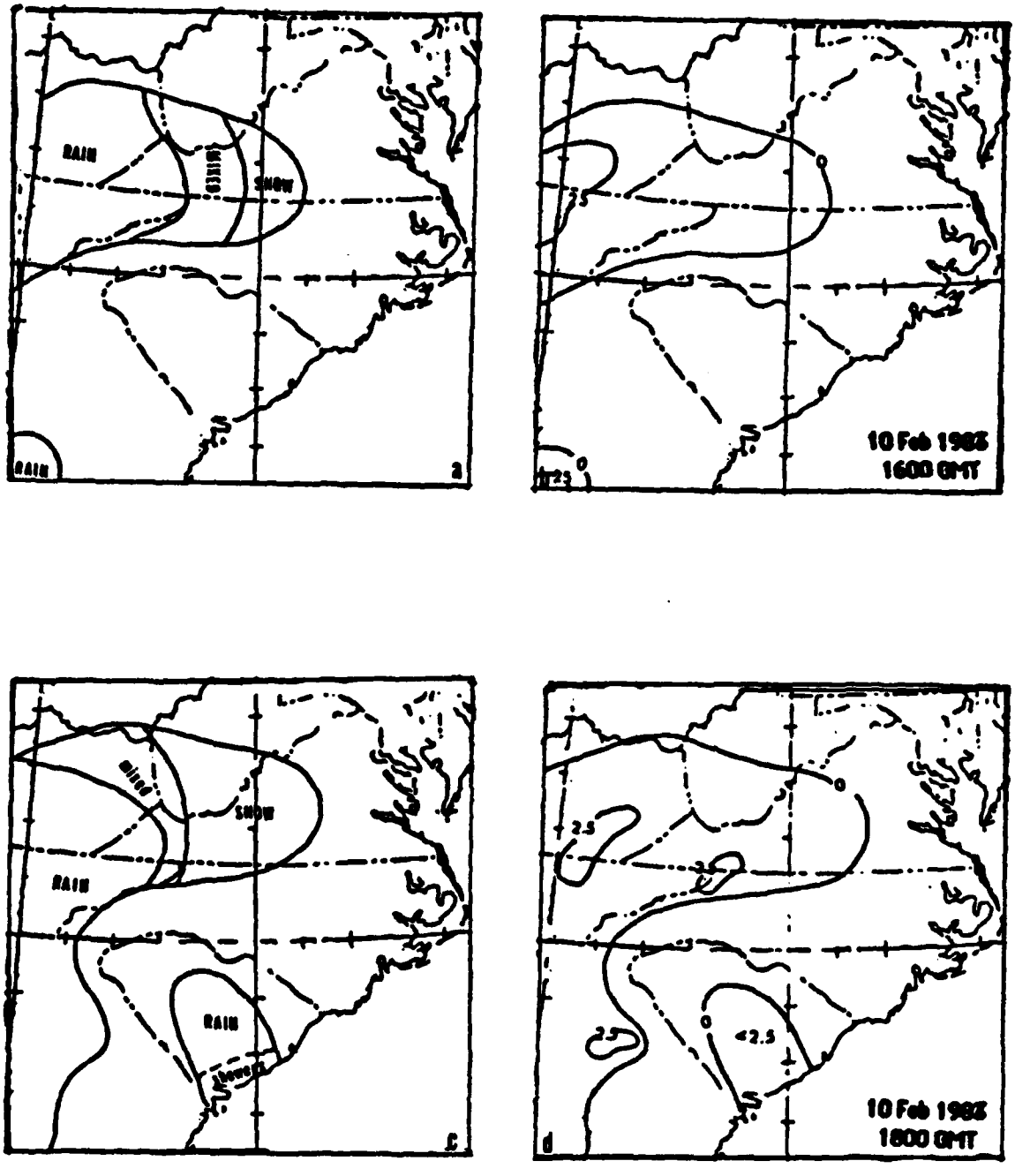


Fig. 2. Hourly precipitation (mm) amounts (a,c) and precipitation type (b,d) for date and time indicated.

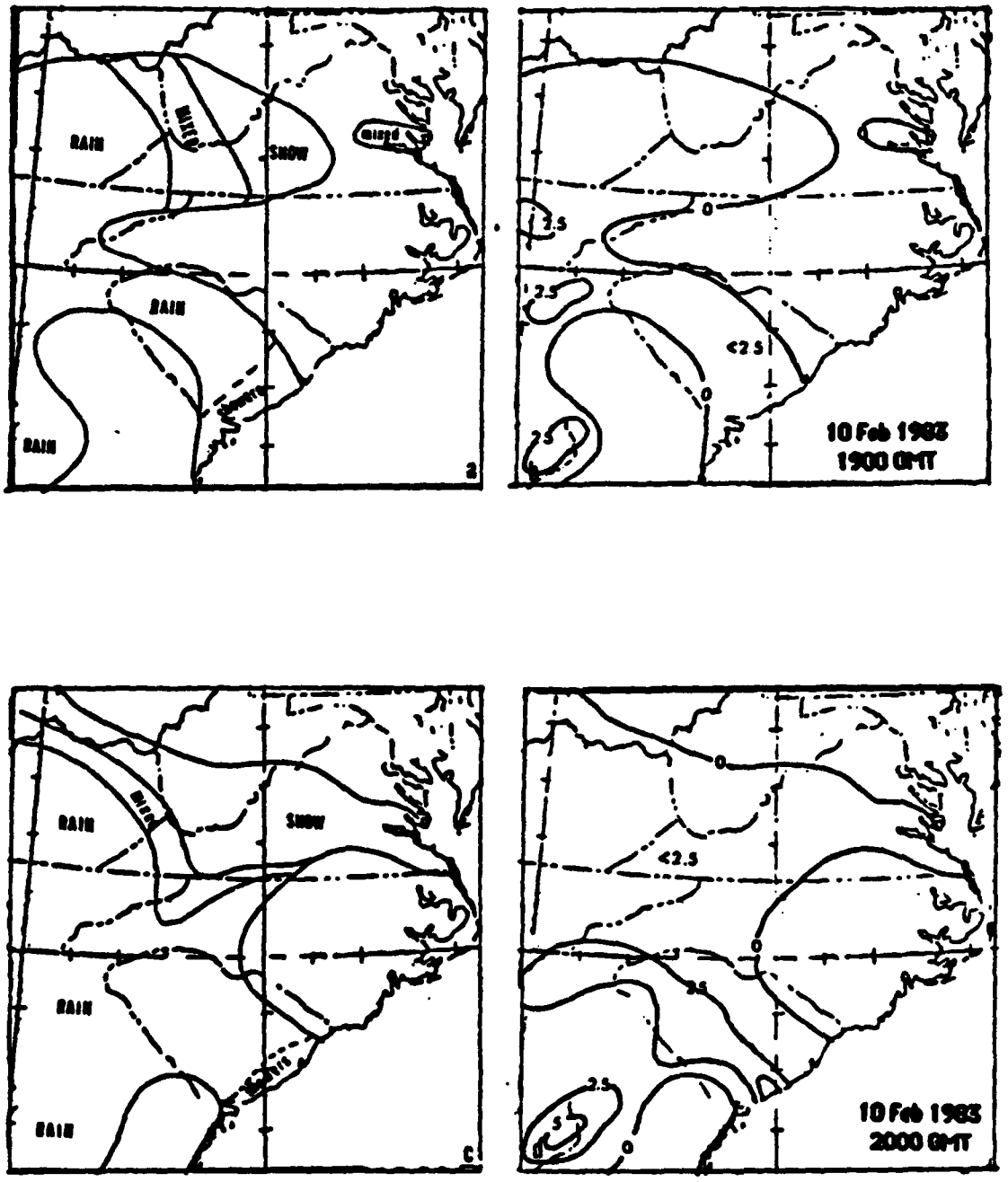


Fig. 3. Hourly precipitation (mm) amounts (a,c) and precipitation type (b,d) for date and time indicated.

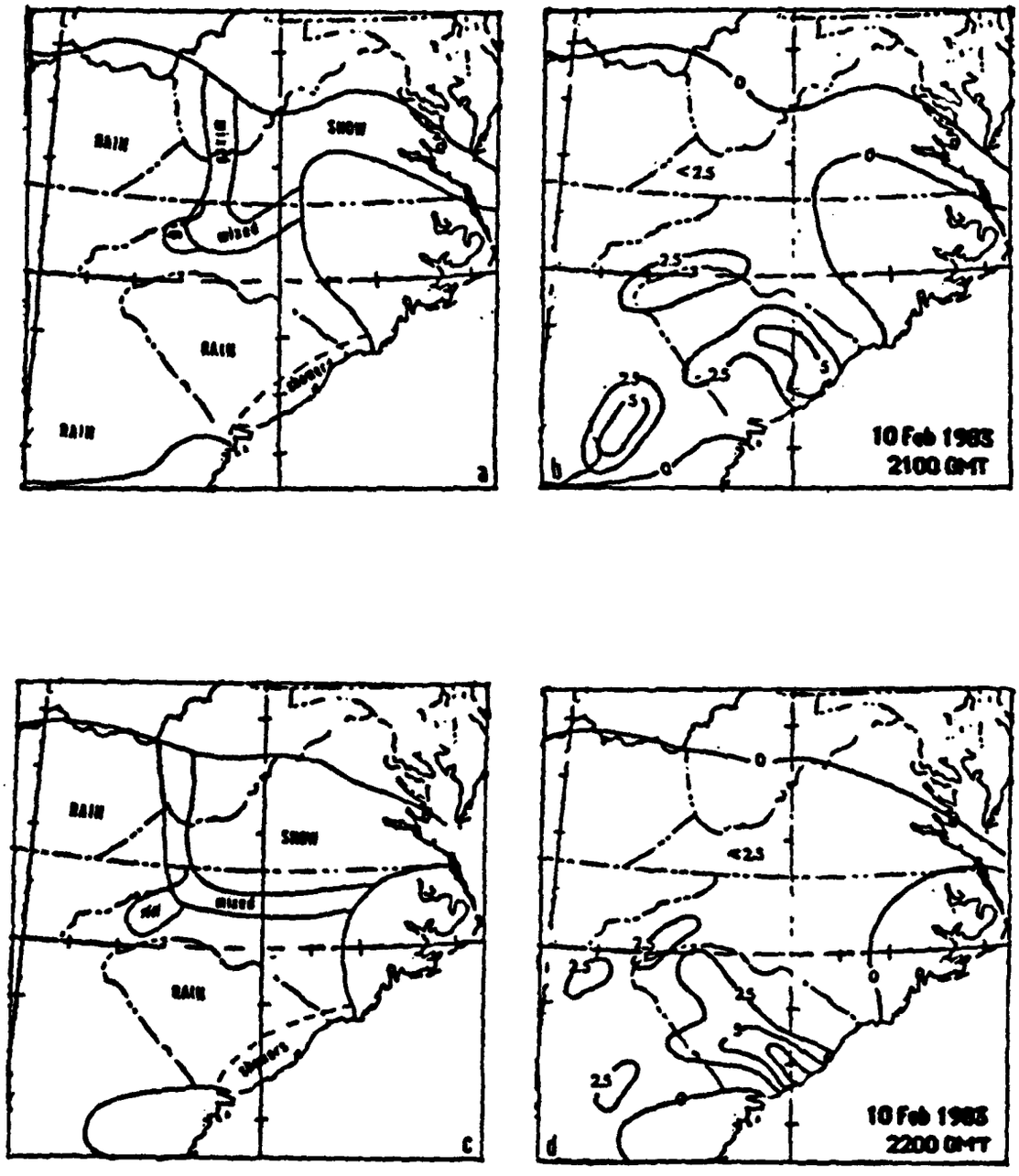


Fig. 4. Hourly precipitation (mm) amounts (a,c) and precipitation type (b,d) for date and time indicated.

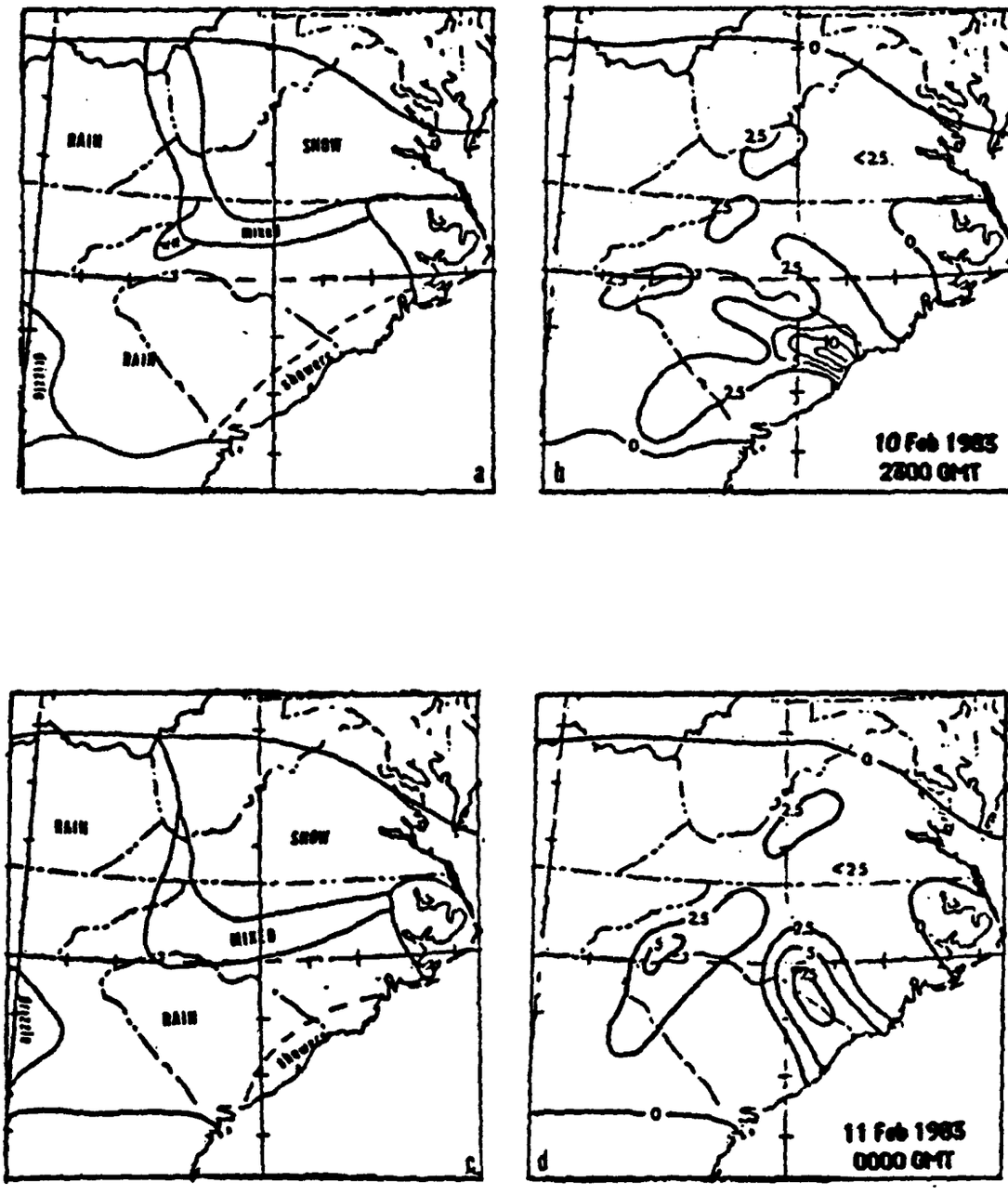


Fig. 5. Hourly precipitation (mm) amounts (a,c) and precipitation type (b,d) for date and time indicated.

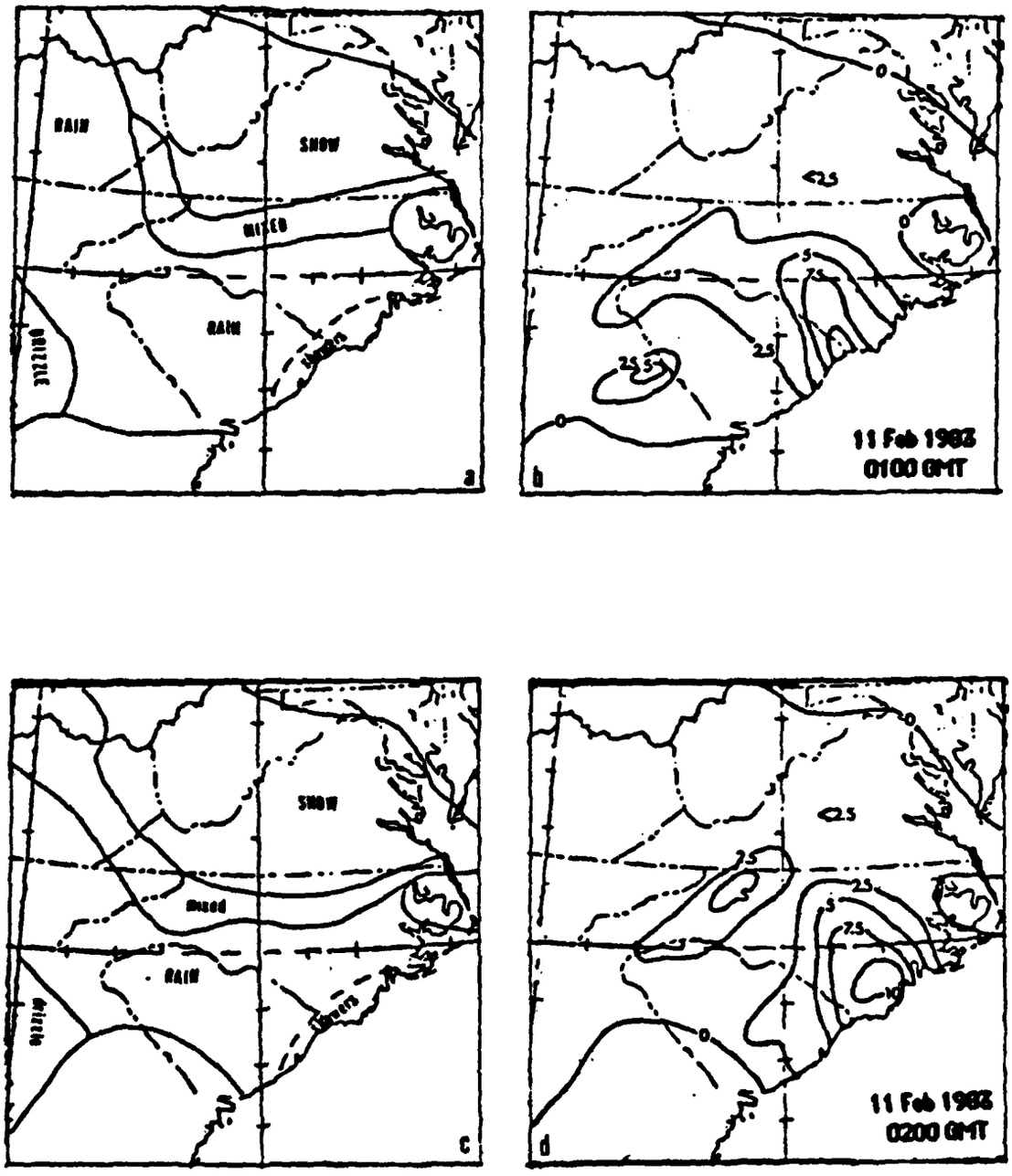


Fig. 6. Hourly precipitation (mm) amounts (a,c) and precipitation type (b,d) for date and time indicated.

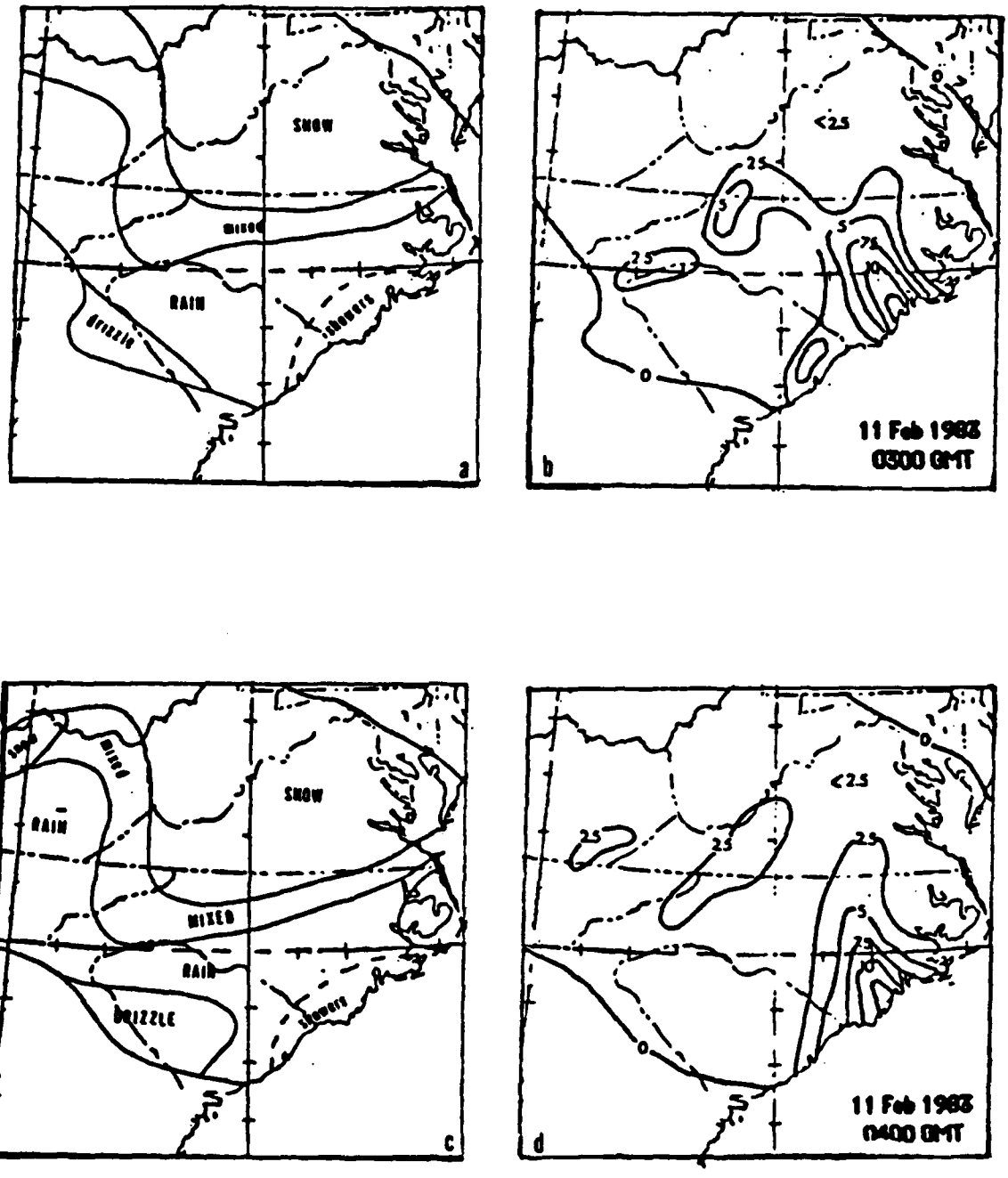


Fig. 7. Hourly precipitation (mm) amounts (a,c) and precipitation type (b,d) for date and time indicated.

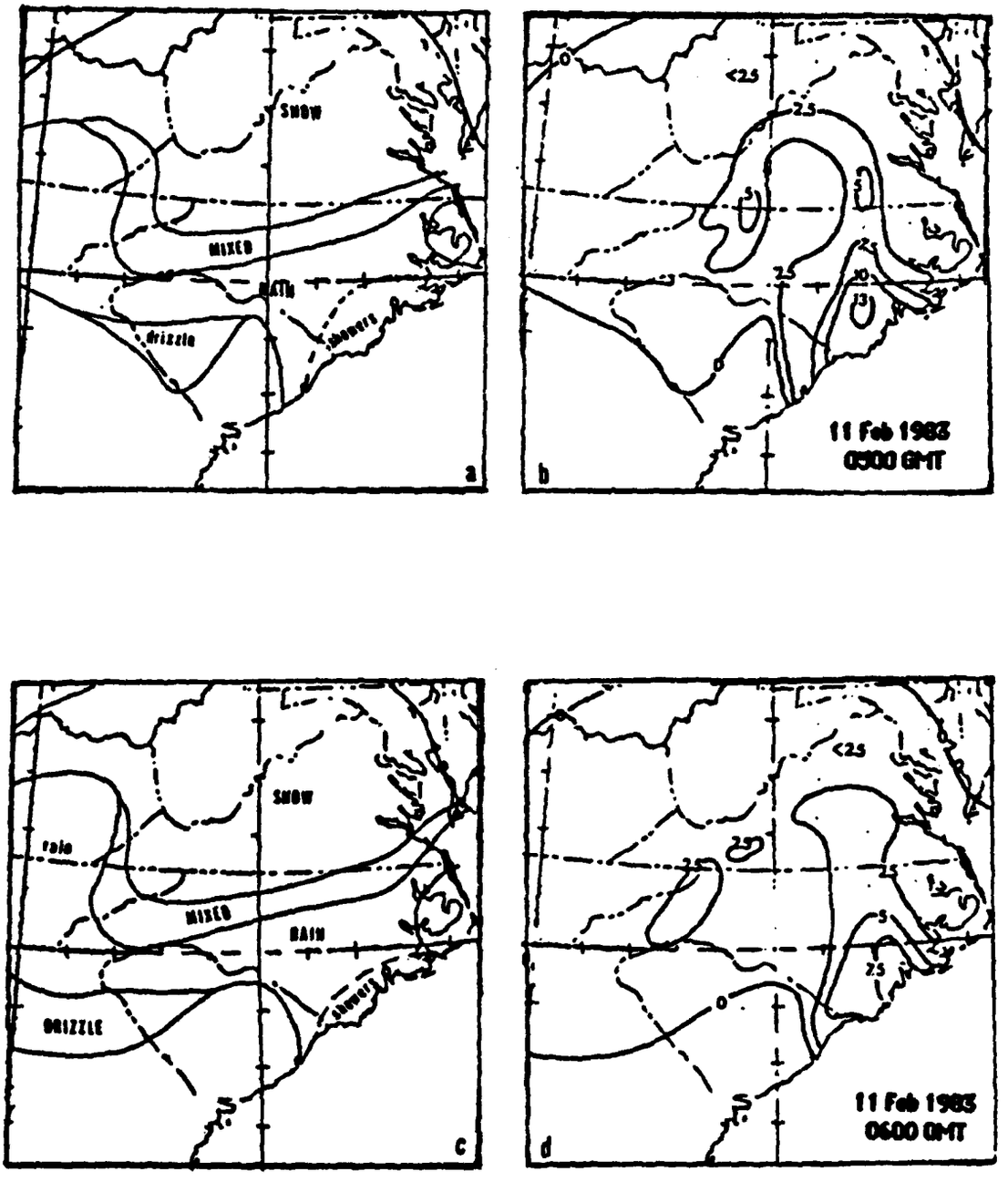


Fig. 8. Hourly precipitation (mm) amounts (a,c) and precipitation type (b,d) for date and time indicated.

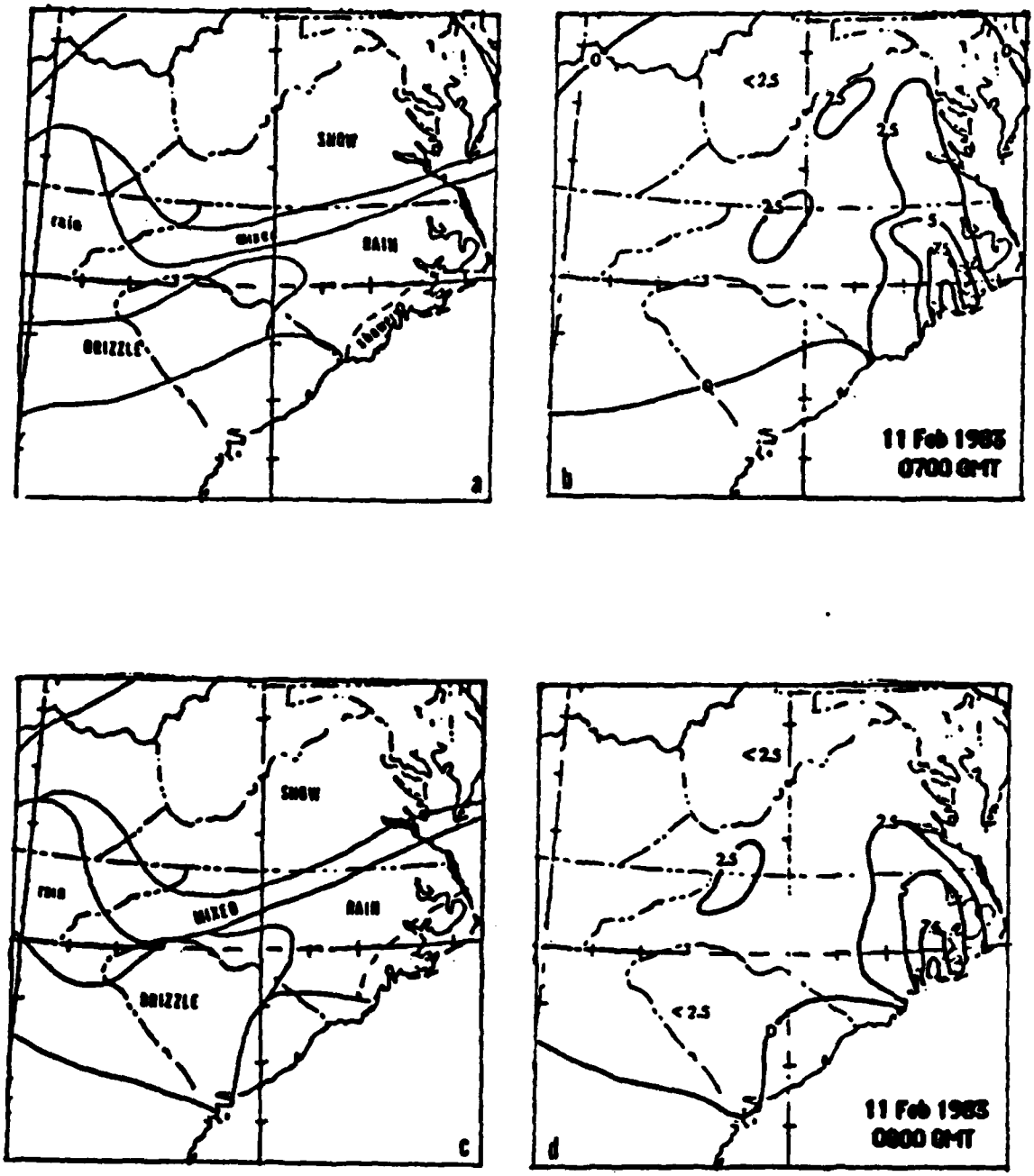


Fig. 9. Hourly precipitation (mm) amounts (a,c) and precipitation type (b,d) for date and time indicated.

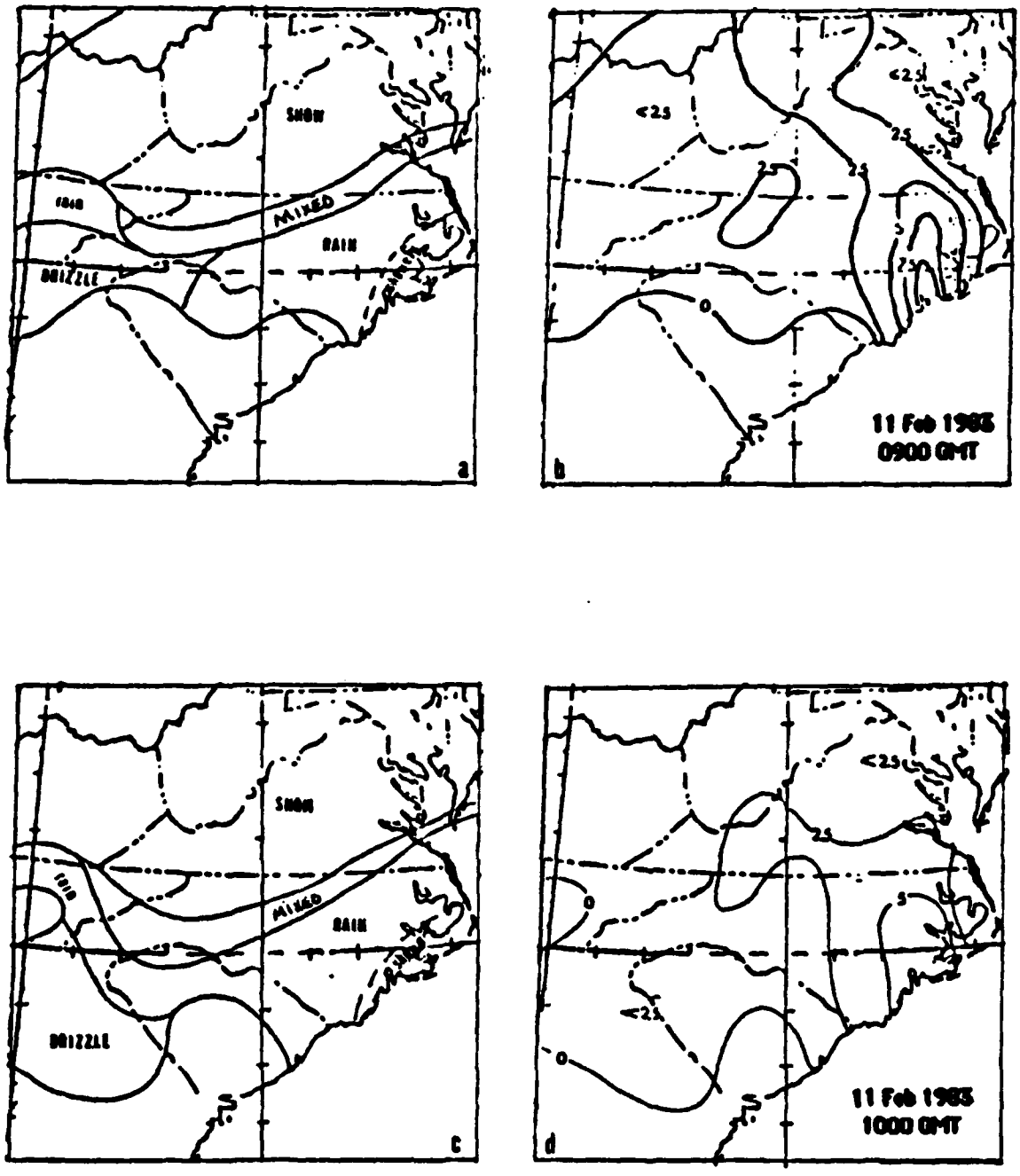


Fig. 10. Hourly precipitation (mm) amounts (a,c) and precipitation type (b,d) for date and time indicated.

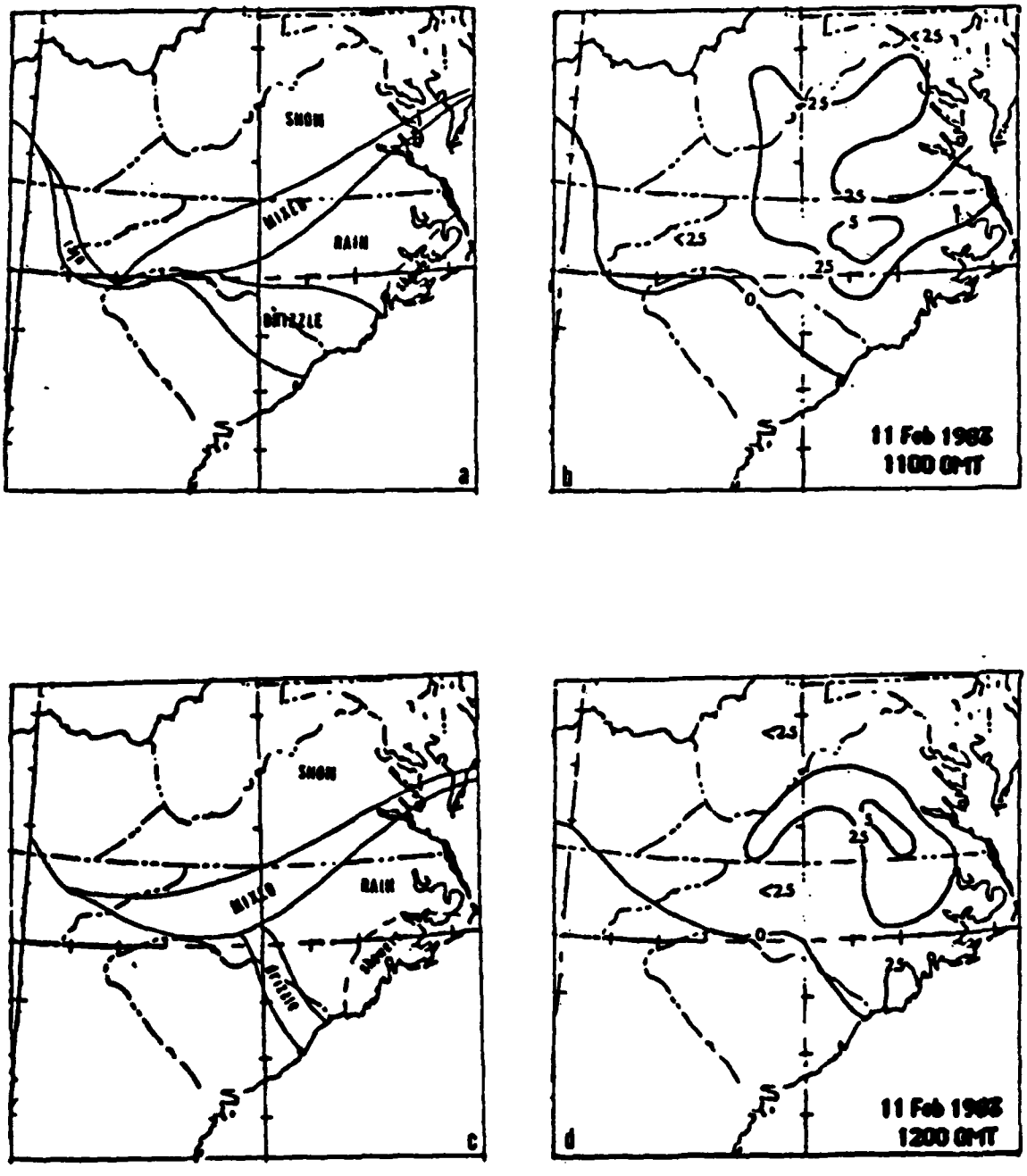


Fig. 11. Hourly precipitation (mm) amounts (a,c) and precipitation type (b,d) for date and time indicated.

END

DTIC

5-86